Vapor-liquid equilibrium data for the carbon dioxide and nitrogen (CO_2+N_2) system at the temperatures 223, 270, 298 and 303 K and pressures up to 18 MPa

Snorre Foss Westman[a,*], H. G. Jacob Stang[b], Sigurd W. Løvseth[b,**], Anders Austegard[b], Ingrid Snustad[b], Sigmund Ø. Størset[b], Ivar S. Ertesvåg[a]

[a]*Norwegian University of Science and Technology, Department of Energy and Process Engineering, Kolbjørn Hejes vei 1b, NO-7491 Trondheim, Norway*
[b]*SINTEF Energy Research, NO-7465 Trondheim, Norway*

Abstract

A new setup for the measurement of vapor-liquid phase equilibria of CO_2-rich mixtures relevant for carbon capture and storage (CCS) transport conditions is presented. An isothermal analytical method with a variable volume cell is used. The apparatus is capable of highly accurate measurements in terms of pressure, temperature and composition, also in the critical region. Vapor-liquid equilibrium (VLE) measurements for the binary system CO_2+N_2 are reported at 223, 270, 298 and 303 K, with estimated standard uncertainties of maximum 0.006 K in the temperature, maximum 0.003 MPa in the pressure, and maximum 0.0004 in the mole fractions of the phases. These measurements are verified against existing data. Although some data exists, there is little trustworthy data around critical conditions, and our data indicate a need to revise the parameters of existing models. A fit made against our data of the vapor-liquid equilibrium prediction of GERG-2008/EOS-CG for CO_2+N_2 is presented. At 223 and 298 K, the critical region of the isotherm are fitted using a scaling law, and high accuracy estimates for the critical composition and pressure are found.

Keywords:
vapor-liquid equilibrium, experimental measurements, carbon dioxide, nitrogen, CO_2 capture and storage

1. Introduction

Knowledge about how CO_2-rich mixtures behave under different conditions is important for the development of carbon capture, transport and storage (CCS) processes. For instance, an accurate equation of state (EOS) describing the thermodynamic properties of these mixtures is needed to model and dimension the various processes along the CCS value chain. Moreover, an EOS can be used to set requirements on the amount of impurities present in the CO_2 to be transported. Even with the recent progress of molecular modeling, empirical EOSs still provide the most accurate description of thermodynamic properties of such systems. Unfortunately, even for relatively simple binary mixtures, the data situation is not satisfactory for all relevant mixtures and conditions [1, 2, 3]. Hence, new and accurate experimental data are needed in order to improve the thermodynamic property predictions, by developing new EOS models or modifying the parameters and structure of existing ones.

Even small amounts of impurities in CO_2-rich mixtures can significantly affect the behavior of the fluid [3, 4]. As an example, the maximum pressure at which a mixture of CO_2 and only 5 % N_2 can be in the two-phase region, the cricondenbar, will increase to approximately 8.4 MPa compared to the critical pressure of CO_2, 7.3773 MPa [4, 5, 6].

Until recently, the most accurate EOS model describing CO_2-rich mixtures has been the GERG-2008 [7, 8]. This EOS [7] covers most of the relevant mixtures expected in CO_2 conditioning and transport found in CCS [8, 3, 9]. The structure and parameters in this EOS were developed and fitted with focus on natural gas mixtures.

In the works by Gernert and Span [1] and Gernert [2], an equation of state called EOS-CG (Equation Of State for Combustion Gases and combustion gas like mixtures) has been developed specifically for CO_2-rich mixtures. The EOS was based on the structure of GERG-2008, with modifications for the binary CO_2-rich systems found within CCS. The EOS was fitted against a significantly extended literature data base for CO_2-rich mixtures compared to the GERG-2008 data base [1, 2].

However, as Gernert and Span [1] and Gernert [2] pointed out in the review of available literature data, large gaps occur in the experimental data for thermophysical properties of CO_2-rich mixtures [3, 10]. Moreover, some of the existing data from different authors are systematically inconsistent with those of other authors within the stated uncertainty estimates. As a consequence, the accuracy of the equations of state fitted to the data could be increased significantly by reconciling the inconsistencies and filling in the gaps in the available data.

*Corresponding author. +47 735 93 860
**Corresponding author. +47 735 97 200
Email addresses: snorre.f.westman@ntnu.no (Snorre Foss Westman), sigurd.w.lovseth@sintef.no (Sigurd W. Løvseth)

The work to be presented here is part of a project called CO_2Mix. As described by Løvseth et al. [5], the CO_2Mix project aims at performing accurate vapor-liquid equilibrium (VLE), speed of sound and density measurements of CO_2-rich mixtures at conditions relevant for transport and conditioning in CCS [3, 9]. As part of this project, a setup has been specifically designed and constructed in order to perform highly accurate phase equilibria measurements on CO_2-rich mixtures under relevant conditions for CCS.

The present paper reports the results of VLE measurements on the CO_2+N_2 binary system, with measurements over the whole VLE pressure region at the temperatures 223, 298 and 303 K, and one VLE data point at 270 K. For some conditions, high quality literature data exist for this system, making it suitable to validate the operation of the experimental setup. Furthermore, several measurements were taken at conditions where no previous data or only data of dubious quality could be found, for instance at pressures close to the critical point of the binary mixture at the measured temperatures. Additionally, measurements were performed at temperatures close to the critical temperature of CO_2. The results are compared to existing EOS models, and new fits are presented.

Special care has been taken by the authors to present the results and analysis in accordance with the IUPAC Guidelines for reporting of phase equilibrium measurements given in the work by Chirico et al. [11]. One of the most important aspects of this is the thorough estimation of the standard uncertainties, as specified in the ISO Guide for the Estimation of Uncertainty in Measurement, commonly referred to as "GUM" [12]. Error-free dissemination of the resulting experimental data with the uncertainty estimates is ensured by supplying the data in a file written in the NIST ThermoML format [13, 14, 15, 16].

In the current work, the experimental setup and the operational procedures applied will be described in detail in Section 2. In Section 3, an analysis of the pressure, temperature and composition measurement uncertainty will be presented, with references to further details in the appendix. The measurement results will be provided in Section 4, before an analysis of the data with regards to existing data and models in Section 5. Section 5 will also present fitting of existing models to the new data.

2. Experimental apparatus

2.1. Description of setup

The experimental setup has been described briefly in [17]. A more detailed description will be given here. Additional details necessary for the uncertainty analysis for the measurement of pressure, temperature, and composition will be given in Sections 3.2, 3.3, and 3.4, respectively.

The vapor-liquid equilibrium measurements were carried out using an isothermal analytical method with a variable-volume cell, as described by [18]. This method involves determination of the equilibrium composition of both phases at given temperature and pressure. A diagram of the cell and the ancillary apparatus is shown in Fig. 1.

In our experiments with 2 components, CO_2 and N_2, Gibbs' phase rule states that we can vary 2 intensive properties freely when we have 2 coexisting phases present. We controlled the temperature T by means of a thermostatic bath, and the pressure p by the injection of CO_2 and N_2 into the cell. We can then state the equilibrium compositions of the liquid and vapor phases, x_{CO_2} and y_{CO_2}, respectively, as functions of T and p:

$$x_{CO_2} = f(T,p)\,, \tag{1}$$

$$y_{CO_2} = f(T,p)\,. \tag{2}$$

The cell consisted of a transparent sapphire cylinder tube placed between two titanium flanges. The internal volume of the cell was approximately 100 ml. To keep the temperature constant, the cell was placed in a thermostatic bath kept at the desired temperature (Fluke Hart Scientific model 7080 for subambient temperatures, and model 6020 with external cooling water for temperatures above ambient). The following two bath fluids were used: at temperatures below ambient, ethanol, and for temperatures close to the critical temperature of CO_2, distilled water.

The temperature of the cell was monitored by two Fluke model 5686 glass capsule standard platinum resistance thermometers (SPRT) placed inside the top and bottom flanges.

The cell pressure was measured indirectly through a Rosemount 1199 diaphragm connected by an oil-filled circuit to a Rosemount 3051 differential pressure transmitter with an array of four absolute pressure sensors p_i, where $i = 1, 2, 3, 4$, (Keller model PAA-33X) with full scales of 1, 3, 10 and 20 MPa respectively, on the other side. The absolute pressure sensor circuit was filled with nitrogen and maintained at a pressure such that the differential pressure between this circuit and the cell circuit was close to zero, using syringe pump 5 (TOP Industrie, model PMHP 100-500).

Three different syringe pumps (from TOP Industrie) were used to fill the components into the cell. Pump 2 was dedicated to injecting CO_2 (model PMHP 100-500). Pump 3 was used to inject an impurity, which was N_2 in the case of the present work (model PMHP 200-200). The surface of the parts of the pump and the tubing in contact with the fluid was sulfinert treated to minimize adsorption. Pump 4 could be used to inject fluids in liquid state, such as water, in later work (model PMHP 100-500). All three pumps could be evacuated through a connection to a vacuum pump (Trivac® E 2 from Leybold).

These pumps were connected via tubing to valves that were integrated in the cell flanges. Integrated valves were used to minimize the dead volume inside the cell. An additional integrated valve could be opened to ventilation when the cell pressure needed to be reduced.

The vacuum pump was connected to an integrated valve, enabling evacuation of the cell before the filling took place.

A magnetic stirrer was placed at the bottom of the cell, and could be rotated at up to 800 rpm to reach VLE faster.

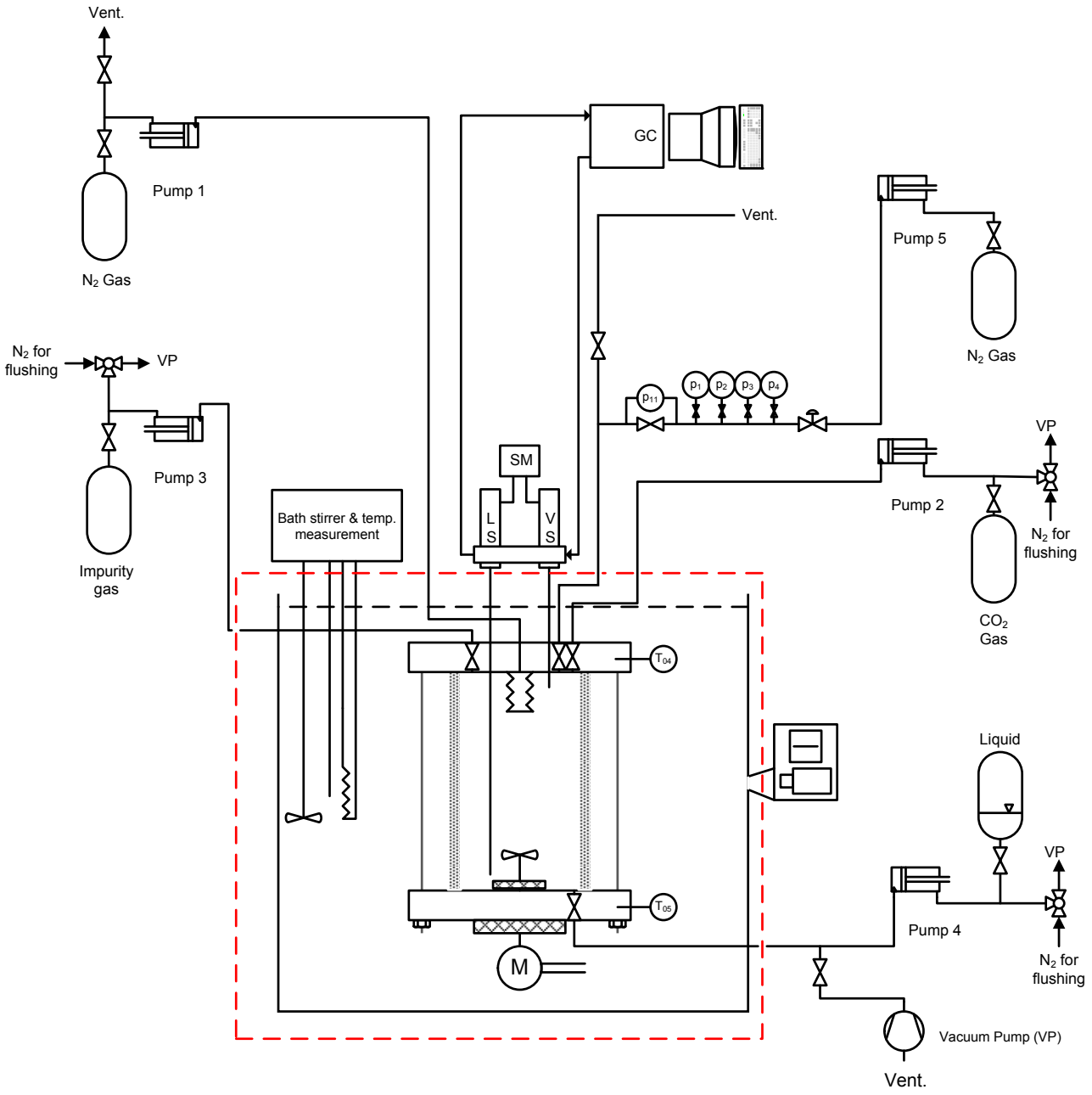

Fig. 1. Principal diagram of cell and ancillary apparatus. LS,VS: Liquid and vapor phase Rolsi^{TM} samplers, respectively. SM: Rolsi^{TM} controller. M: Gear for rotating permanent magnet below cell, which rotates stirrer inside cell. Gear connected to electric motor outside bath. T_{04}: Top flange SPRT. T_{05}: Bottom flange SPRT.

A borescope was used to inspect the content of the cell through the transparent sapphire cylinder, to ensure that the liquid level was appropriate.

A custom made National Instruments LabVIEW program was used for data acquisition of the measured pressure and temperature values, which were logged every second.

The resistance of the two SPRTs were measured one at a time using an ASL SB148 switchbox to change between the two SPRTs, which in turn was connected to an ASL F650AC thermometry bridge. A resistance measurement point of one resistor was obtained once every 20 seconds when the ASL bridge was set to obtain the most accurate ratio value. The ASL bridge measured ratio values were obtained by the logging program through an USB connection.

The update rates of the four pressure sensors p_i were 400 Hz, and the dead time of the differential pressure sensor p_{11} was approximately 45 ms. The measured pressure values of p_i were obtained by the logging program using the digital output of the sensors through a RS485 serial connection. The values of p_{11} were obtained using a conversion of the analog 4-20 mA DC current output of the sensor to a digital output read through a RS485 serial connection by the logging program.

The compositions of the vapor and liquid phases were measured by extracting a sample from a phase using Rolsi™ electromagnetic samplers (Armines patent [19]. Pneumatic version of the Rolsi™ sampler described in [20]). The vapor phase sampling capillary inlet was placed close to the top flange inside the cell, while the liquid phase capillary inlet could be moved vertically inside the cell to be at an appropriate position in the liquid phase. The use of these Rolsi™ samplers for VLE measurements was first described in [21].

Using the LabVIEW program, the electromagnetically controlled valves of the Rolsi™ samplers were opened for a specified time period to let a sample flow out of the cell. The sample flowed out through the capillaries into a heated gas chromatograph (GC) helium carrier gas circuit at close to atmospheric pressure. The low-pressure side of the Rolsi™ valves and piping between the valves and GC were also heated above the critical temperature of CO_2, ensuring that both the vapor and liquid samples were in gaseous form. The sample was swept by the carrier gas into the GC (Agilent 7890A) equipped with a Supelco Carboxen-1010 PLOT Capillary GC Column (from Sigma-Aldrich, column length 30 m, internal diameter 0.53 mm) where the CO_2 and N_2 were separated. Downstream of the column, a thermal conductivity detector (TCD) measured the difference in voltage needed to keep the gas passing the detector at a constant temperature. The detector response was monitored as a function of time at 5 Hz, resulting in two separate peaks corresponding to N_2 and CO_2. At sampling, the logging of the detector response was started automatically with the Agilent OpenLAB CDS EZChrom GC data acquisition and control software.

When a sample was taken, pump 1 was used to apply an increased N_2 overpressure compared to the cell pressure on a plate bellows inside the cell, to expand the bellows and thereby decreasing the cell volume, preventing a decrease in cell pressure after each sample. Fully expanded, the bellows caused an approximate volume decrease inside the cell of maximum 1 cm^3.

The internal diameter of the Rolsi™ capillaries were 150 μm, and the length of the liquid and vapor phase capillaries were 0.4 and 0.3 m, respectively. The internal volumes of the liquid and vapor capillaries corresponded to approximately 0.007 and 0.005 % of the cell volume, respectively. The upper part of the both the liquid and the vapor capillaries were outside the thermostatic bath, and were heated to 313 K to avoid condensation.

As the liquid in the heated upper part of the liquid capillary would boil off, too small samples would only consist of the boil-off gas with a composition that would not be representative of the liquid phase in the cell. In order to be sure to measure the true liquid composition, the number of moles of each liquid sample should at least be as large as what is found in a volume of the whole liquid capillary with the same density and composition as the liquid phase inside the cell. As some of the volume of the liquid sampler was occupied by a vapor phase with lower density than a liquid phase, the calculated liquid sample size was probably an overestimate, but helped ensure thorough flushing of the liquid capillary for each sample. Because the sample size should be sufficient to flush the capillaries, the expansion of the bellows was necessary to prevent a significant change in the cell pressure. For the vapor samples, the first samples of a series at a pressure / temperature point were of a sufficient size to flush the vapor capillary. Consecutive sample sizes were set large enough to give a good repeatability in the composition measurements. The repeatability as a function of sample size was determined from the calibration of the GC using the calibration gas mixtures.

In practical terms, the sample volumes discussed above were estimated from the GC traces. The liquid phase density and composition were calculated using the GERG-2008 EOS [7] at the cell pressure and temperature. An estimate of the number of moles in a sample as a function of the peak areas of each component in the GC traces was established by injecting each of the components into the GC through a sample loop with a known volume, kept at ambient temperature and slightly higher than atmospheric pressure. The densities of the pure components were calculated using the EOSs by [6] and [22].

2.2. Calibration

The two SPRTs used for temperature measurements had been calibrated in-house according to the International Temperature Scale of 1990 (ITS-90) [23], against fix point cells calibrated at accredited calibration laboratories. Details about the calibration of the SPRTs can be found in Section 3.3.

The absolute pressure sensors had been calibrated in-house against a dead weight tester recently calibrated at an accredited calibration laboratory. For details, see Section 3.2.

The GC had been calibrated against gravimetrically prepared calibration gas mixtures made in-house. See Section 3.4 for details.

Table 1
Chemical samples used.

Chemical name	CASRN	Source	Initial mole fraction purity	Purification method	Final mole fraction purity	Analysis method
Carbon dioxide	124-38-9	Yara Praxair	0.99999	None	0.99999	None
Nitrogen	7727-37-9	Yara Praxair	0.999999	None	0.999999	None
Helium[1]	7440-59-7	Yara Praxair/AGA	0.999999	None	0.999999	None

[1] GC carrier gas

The manufacturer's specified purity of the CO_2 and N_2 samples used for both the VLE experiments, and for preparing the calibration gas mixtures, are listed in Table 1. We did not perform any additional analysis of the specified purity of the samples by for instance mass spectroscopy. However, as we performed vapor pressure measurements of CO_2 at the different temperatures where VLE measurements were performed, we asserted that the vapor pressures were in agreement with the calculated vapor pressures from the EOS by Span and Wagner [6], within the combined uncertainty in our pressure measurements and in the EOS calculations.

2.3. Experimental procedures

Before starting a VLE experiment, the whole circuit in connection with the VLE cell was evacuated, using the vacuum pump. The evacuation included the gas lines to the cell from the gas cylinders of pure CO_2 and N_2, and all lines transporting the gases into the cell.

The CO_2 pump and N_2 impurity pump and lines were first evacuated once, and then flushed with the respective gases to dilute any remaining impurities in the lines and pumps. This evacuation and flushing were repeated 5 times for each pump. After the final evacuation, the gases were filled onto their respective lines and pumps, and maintained at a pressure of at least 0.5 MPa to prevent contamination of the gases.

After the flushing of the gas lines and pumps, the cell was flushed with CO_2, and evacuated. As with the pumps, the flushing and evacuation were repeated 5 times.

Following the flushing, and with the thermostatic bath kept at the desired temperature, CO_2 was injected until the volume fraction of liquid CO_2 was approximately 50 % of the cell.

The stirrer then ran until the pressure and temperature measurements had stabilized. After the stirrer had been turned off, the vapor pressure of CO_2 was measured. If the measured vapor pressure were within the combined uncertainty of the Span-Wagner EOS [6] and our measurements, the purity of the CO_2 in the cell was deemed to be sufficient.

After the CO_2 vapor pressure measurements, N_2 was filled onto the cell to increase the pressure, and the stirrer was run until the temperature and pressure had stabilized. The liquid level in the cell was adjusted to keep a liquid volume fraction of approximately 50 %, by either injecting more CO_2 or venting out either some of the vapor or liquid phase. The liquid phase capillary inlet was placed such as to always be more than 10 mm below the liquid level in the cell.

After this, the borescope was removed from the thermostatic bath to prevent heat transfer from the surroundings into the bath fluid. When the cell pressure and temperature had stabilized, the stirrer was turned off, and the vapor and liquid phases were left to settle before sampling started.

From this point on, there were two different procedures employed in this work. The series of experiments started off with VLE measurements at 298 K, and then 303, 223 and 270 K. At the end of the VLE experiments at 303 K, the bellows started leaking N_2 into the cell. To avoid delay in the measurements, it was decided to replace the bellows with a blind plug, and proceed with VLE experiments at the 223 and 270 K without pressure compensation of sampling, and hence using slightly different procedures than for the previous isotherms.

For the measurements at 298 and 303 K, with the pressure drop due to sampling compensated by using the bellows, a sample was withdrawn from the cell every 25 minutes.

For the measurements at 223 and 270 K, the pressure dropped slightly after each sample. Two different methods were used to approach the VLE state of the new pressure value. In the first method, the stirrer was run for 15 minutes after each sampling, and then turned off to allow the phases to separate for the remaining 10 minutes before the next sample was taken. In the second method, the stirrer was not used between the samples. Instead, the period between each sample was increased from 25 minutes to 2-3 hours.

3. Uncertainty analysis

3.1. Definitions

The "GUM" [12] terms and definitions will be used in the following analysis. For ease of reading, and, since several of the estimation methods will be used repeatedly, some of the symbols used will be defined here.

The uncertainty components will be evaluated as standard uncertainties, with symbol $u(y)$, where y is the estimate of the measurand Y, that is, the measurement result. Standard uncertainty is the uncertainty of the result of a measurement expressed as an estimated experimental sample standard deviation, with symbol $s(y)$ [12].

Type A evaluation of uncertainty refers to uncertainties evaluated by statistical analysis of a series of observations [12]. Examples include the evaluation of the uncertainty of the mean values of pressure and temperature in the time

before a single sample is taken of the composition of the phases in the cell.

Type B evaluation of uncertainty refers to uncertainties evaluated by other means, for example specifications of measurement equipment provided by the manufacturer, or when the uncertainty of a value has to be subjectively evaluated, as in the case of measured physical distances on the laboratory apparatus for the calculation of the hydrostatic pressure. Common for these type of evaluations is that the uncertainties have to be modeled using an applicable probability distribution [12].

The propagation of the standard uncertainties in the input quantities X_i to the standard uncertainty in the final estimate of the measurand is described by the combined standard uncertainty, symbol $u_c(y)$.

For N uncorrelated input quantities, the general expression for $u_c(y)$ is given by [12] as

$$u_c^2(y) = \sum_{i=1}^{N} \left(\frac{\partial f}{\partial x_i} \right)^2 u^2(x_i) \,, \tag{3}$$

where $Y = f(X_1, X_2, ..., X_N)$.

When it is difficult to determine if the input quantities are independent, or if the correlation of the quantities is not possible to determine, the most conservative estimate is assumed, that the maximum errors in each contribution occurs simultaneously:

$$u_c(y) = \sum_{i=1}^{N} \left| \frac{\partial f}{\partial x_i} \right| |u(x_i)| \,. \tag{4}$$

Some of the standard uncertainty terms $u(x_i)$ in these equations have to be evaluated from other underlying standard uncertainties without knowing the functional form of f. This is the case, for example, for manufacturers' specifications of several sources of uncertainties contributing to the total uncertainty in the measured value. When this is the case, and the contributions are assumed to be independent, the total standard uncertainty is evaluated with Eq. (5a).

When the contributions cannot be assumed to be independent, the most conservative estimate is assumed, similar to Eq. (4), shown in Eq. (5b).

$$u(x_i) = \begin{cases} \sqrt{\Sigma_{k=1}^{N} u^2(x_k)} & \text{if independent,} \quad (5a) \\ \Sigma_{k=1}^{N} |u(x_k)| & \text{if not independent.} \quad (5b) \end{cases}$$

These maximum estimates are also used in cases where such a maximum estimate does not contribute significantly to the final combined uncertainty in a value. Examples include cases where another source of uncertainty completely dominates the final combined uncertainty.

It is sometimes only possible to assume that a quantity X_i lies within an interval $[a_-, a_+]$ with a probability equal to one. In these cases, the quantity is modeled using either a rectangular or triangular probability distribution. If the expected value of X_i is estimated as $x_i = (a_- + a_+)/2$, and $a = |a_- - a_+|/2$, the standard uncertainty is estimated as $u(x_i) = a/\sqrt{3}$ for the rectangular distribution, and $u(x_i) = a/\sqrt{6}$ for the triangular distribution.

3.2. Pressure

The standard uncertainties connected to the measurement of pressure p at VLE are summarized in Table 2, and the justification for these uncertainties is presented in Appendix A.1.

To illustrate the final estimated uncertainty in the pressure measurements resulting from the analysis in Appendix A.1, Fig. 2 shows the pressure standard uncertainty relative to the measured pressure for the VLE measurements performed in this work.

3.3. Temperature

The standard uncertainties connected to the measurement of temperature T at VLE are summarized in Table 3, and the justification for these uncertainties is presented in Appendix A.2.

The temperature standard uncertainty estimated in Appendix A.2 is illustrated by Fig. 3, which shows the temperature uncertainty for the VLE experiments performed in this work.

3.4. Composition

The results of the calibration of the GC, and the analysis of the estimated uncertainty in the measured compositions of the phases, are given in detail in Appendix A.3. The standard uncertainty in the CO_2 mole fractions of the phases is estimated to be $u(x_{CO_2}) = u(y_{CO_2}) = 2.7 \cdot 10^{-4}$.

Table 2
Summary of standard uncertainty components for pressure measurements.

Symbol	Description and unit	u
Hydrostatic pressure p_{hs}		
$u(\rho_1)$	EOS-CG[2] vapor density of CO_2+N_2 (kg m^{-3})	$3 \cdot 10^{-3} \cdot \rho_1$
$u(\rho_2)$	Same as $u(\rho_1)$ (kg m^{-3})	$3 \cdot 10^{-3} \cdot \rho_2$
$u(\rho_{4,1})$	SW[1] density at 313.15 K (kg m^{-3})	$3 \cdot 10^{-4} \cdot \rho_{4,1}$
$u(\rho_{4,2})$	Same as $u(\rho_1)$ (kg m^{-3})	$3 \cdot 10^{-3} \cdot \rho_{4,2}$
u(CAD)	(m)	0
$u_{\mathrm{c}}(h_1)$	(m)	0.0048
$u(h_{\mathrm{liq}})$	(m)	0.0048
$u(h_{\mathrm{liq}},1)$	Borescope h_{liq} (m)	0.0048
$u(h_{\mathrm{liq}},2)$	Variation in h_{liq} (m)	0
$u(h_2)$	Bath liquid level variation (m)	0.006
$u_{\mathrm{c}}(h_3)$	(m)	0.006
$u(h_4)$	Same as u(CAD) (m)	0
$u(g_{\mathrm{L}})$	Local g (m s^{-2})	$2 \cdot 10^{-7}$
Differential pressure p_{11}		
$u(p_{11},1)$	Ambient temperature (MPa)	0
$u(p_{11},2)$	Line pressure zero (MPa)	0
$u(p_{11},3)$	Line pressure span (MPa)	$4.9 \cdot 10^{-5}$ MPa^{-1} $\cdot p_i \cdot p_{11}$
$u(p_{11},4)$	Mounting (MPa)	0
$u(p_{11},5)$	Vibration (MPa)	$2.8 \cdot 10^{-5}$
$u(p_{11},6)$	Power supply (MPa)	0
$u(p_{11},7)$	A/D conversion (MPa)	$2.4 \cdot 10^{-4}$
Pressure sensors p_i		
$u(p_1)$	1 MPa sensor (MPa)	$2.24 \cdot 10^{-4}$
$u(p_2)$	3 MPa sensor (MPa)	$2.33 \cdot 10^{-4}$
$u(p_3)$	10 MPa sensor (MPa)	$7.64 \cdot 10^{-4}$
$u(p_4)$	20 MPa sensor (MPa)	$1.965 \cdot 10^{-3}$

[1] Span and Wagner [6] [2] Gernert and Span [1] and Gernert [2]

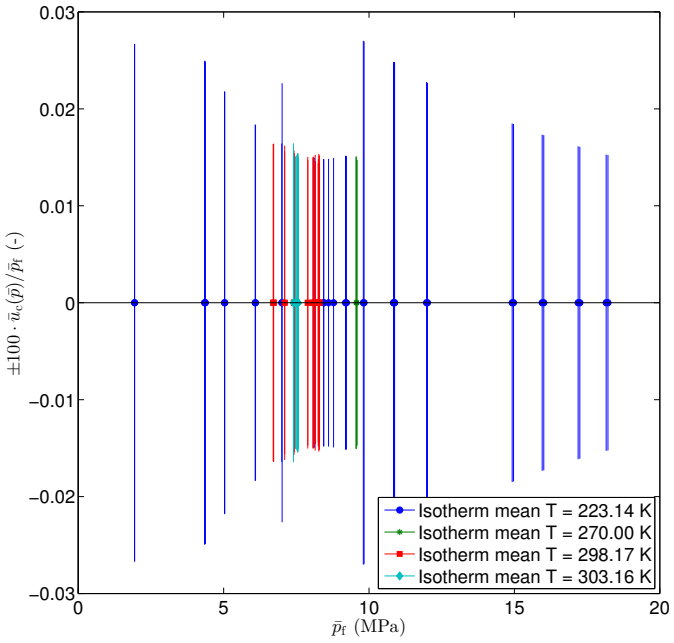

Fig. 2. Pressure standard uncertainty relative to the measured pressure for the VLE measurements performed, expressed as $100 \cdot \bar{u}_c(\bar{p})/\bar{p}_f$. Measured pressure $\bar{p}_f$. Standard uncertainty $\bar{u}_c(\bar{p})$.

Table 3
Summary of standard uncertainty components for temperature measurements.

Symbol	Unit	u
$u(W_{\mathrm{b}})$	(-)	$0.35 \cdot 10^{-6}$
$u(R_{\mathrm{ref}})$	(Ω)	$8.5 \cdot 10^{-6}$
$u(T_{H_2O})$	(mK)	0.51
$u(T_{\mathrm{Hg}})$	(mK)	1.43
$u(T_{\mathrm{Ga}})$	(mK)	0.85
For experiments at 298 K and 303.15 K		
$u(R_{H_2O}(T_{04}))$	(Ω)	$2.06 \cdot 10^{-5}$
$u(R_{H_2O}(T_{05}))$	(Ω)	$2.41 \cdot 10^{-5}$
$u(R_{\mathrm{Hg}}(T_{04}))$	(Ω)	$2.29 \cdot 10^{-5}$
$u(R_{\mathrm{Hg}}(T_{05}))$	(Ω)	$1.84 \cdot 10^{-5}$
$u(R_{\mathrm{Ga}}(T_{04}))$	(Ω)	$2.19 \cdot 10^{-5}$
$u(R_{\mathrm{Ga}}(T_{05}))$	(Ω)	$2.37 \cdot 10^{-5}$
$u(W_{\mathrm{Hg}}(T_{04}))$	(-)	$6.1 \cdot 10^{-6}$
$u(W_{\mathrm{Hg}}(T_{05}))$	(-)	$6.1 \cdot 10^{-6}$
$u(W_{\mathrm{Ga}}(T_{04}))$	(-)	$4.2 \cdot 10^{-6}$
$u(W_{\mathrm{Ga}}(T_{05}))$	(-)	$4.3 \cdot 10^{-6}$
For experiments at 223.15 K and 270.00 K		
$u(R_{H_2O}(T_{04}))$	(Ω)	$3.94 \cdot 10^{-5}$
$u(R_{H_2O}(T_{05}))$	(Ω)	$2.57 \cdot 10^{-5}$
$u(R_{\mathrm{Hg}}(T_{04}))$	(Ω)	$2.29 \cdot 10^{-5}$
$u(R_{\mathrm{Hg}}(T_{05}))$	(Ω)	$1.84 \cdot 10^{-5}$
$u(R_{\mathrm{Ga}}(T_{04}))$	(Ω)	$2.69 \cdot 10^{-5}$
$u(R_{\mathrm{Ga}}(T_{05}))$	(Ω)	$2.37 \cdot 10^{-5}$
$u(W_{\mathrm{Hg}}(T_{04}))$	(-)	$6.2 \cdot 10^{-6}$
$u(W_{\mathrm{Hg}}(T_{05}))$	(-)	$6.1 \cdot 10^{-6}$
$u(W_{\mathrm{Ga}}(T_{04}))$	(-)	$4.5 \cdot 10^{-6}$
$u(W_{\mathrm{Ga}}(T_{05}))$	(-)	$4.3 \cdot 10^{-6}$

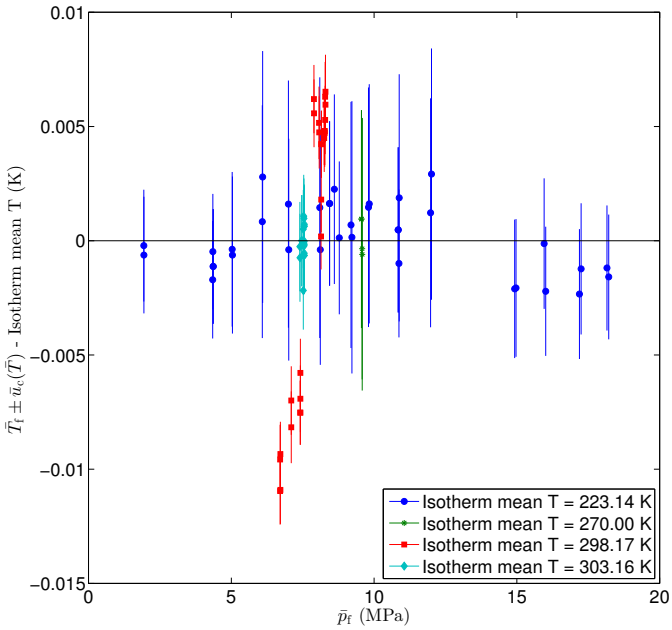

Fig. 3. Temperature deviations for each VLE measurement from isotherm mean temperature, and temperature standard uncertainty, expressed together as $\bar{T}_f \pm \bar{u}_c(\bar{T})$ - isotherm mean temperature, versus VLE experiment pressure $\bar{p}_f$. VLE experiment mean temperature $\bar{T}_f$. Temperature standard uncertainty $\bar{u}_c(\bar{T})$.

3.5. Data reduction

As mentioned in Section 2.3, there is a small pressure drop after each composition sample is withdrawn from the cell. The experiments at 298 and 303 K were carried out using pressure compensation after each composition sample was extracted, while no pressure compensation was done at 223 and 270 K.

For the experiments at 298 and 303 K, the cell pressure returned to its original value around 3-5 minutes after liquid or vapor sampling, after which the cell pressure was stable for the remaining 20 minutes until the next composition sample was taken. In these measurements, it was not possible to see a trend in the composition from sample to sample. Therefore, it was assumed that each composition sample represented the equilibrium composition at the pressure and temperature just before the sample was withdrawn from the cell. With respect to temperature, it has not been possible to see any variations caused by the withdrawal of a composition sample from the cell.

For the experiments at 223 and 270 K, the cell pressure decreased after each composition sample. To reach equilibrium at this new lowered pressure, the stirrer inside the cell was run for 10 minutes right after the composition sample was extracted, and then turned off to let the contents of the cell settle for the remaining 15 minutes until the next composition sample. For some of the series, instead of stirring after each sample, we waited for 2 or 3 hours to let the cell reach VLE again before a new sample was taken. The changes in composition from sample to sample were consistent with the decrease in pressure, considering the derivatives $\partial x_{\mathrm{CO}_2}/\partial p$ and $\partial y_{\mathrm{CO}_2}/\partial p$ evaluated numerically from the fitted version of EOS-CG (See Section 5.4.2). Hence, the composition of each sample withdrawn was assumed to represent the equilibrium composition at the pressure and temperature just before the composition sample was withdrawn.

For each sample, the equilibrium pressure and temperature were assumed to be represented by the pressure and temperature measurements averaged over a time period equal to 75 % of the sampling period ending just before the sample extraction starts, denoted $\bar{p}$ and $\bar{T}$, respectively. During these time periods, no systematic trends in pressure and temperature were seen.

The standard systematic uncertainty of these mean values, $\bar{u}(p)$ and $\bar{u}(T)$, were assumed to be equal to the arithmetic mean values of the standard systematic uncertainties of the p_i and T_i measurements, $u_c(p_i)$ and $u(T_i)$, used to calculate the mean pressure and temperature. $u_c(p_i)$ and $u(T_i)$ were obtained from the analysis presented in Sections Appendix A.1.4 and Appendix A.2.1, in Eqs. (A.8) and (A.16), respectively.

The standard random uncertainties of $\bar{p}$ and $\bar{T}$, $s(\bar{p})$ and $s(\bar{T})$, cannot be evaluated in the form $s/\sqrt{n}$, as the measurements used to calculate the mean values were autocorrelated. Using the approach of Box et al. [24] and Law and Kelton [25], approximate values can be obtained as

$$s(\bar{z}) \approx \frac{s(z)}{\sqrt{n}} \cdot \sqrt{\frac{n-1}{n/a-1}}\,, \tag{6}$$

where $z = p$ or T, and

$$s(z) = \sqrt{\sum_{i=1}^{n} \frac{(z_i - \bar{z})^2}{n-1}}\,, \tag{7}$$

$$a = 1 + 2\sum_{k=1}^{n-1}(1-k/n)\hat{\rho}_k\,, \tag{8}$$

$$\hat{\rho}_k = \frac{\sum_{i=1}^{n-k}(z_i - \bar{z})(z_{i+k} - \bar{z})}{\sum_{i=1}^{n}(z_i - \bar{z})^2}\,. \tag{9}$$

The combined standard uncertainty of the mean values $\bar{p}$ and $\bar{T}$ are then given as

$$\begin{aligned} u_c(\bar{p}) &= \sqrt{s^2(\bar{p}) + \bar{u}^2(p)}\,, \\ u_c(\bar{T}) &= \sqrt{s^2(\bar{T}) + \bar{u}^2(T)}\,. \end{aligned} \tag{10}$$

For each series of pressure, temperature and composition samples, the arithmetic mean values, $\bar{p}_f$, $\bar{T}_f$ and $\bar{x}_{\mathrm{CO}_2}$ or $\bar{y}_{\mathrm{CO}_2}$, were calculated. The subscript f is used to differentiate between the pressure and temperature values for each composition sample, and the mean values of the pressure and temperature for each series of samples. With $\bar{u}_c(\bar{p})$, $\bar{u}_c(\bar{T})$, $\bar{u}_{\mathrm{tot}}(x_{\mathrm{CO}_2})$ and $\bar{u}_{\mathrm{tot}}(y_{\mathrm{CO}_2})$ calculated as the means of $u_c(\bar{p})$, $u_c(\bar{T})$, $u_{\mathrm{tot}}(x_{\mathrm{CO}_2})$ and $u_{\mathrm{tot}}(y_{\mathrm{CO}_2})$ in each series, respectively, the propagation of uncertainty is calculated in the following manner:

$$u_c(\bar{p}_f) = \sqrt{s^2(\bar{p}_f) + \bar{u}_c(\bar{p})^2}\,, \tag{11}$$

$$u_c(\bar{T}_f) = \sqrt{s^2(\bar{T}_f) + \bar{u}_c(\bar{T})^2}\,, \tag{12}$$

$$u_c(\bar{x}_{\mathrm{CO}_2}) = \sqrt{s^2(\bar{x}_{\mathrm{CO}_2}) + \bar{u}_{\mathrm{tot}}(x_{\mathrm{CO}_2})^2}\,, \tag{13}$$

$$u_c(\bar{y}_{\mathrm{CO}_2}) = \sqrt{s^2(\bar{y}_{\mathrm{CO}_2}) + \bar{u}_{\mathrm{tot}}(y_{\mathrm{CO}_2})^2}\,, \tag{14}$$

with $s(\bar{p}_f)$, $s(\bar{T}_f)$, $s(\bar{x}_{\mathrm{CO}_2})$ and $s(\bar{y}_{\mathrm{CO}_2})$ calculated according to Eq. (7) divided by $\sqrt{n}$.

4. Results

VLE measurements at 223.14, 270.00, 298.17 and 303.16 K were conducted.

The existence of liquid and vapor phases was confirmed visually before the sampling of the phase compositions. Furthermore, the volumes occupied by the liquid and vapor phases inside the cell were measured visually. This visual inspection also assisted in determining the proximity to the critical point, that is, when the liquid and vapor phases for the CO_2+N_2 system become clouded due to the small density

difference of the phases, caused by critical opalescence, see e.g. [26]. The difference in the appearance of the phases as the VLE pressure was increased at 303.16 K is shown in Fig. 4, where Fig. 4a shows the appearance of the phases at a pressure relatively far from the critical point at 303.16 K, and Fig. 4b at a pressure closer to the critical point.

The pressure $\bar{p}$, temperature $\bar{T}$ and composition x_{CO_2} or y_{CO_2} for each VLE sample are given with the corresponding uncertainties in Tables B.2 and B.3. The mean pressure $\bar{p}_f$, temperature $\bar{T}_f$ and composition $\bar{x}_{CO_2}$ or $\bar{y}_{CO_2}$ and corresponding uncertainties for each series are given in Tables 4 and 5. These averaged measured data and estimated uncertainties are plotted in Figs. 7 to 10 for the temperatures 223.14, 270.00, 298.17 and 303.16 K, respectively. The measured relative volatility for the different temperatures is plotted as a function of pressure in Fig. 11.

At 223 and 270 K, the approach used to calculate the values in Tables 4 and 5 described in Section 3.5 will yield too high estimates for the sample standard deviation of the mean for the measurements, $s(\bar{p}_f)$, $s(\bar{x}_{CO_2})$ and $s(\bar{y}_{CO_2})$. The reason is that the pressure, and thereby the composition, from sample to sample changes to a new equilibrium condition. The data shown in the tables for these two temperatures should only be regarded as a summary of the data, and the more detailed values found in Tables B.2 and B.3 should be considered for further modeling work.

For the measurements at 298.17 and 303.16 K, where the bellows was used to prevent a decrease in cell pressure after sampling, the variation in the compositions of the samples was expected to be minimal. With reference to Tables 4 and 5, the maximum value of the sample standard deviation of the mean of the mole fractions in the liquid phase, $s(\bar{x}_{CO_2})$, was $3.2 \cdot 10^{-5}$, and the corresponding maximum value for the vapor phase was $9.0 \cdot 10^{-5}$. It was not possible to see any significant increasing trend in these sample standard deviations for the measurements in the critical region compared to the measurements at lower pressures.

With reference to Tables B.2 and B.3, it can be seen that the combined standard uncertainty in temperature, $u_c(\bar{T})$, was below 6 mK for all VLE measurements. The standard uncertainty in pressure, $u_c(\bar{p})$, ranged from 0.5 kPa at the lowest measured pressure around 0.68 MPa (0.07 %), to 3 kPa at 18 MPa (0.02 %). The standard uncertainty in phase mole fractions, $u_{tot}(x_{CO_2})$ and $u_{tot}(y_{CO_2})$, were for most of the samples around $2.8 \cdot 10^{-4}$. For the samples at the highest pressures at 223.14 K, the uncertainty increased to around $3.6 \cdot 10^{-4}$. Due to the proximity to the critical point, the uncertainty in pressure contributed at a greater effect to the total uncertainty in the mole fractions, as described by Eq. (A.33). This same increase in uncertainty in the mole fractions is not seen in Tables B.2 and B.3 for the VLE measurements in the critical region at 298.17 and 303.16 K, which was caused by lack of match between the fitted version of EOS-CG and the measured data in this region. The uncertainty in the mole fractions in this region should therefore be higher than what is given in Tables B.2 and B.3.

5. Analysis and discussion

5.1. Comparison with literature data

Identified literature data around the temperatures 223, 270, 298 and 303 K are plotted together with the measurement data and uncertainties of this work in Figs. 7 to 10.

The only literature data found in the vicinity of 223.14 K were the bubble and dew point measurements at 5 and 10 MPa by Weber et al. [27]. Their measurements at 5 MPa were in very good agreement with our measurements. Their measurements at 10 MPa seemed to be slightly off in composition, compared with our neighboring data points at 9.8 and 10.9 MPa.

There was very good agreement between our measurements at 270.00 K and 9.6 MPa, and the corresponding high quality data points of Brown et al. [28]. The differences were within their stated pressure and composition uncertainties.

At 298.17 K, there were very little high quality literature data. Our liquid and vapor points at 7.41 MPa and our liquid points at 8.15 MPa and the data of Yorizane et al. [29] were in good agreement, given their stated composition and pressure uncertainty. The remaining data of Yorizane et al. [29] were not in agreement with our measurements, and they predicted a higher critical point, compared to our measurements.

At 303.16 K, our data and the recent data by Fandiño et al. [30] seemed to be in good agreement up to their liquid and vapor points at 7.42 MPa. Above this pressure, their bubble point at 7.5 MPa was lower in CO_2 content than the bubble point line predicted by our data. In addition, their data contained a bubble point at 7.5717 MPa, which was 0.014 MPa higher than the maximum pressure of our bubble and dew points. Our data at the highest pressures suggested close proximity to the critical point, lower than what was suggested by the bubble point of Fandiño et al. [30]. At 303.16 K, some instability was seen in the composition of our vapor data. This was probably due to a small leakage in the nitrogen filled bellows into the VLE cell, which were later detected. However, this leakage did not explain the apparent difference in critical pressure between our measurements and those of Fandiño et al. [30]. For comparison, in our apparatus, the transition between the two-phase region into the supercritical region could visually be observed and accurately determined within approximately 0.02 MPa for the VLE measurements at 298.17 K.

There was a possibility that some of our measurements close to the critical point at 303.16 K were affected by incomplete separation of the liquid and vapor phase before sampling took place, causing the measured liquid and vapor compositions to be closer to the total composition in the cell than the actual VLE composition at the actual temperature and pressure.

5.2. Critical point estimation

For binary mixtures the critical point in terms of pressure and temperature is dependent on the composition. For a given temperature, we denote the composition, if any, where

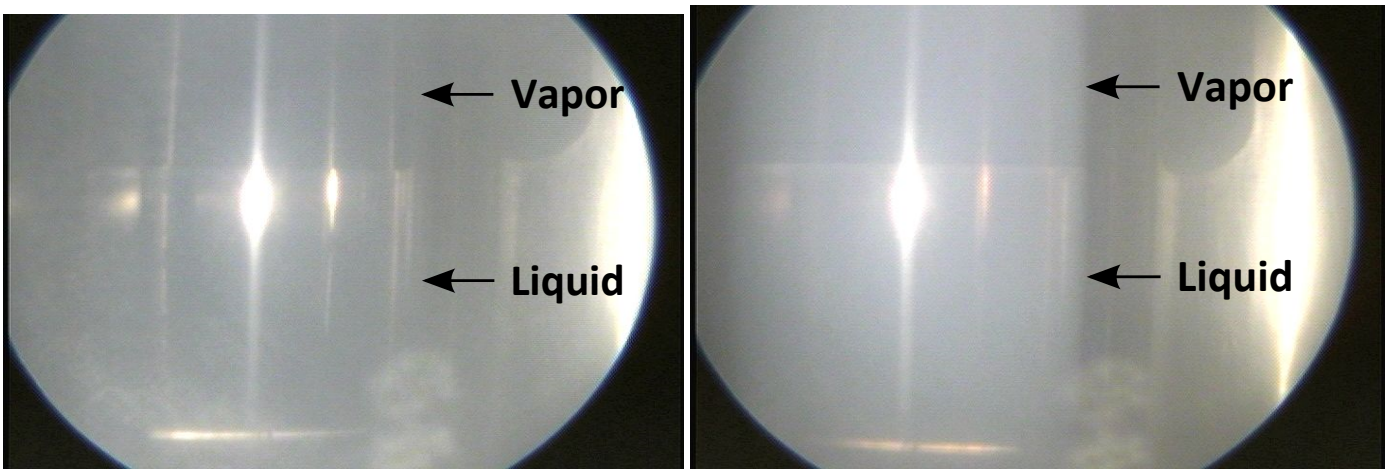

(a) Before sampling liquid point L30 at 7.4035 MPa. Far from critical point.

(b) Before sampling liquid point L34 at 7.5531 MPa. Closer to critical point, more similar density and composition in phases.

Fig. 4. Borescope pictures of liquid and vapor interface at 303.16 K for two different pressures.

the critical point is attained for the critical composition, as $z_{CO_2,c}$. The critical composition and pressure, p_c, are identified as the maximum pressure point in closed isothermal pressure-composition phase envelopes of binary mixtures, as seen in e.g. Figs. 7 to 10. For a long time, thermodynamic behavior around critical points in a range of different systems including VLE has been estimated using scaling laws from statistical mechanics [31, 32, 33]. For binary mixtures, the following scaling law can be applied [34, 35]:

$$z_{CO_2} = z_{CO_2,c} + \left(\lambda_1 + \epsilon\frac{\lambda_2}{2}\right)(p_c - p) + \epsilon\frac{\mu}{2}(p_c - p)^{\beta}, \quad \text{where,} \tag{15}$$

$$\epsilon = \begin{cases} 1 \text{ for bubble points} \\ -1 \text{ for dew points} \end{cases}$$

Here, z_{CO_2} is the boiling point $\left(z_{CO_2} = x_{CO_2}\right)$ or dew point $\left(z_{CO_2} = y_{CO_2}\right)$ CO_2 mole fraction at pressure p, p_c is the critical pressure, and $z_{CO_2,c}$ is the critical composition. β is an universal scaling exponent, which here was fixed at 0.325 [36]. The other parameters of Eq. (15) are regressed by using data close to the critical point. In this work, the fitting parameters were regressed using data reported in Tables 4 and 5 at 223.14 and 298.17 K. The regression was performed using ordinary least squares method. No weighing of data was performed. Based on the standard error of regression and estimated uncertainty of the measured data, an estimate of the uncertainties of the critical point can be found:

$$u_{z_{CO_2,c}} = \sqrt{S_E^2\left(\hat{z}_{CO_2,c}\right) + \left[\frac{1}{n_p}\sum_{i=1}^{n_p} u_c\left(\bar{x}_{i,CO_2}\right)\right]^2} \tag{16}$$

$$u_{p_c} = \sqrt{S_E^2\left(\hat{p}_c\right) + \left[\frac{1}{n_p}\sum_{i=1}^{n_p} u_c\left(\bar{p}_{i,f}\right)\right]^2} \tag{17}$$

Here $\hat{z}_{CO_2,c}$ and $\hat{p}_c$ are the regressed estimates for the critical composition and pressure based on (15) and the n_p number of data points i used in the regression. S_E are standard errors of regression coefficients, and $u_c\left(\bar{x}_{i,CO_2}\right)$ and $u_c\left(\bar{p}_{i,f}\right)$ are the estimated uncertainties of data point i taken from Tables 4 and 5. The uncertainties estimates provided in Eqs. (16)-(17) are conservative in that it was assumed that the measurement errors were systematic, but the uncertainty estimates of the critical points did not fully take into account possible model errors.

The regression parameters and the uncertainties are provided in Table 6, and the fits, critical points and data points used are shown in Fig. 5. The critical points are also included in Figs. 7 and 9 together with the other data and equations of state to be discussed in the following. The scaling law of Eq. (15) appeared to provide an adequate fit of the data of this work around the critical region. The estimated uncertainties of the critical mole fraction area were around 10^{-3} at 223.14 K and $4{\cdot}10^{-4}$ at 298.17 K, whereas the corresponding estimated relative uncertainties in pressure were 0.05 and 0.02 %, respectively. The pressure measurement uncertainty was a significant contributor to the critical point estimate uncertainty at 223.14 K. As discussed in Section 4, the uncertainty estimates for the data at 223.14 K without pressure compensation were probably exaggerated. In Fig. 5b, also some supercritical data points are included, which were outside the estimated uncertainty bounds of the critical point at 298.17 K. Also the measurement points not used in the regression included in Fig. 5a seemed to confirm that the scaling law was suitable for our measurements.

5.3. Comparison to EOS-CG

In the development of EOS-CG, the parameters and mixture model used by Gernert and Span [1] and Gernert [2] for the description of CO_2+N_2, were the same as in the GERG-2008 EOS [7].

Table 4
Experimental VLE data for CO_2 (1) + N_2 (2) at mean temperature $\bar{T}_f$, mean pressure $\bar{p}_f$, and mean liquid phase mole fraction $\bar{x}_{CO_2}$ [a].

ID	Data			Temperature			Pressure			Composition			
	$\bar{T}_f$ (K)	$\bar{p}_f$ (MPa)	$\bar{x}_{CO_2}$ (-)	$s(\bar{T}_f)$ (K)	$\bar{u}_c(\bar{T})$ (K)	$u_c(\bar{T}_f)$ (K)	$s(\bar{p}_f)$ (MPa)	$\bar{u}_c(\bar{p})$ (MPa)	$u_c(\bar{p}_f)$ (MPa)	$s(\bar{x}_{CO_2})$ (-)	$\bar{u}_{tot}(x_{CO_2})$ (-)	$u_c(\bar{x}_{CO_2})$ (-)	$x_{CO_2,calc}$ (-)
P1	223.138	0.6829[1]	0.99999	5.3e-5	2.5e-3	2.5e-3	2.5e-6	5.0e-4	5.0e-4				
L1	223.140	1.9354	0.98156	4.5e-5	2.4e-3	2.4e-3	4.4e-5	5.2e-4	5.2e-4	9.3e-6	2.7e-4	2.7e-4	0.98346
L2	223.138	4.3468	0.94422	1.1e-4	2.6e-3	2.6e-3	2.5e-4	1.1e-3	1.1e-3	4.2e-6	2.7e-4	2.7e-4	0.94892
L3	223.139	5.0287	0.93314	1.4e-4	3.4e-3	3.4e-3	6.2e-4	1.1e-3	1.3e-3	8.0e-6	2.7e-4	2.7e-4	0.93846
L4	223.143	6.0976	0.91557	1.7e-4	5.5e-3	5.5e-3	7.8e-4	1.1e-3	1.4e-3	1.0e-5	2.7e-4	2.7e-4	0.92134
L5	223.141	6.9979	0.90041	7.6e-5	5.4e-3	5.4e-3	1.1e-3	1.1e-3	1.6e-3	2.1e-5	2.7e-4	2.7e-4	0.90618
L6	223.139	8.1151	0.88108	1.9e-4	5.0e-3	5.0e-3	1.0e-3	1.2e-3	1.6e-3	1.1e-5	2.7e-4	2.7e-4	0.88632
L7	223.140	8.7815	0.86908	6.5e-5	3.3e-3	3.3e-3	2.1e-3	1.3e-3	2.5e-3	4.4e-5	2.7e-4	2.8e-4	0.87386
L8	223.140	9.2232	0.86112	2.6e-4	6.0e-3	6.0e-3	1.8e-3	1.4e-3	2.2e-3	3.3e-5	2.7e-4	2.8e-4	0.86532
L9	223.141	9.8292	0.85043	6.2e-5	5.2e-3	5.2e-3	3.0e-3	2.7e-3	4.0e-3	1.2e-5	2.8e-4	2.8e-4	0.85322
L10	223.140	10.8430	0.82974	5.8e-5	3.6e-3	3.6e-3	3.3e-3	2.7e-3	4.3e-3	4.6e-5	2.8e-4	2.8e-4	0.83187
L11	223.142	10.8779	0.82920	7.6e-5	5.4e-3	5.4e-3	2.7e-3	2.7e-3	3.8e-3	5.4e-5	2.8e-4	2.8e-4	0.83111
L12	223.143	12.0106	0.80546	8.9e-5	5.5e-3	5.5e-3	4.2e-3	2.7e-3	5.0e-3	8.4e-5	2.8e-4	2.9e-4	0.80527
L13	223.138	14.9228	0.73343	1.8e-4	3.0e-3	3.0e-3	5.8e-3	2.8e-3	6.4e-3	1.6e-4	2.9e-4	3.3e-4	0.72553
L14	223.140	15.9554	0.70046	7.6e-5	2.9e-3	2.9e-3	6.9e-3	2.8e-3	7.5e-3	2.5e-4	2.9e-4	3.8e-4	0.68981
L15	223.137	17.1911	0.64879	1.6e-4	2.8e-3	2.8e-3	8.0e-3	2.8e-3	8.4e-3	4.2e-4	3.1e-4	5.2e-4	0.63665
L16	223.139	18.1560	0.57419	1.1e-4	2.7e-3	2.7e-3	8.4e-3	2.8e-3	8.8e-3	1.2e-3	3.5e-4	1.3e-3	0.57689
L17	269.996	9.5824	0.86046	1.2e-4	5.7e-3	5.7e-3	2.2e-3	1.4e-3	2.6e-3	5.1e-5	2.8e-4	2.8e-4	0.85932
P2	298.174	6.4369[2]	0.99999	1.9e-5	1.6e-3	1.6e-3	8.0e-6	1.2e-3	1.2e-3				
L18	298.158	6.7090	0.99359	2.2e-4	1.5e-3	1.5e-3	1.1e-4	1.1e-3	1.1e-3	2.7e-6	2.7e-4	2.7e-4	0.99371
L19	298.160	6.7192	0.99334	5.5e-5	1.4e-3	1.4e-3	5.0e-5	1.1e-3	1.1e-3	3.7e-6	2.7e-4	2.7e-4	0.99347
L20	298.161	7.1003	0.98384	3.6e-4	1.6e-3	1.6e-3	1.0e-4	1.1e-3	1.1e-3	9.9e-7	2.7e-4	2.7e-4	0.98411
L21	298.162	7.4191	0.97525	1.6e-4	1.5e-3	1.5e-3	1.7e-4	1.2e-3	1.2e-3	3.0e-6	2.7e-4	2.7e-4	0.97557
L22	298.175	7.8946	0.96050	4.3e-4	1.5e-3	1.5e-3	3.0e-4	1.2e-3	1.2e-3	3.7e-6	2.8e-4	2.8e-4	0.96091
L23	298.174	8.0782	0.95344	1.2e-4	1.6e-3	1.6e-3	3.0e-5	1.2e-3	1.2e-3	4.8e-6	2.8e-4	2.8e-4	0.95412
L24	298.171	8.1479	0.95029	1.5e-4	1.4e-3	1.4e-3	2.2e-4	1.2e-3	1.3e-3	1.1e-5	2.8e-4	2.8e-4	0.95126
L25	298.173	8.1544	0.94976	2.5e-4	1.5e-3	1.5e-3	4.0e-4	1.2e-3	1.3e-3	2.3e-6	2.8e-4	2.8e-4	0.95099
L26	298.174	8.2531	0.94359	3.6e-4	1.5e-3	1.5e-3	3.1e-4	1.2e-3	1.2e-3	3.2e-5	2.8e-4	2.8e-4	0.94654
L27	298.174	8.2743	0.94155	4.4e-4	1.5e-3	1.6e-3	1.4e-4	1.3e-3	1.3e-3	1.8e-5	2.8e-4	2.8e-4	0.94551
L28	298.174	8.2862	0.94041	2.8e-4	1.5e-3	1.5e-3	1.5e-5	1.3e-3	1.3e-3	6.4e-6	2.8e-4	2.8e-4	0.94492
L29	298.176	8.2971	0.93797	2.0e-5	1.6e-3	1.6e-3	1.8e-4	1.2e-3	1.2e-3	2.0e-5	2.8e-4	2.8e-4	0.94437
P3	303.158	7.2105[3]	0.99999	9.5e-6	2.0e-3	2.0e-3	3.0e-5	1.1e-3	1.1e-3				
L30	303.156	7.4035	0.99450	5.0e-4	1.9e-3	2.0e-3	3.0e-5	1.1e-3	1.1e-3	1.4e-6	2.7e-4	2.7e-4	0.99457
L31	303.155	7.5216	0.99044	3.0e-4	1.7e-3	1.7e-3	3.2e-5	1.1e-3	1.1e-3	1.2e-6	2.8e-4	2.8e-4	0.99078
L32	303.157	7.5345	0.98985	3.1e-5	1.7e-3	1.7e-3	4.3e-5	1.1e-3	1.1e-3	3.3e-6	2.8e-4	2.8e-4	0.99035
L33	303.157	7.5452	0.98928	8.9e-5	1.7e-3	1.7e-3	2.8e-5	1.2e-3	1.2e-3	5.1e-6	2.8e-4	2.8e-4	0.98997
L34	303.157	7.5531	0.98883	5.8e-5	1.8e-3	1.8e-3	2.5e-5	1.2e-3	1.2e-3	2.0e-6	2.8e-4	2.8e-4	0.98969
L35	303.157	7.5539	0.98894	5.2e-5	1.7e-3	1.7e-3	6.7e-5	1.1e-3	1.1e-3	1.8e-6	2.8e-4	2.8e-4	0.98966
L36	303.157	7.5575	0.98840	1.7e-4	1.7e-3	1.7e-3	4.6e-5	1.1e-3	1.1e-3	5.2e-6	2.8e-4	2.8e-4	0.98954

[a] Sample standard deviation of the mean of the temperatures $s(\bar{T}_f)$, mean of the standard systematic uncertainty of the temperatures $\bar{u}_c(\bar{T})$, total standard uncertainty of the temperature $u_c(\bar{T}_f)$, sample standard deviation of the mean of the pressures $s(\bar{p}_f)$, mean of the standard systematic uncertainty of the pressures $\bar{u}_c(\bar{p})$, total standard uncertainty of the pressure $u_c(\bar{p}_f)$, sample standard deviation of the mean of the mole fractions $s(\bar{x}_{CO_2})$, mean of the total standard uncertainty of the mole fractions $\bar{u}_{tot}(x_{CO_2})$, total standard uncertainty of the mole fraction $u_c(\bar{x}_{CO_2})$, fitted EOS-CG calculated mole fraction $x_{CO_2,calc}(\bar{T}_f, \bar{p}_f)$ [1] Span-Wagner CO_2 vapor pressure is 0.6820 ± 0.0002 MPa; [2] Span-Wagner CO_2 vapor pressure is 6.4379 ± 0.0019 MPa; [3] Span-Wagner CO_2 vapor pressure is 7.2149 ± 0.0021 MPa;

At present, EOS-CG (or GERG-2008) gives the best prediction of the VLE of the CO_2+N_2 system. On this basis, it was of interest to determine how well our data agreed with EOS-CG.

The VLE predictions of EOS-CG using the original parameters [1, 2] are shown with the measurement data and uncertainty estimates of the current work in Figs. 7 to 10. The relative volatility of the new data and EOS-CG can be compared in Fig. 11.

At 223.14 K, our data showed very good agreement with EOS-CG up to pressures of 12 MPa. Above this pressure, the estimate for the critical point from Section 5.2 was $\hat{p}_c$ = 18.26 MPa and $\hat{z}_{CO_2,c}$ = 0.4880, while EOS-CG with original parameters indicated $\hat{p}_c$ =19.88 MPa and $\hat{z}_{CO_2,c}$ = 0.479. Hence, it seemed like EOS-CG overpredicted the critical pressure at this temperature by about 1.6 MPa. The deviations between our data and the model were in this region order of magnitudes larger than the estimated uncertainties of our data and critical point estimate.

According to the literature data review of Gernert and Span [1] and Gernert [2], there were no VLE literature data in the critical region at temperatures below the data provided by Al-Sahhaf et al. [37] at 240 K. There were, however, some phase boundary measurements in the temperature region 208 to 240 K with CO_2 mole fractions from 0.4 to 0.5, in the works by Esper [38], [39] and Duarte-Garza et al.

Table 5
Experimental VLE data for CO_2 (1) + N_2 (2) at mean temperature $\bar{T}_f$, mean pressure $\bar{p}_f$, and mean vapor phase mole fraction $\bar{y}_{CO_2}$ [a].

ID	Data			Temperature			Pressure			Composition			
	$\bar{T}_f$ (K)	$\bar{p}_f$ (MPa)	$\bar{y}_{CO_2}$ (-)	$s(\bar{T}_f)$ (K)	$\bar{u}_c(\bar{T})$ (K)	$u_c(\bar{T}_f)$ (K)	$s(\bar{p}_f)$ (MPa)	$\bar{u}_c(\bar{p})$ (MPa)	$u_c(\bar{p}_f)$ (MPa)	$s(\bar{y}_{CO_2})$ (-)	$\bar{u}_{tot}(y_{CO_2})$ (-)	$u_c(\bar{y}_{CO_2})$ (-)	$y_{CO_2,calc}$ (-)
P1	223.138	0.6829[1]	0.99999	5.3e-5	2.5e-3	2.5e-3	2.5e-6	5.0e-4	5.0e-4				
V1	223.139	1.9383	0.40700	1.1e-4	2.6e-3	2.6e-3	3.6e-4	5.2e-4	6.3e-4	1.2e-4	2.9e-4	3.1e-4	0.41050
V2	223.139	4.3535	0.23253	8.2e-5	2.5e-3	2.5e-3	1.2e-3	1.1e-3	1.6e-3	3.8e-5	2.8e-4	2.8e-4	0.23398
V3	223.139	4.3652	0.23239	1.8e-4	2.5e-3	2.5e-3	1.1e-3	1.1e-3	1.5e-3	6.9e-5	2.8e-4	2.8e-4	0.23364
V4	223.139	5.0378	0.21785	1.2e-4	3.4e-3	3.4e-3	1.0e-3	1.1e-3	1.5e-3	4.8e-5	2.7e-4	2.8e-4	0.21745
V5	223.141	6.0853	0.20174	8.5e-5	5.1e-3	5.1e-3	1.8e-3	1.1e-3	2.1e-3	4.7e-5	2.7e-4	2.8e-4	0.20185
V6	223.139	7.0097	0.19326	1.3e-4	4.9e-3	4.9e-3	1.6e-3	1.6e-3	2.2e-3	9.8e-5	2.7e-4	2.9e-4	0.19449
V7	223.141	8.0989	0.18971	1.2e-4	5.7e-3	5.7e-3	1.5e-3	1.2e-3	2.0e-3	6.6e-5	2.7e-4	2.8e-4	0.19118
V8	223.141	8.4403	0.18981	1.7e-4	3.6e-3	3.6e-3	1.7e-3	1.3e-3	2.1e-3	1.1e-5	2.7e-4	2.7e-4	0.19110
V9	223.142	8.6079	0.18980	4.4e-4	4.2e-3	4.2e-3	1.5e-3	1.3e-3	2.0e-3	5.7e-5	2.7e-4	2.8e-4	0.19122
V10	223.140	9.1920	0.19069	2.8e-4	5.4e-3	5.4e-3	1.3e-3	1.4e-3	1.9e-3	3.8e-5	2.7e-4	2.8e-4	0.19234
V11	223.141	9.8050	0.19283	6.6e-5	5.2e-3	5.2e-3	2.0e-3	2.6e-3	3.3e-3	6.9e-5	2.7e-4	2.8e-4	0.19470
V12	223.139	10.8694	0.19990	2.4e-4	3.2e-3	3.2e-3	1.9e-3	2.7e-3	3.3e-3	1.0e-4	2.7e-4	2.9e-4	0.20150
V13	223.141	11.9787	0.20881	3.5e-4	5.0e-3	5.0e-3	2.5e-3	2.7e-3	3.7e-3	9.6e-5	2.8e-4	2.9e-4	0.21230
V14	223.138	14.9699	0.25683	3.6e-4	3.0e-3	3.0e-3	3.3e-3	2.8e-3	4.3e-3	2.6e-4	2.8e-4	3.8e-4	0.26333
V15	223.138	16.0098	0.28507	1.1e-4	2.8e-3	2.8e-3	3.5e-3	2.8e-3	4.5e-3	1.6e-4	2.9e-4	3.3e-4	0.29132
V16	223.139	17.2510	0.33148	1.6e-4	2.9e-3	2.9e-3	3.3e-3	2.8e-3	4.3e-3	1.6e-4	3.0e-4	3.4e-4	0.33698
V17	223.138	18.2173	0.41480	5.8e-5	2.7e-3	2.7e-3	3.3e-3	2.8e-3	4.3e-3	6.1e-4	3.6e-4	7.1e-4	0.39381
V18	269.997	9.5571	0.58169	7.3e-5	4.8e-3	4.8e-3	4.5e-3	1.4e-3	4.8e-3	2.5e-4	2.8e-4	3.8e-4	0.58466
V19	269.996	9.5839	0.58095	1.1e-4	6.0e-3	6.0e-3	2.6e-3	1.4e-3	2.9e-3	2.3e-4	2.8e-4	3.6e-4	0.58453
P2	298.174	6.4369[2]	0.99999	1.9e-5	1.6e-3	1.6e-3	8.0e-6	1.2e-3	1.2e-3				
V20	298.159	6.7088	0.98174	2.2e-5	1.5e-3	1.5e-3	4.2e-5	1.1e-3	1.1e-3	9.0e-5	2.8e-4	3.0e-4	0.98181
V21	298.158	6.7194	0.98097	8.7e-5	1.5e-3	1.5e-3	1.3e-4	1.1e-3	1.1e-3	6.8e-6	2.8e-4	2.8e-4	0.98113
V22	298.162	7.0988	0.95952	5.3e-6	1.5e-3	1.5e-3	2.4e-5	1.2e-3	1.2e-3	1.5e-5	2.8e-4	2.8e-4	0.95949
V23	298.161	7.4163	0.94435	6.9e-5	1.4e-3	1.4e-3	1.0e-4	1.1e-3	1.1e-3	5.6e-5	2.8e-4	2.8e-4	0.94439
V24	298.163	7.4175	0.94434	1.1e-4	1.5e-3	1.5e-3	2.9e-4	1.1e-3	1.2e-3	3.8e-5	2.8e-4	2.8e-4	0.94435
V25	298.175	7.8935	0.92792	1.5e-5	1.5e-3	1.5e-3	1.5e-4	1.2e-3	1.2e-3	2.3e-5	2.8e-4	2.8e-4	0.92736
V26	298.174	8.0724	0.92467	7.7e-5	1.6e-3	1.6e-3	3.0e-4	1.2e-3	1.2e-3	3.9e-5	2.7e-4	2.8e-4	0.92293
V27	298.169	8.1434	0.92461	3.0e-4	1.4e-3	1.5e-3	8.1e-5	1.2e-3	1.2e-3	5.2e-5	2.7e-4	2.8e-4	0.92153
V28	298.173	8.2526	0.92610	7.3e-5	1.5e-3	1.5e-3	1.4e-4	1.2e-3	1.2e-3	4.2e-5	2.7e-4	2.8e-4	0.92011
V29	298.174	8.2721	0.92694	8.9e-5	1.5e-3	1.5e-3	8.8e-5	1.2e-3	1.2e-3	8.4e-5	2.7e-4	2.9e-4	0.91995
V30	298.175	8.2862	0.92730	1.2e-5	1.5e-3	1.5e-3	1.0e-4	1.3e-3	1.3e-3	4.6e-5	2.7e-4	2.8e-4	0.91988
V31	298.175	8.2972	0.93025	3.6e-4	1.6e-3	1.7e-3	7.6e-5	1.2e-3	1.2e-3	3.4e-5	2.7e-4	2.8e-4	0.91982
P3	303.158	7.2105[3]	0.99999	9.5e-6	2.0e-3	2.0e-3	3.0e-5	1.1e-3	1.1e-3				
V32	303.157	7.4007	0.99154	2.7e-4	2.0e-3	2.0e-3	1.7e-5	1.2e-3	1.2e-3	1.4e-5	2.8e-4	2.8e-4	0.99157
V33	303.157	7.4672	0.98904	2.4e-4	2.0e-3	2.0e-3	5.5e-5	1.1e-3	1.1e-3	2.6e-5	2.8e-4	2.8e-4	0.98888
V34	303.158	7.5217	0.98695	1.8e-5	1.7e-3	1.7e-3	7.9e-5	1.1e-3	1.1e-3	1.5e-5	2.8e-4	2.8e-4	0.98682
V35	303.158	7.5350	0.98699	3.5e-5	1.8e-3	1.8e-3	5.7e-5	1.2e-3	1.2e-3	9.4e-6	2.8e-4	2.8e-4	0.98635
V36	303.158	7.5450	0.98683	2.0e-5	1.7e-3	1.7e-3	2.1e-5	1.2e-3	1.2e-3	2.3e-5	2.8e-4	2.8e-4	0.98600
V37	303.158	7.5532	0.98681	2.4e-4	1.8e-3	1.8e-3	1.1e-4	1.2e-3	1.2e-3	6.6e-5	2.8e-4	2.8e-4	0.98571
V38	303.158	7.5540	0.98662	3.2e-5	1.8e-3	1.8e-3	6.2e-5	1.1e-3	1.1e-3	1.6e-5	2.8e-4	2.8e-4	0.98568
V39	303.157	7.5543	0.98641	1.0e-4	1.7e-3	1.7e-3	1.9e-5	1.1e-3	1.1e-3	1.1e-5	2.8e-4	2.8e-4	0.98571
V40	303.158	7.5574	0.98708	2.3e-5	1.7e-3	1.7e-3	6.2e-5	1.1e-3	1.1e-3	8.2e-6	2.8e-4	2.8e-4	0.98568

[a] Sample standard deviation of the mean of the temperatures $s(\bar{T}_f)$, mean of the standard systematic uncertainty of the temperatures $\bar{u}_c(\bar{T})$, total standard uncertainty of the temperature $u_c(\bar{T}_f)$, sample standard deviation of the mean of the pressures $s(\bar{p}_f)$, mean of the standard systematic uncertainty of the pressures $\bar{u}_c(\bar{p})$, total standard uncertainty of the pressure $u_c(\bar{p}_f)$, sample standard deviation of the mean of the mole fractions $s(\bar{y}_{CO_2})$, mean of the total standard uncertainty of the mole fractions $\bar{u}_{tot}(y_{CO_2})$, total standard uncertainty of the mole fraction $u_c(\bar{y}_{CO_2})$, fitted EOS-CG calculated mole fraction $y_{CO_2,calc}(\bar{T}_f, \bar{p}_f)$ [1] Span-Wagner CO_2 vapor pressure is 0.6820 ± 0.0002 MPa; [2] Span-Wagner CO_2 vapor pressure is 6.4379 ± 0.0019 MPa; [3] Span-Wagner CO_2 vapor pressure is 7.2149 ± 0.0021 MPa;

[40]. As Gernert and Span [1] and Gernert [2] noted, these phase boundary measurements indicated that EOS-CG overpredicted the critical pressure at these lower temperatures, which was in accordance with our measurements.

Both at 298.17 and 303.16 K, our data indicated a critical point at lower pressures and higher total CO_2 compositions than EOS-CG.

At 298.17 K, EOS-CG indicated a critical point at approximately $\hat{p}_c = 8.449$ MPa and $\hat{z}_{CO_2,c} = 0.9286$, while the estimation of the critical point from Section 5.2 was $\hat{p}_c = 8.295$ MPa and $\hat{z}_{CO_2,c} = 0.9342$. Hence, the new data indicated that EOS-CG overpredicts the critical pressure by approximately 0.15 MPa.

At 303.16 K, the critical point indicated by EOS-CG was approximately $\hat{p}_c = 7.665$ MPa and $\hat{z}_{CO_2,c} = 0.9834$, while the data of this work indicated $\hat{p}_c = 7.558$ MPa and $\hat{z}_{CO_2,c} = 0.9877$. Based on this comparison, EOS-CG overpredicts the critical pressure by approximately 0.11 MPa.

Overall, EOS-CG seems to predict higher critical pressures than indicated by our data.

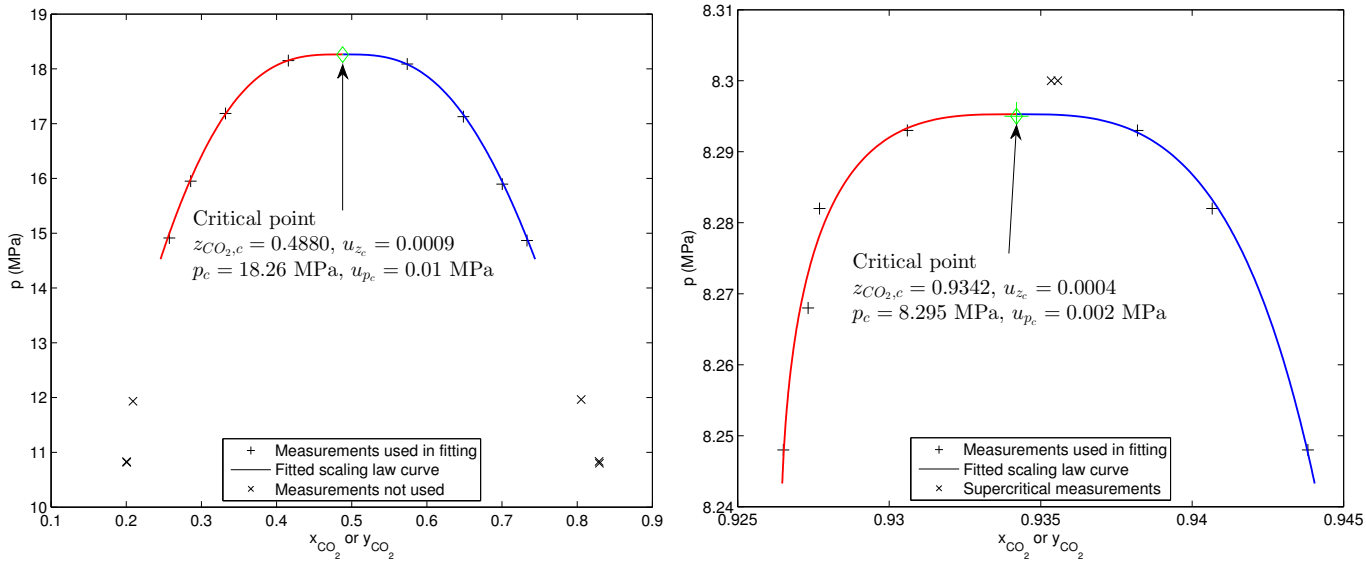

(a) 223.14 K **(b)** 298.17 K

Fig. 5. Estimation of phase behavior around the critical point by regression analysis of scaling law in Eq. (15). Note that that the scales are very different in the two graphs.

5.4. Model fitting

5.4.1. Introduction

The parameters of two different equations of state were fitted against the experimental data. First, EOS-CG [1, 2] was fitted to obtain the best possible description of the critical region. Second, the Peng-Robinson (PR) cubic EOS [41] with the alpha correction by Mathias and Copeman [42] (MC), the mixing rules by Wong and Sandler [43] (WS) and the NRTL [44] excess Gibbs energy model, were chosen. This combination of EOS, alpha correction, mixing rule and excess Gibbs energy model, designated here as PR-MC-WS-NRTL, has previously been used with some success to fit VLE data of the CO_2-Ar system [45], for instance with regard to the critical region at a certain temperature. This EOS is computationally less time-consuming than EOS-CG.

The phase equilibrium calculations were performed by solving the equation of state using the equilibrium condition, expressed as an equality of the fugacities of each component, $i = \mathrm{CO_2}, \mathrm{N_2}$, in the liquid and vapor phase [46]:

$$f_{i,\mathrm{L}}(T,p,x_i) = f_{i,\mathrm{V}}(T,p,y_i)\,. \tag{18}$$

The solution of this equation was performed using an in-house software.

The model fit was performed using orthogonal distance regression (ODR), which in our case consisted of minimizing an objective function with weighting of the error between data and model prediction in both composition $x_{\mathrm{CO_2}}$ and $y_{\mathrm{CO_2}}$, and in pressure $\bar{p}$, at a fixed temperature. The Python$^{\mathrm{TM}}$ implementation of NIST's ODRPACK [47] was used to perform the regression. With $z_{\mathrm{CO_2}}$ equal to $x_{\mathrm{CO_2}}$ or $y_{\mathrm{CO_2}}$,

Table 6
Regressed parameters of scaling law in Eq. (15) in this work and other parameters relevant for fit.

Symbol	Unit	T=223.14 K	T=298.17 K
n_p		8	7
$\hat{\lambda}_1(T)$	(MPa^{-1})	$1.8247{\cdot}10^{-3}$	0.020517
$\hat{\lambda}_2(T)$	(MPa^{-1})	0.012694	-0.075047
$\hat{\mu}(T)$	($\mathrm{MPa}^{-\beta}$)	0.29375	0.056131
$\hat{z}_{\mathrm{CO_2},c}(T)$		0.4880	0.9342
$\hat{p}_c(T)$	(MPa)	18.26	8.295
$s_{z_{\mathrm{CO_2},c}}$		0.0008	0.0002
$u_{z_{\mathrm{CO_2},c}}$		0.0009	0.0004
s_{p_c}	(MPa)	0.008	0.001
u_{p_c}	(MPa)	0.01	0.002

the objective function S minimized can be stated as:

$$S^2 = \frac{1}{n-n_\mathrm{p}} \sum_i \left(\frac{p_{i,\mathrm{calc}} - \bar{p}_i}{u_\mathrm{c}(\bar{p}_i)} \right)^2 + \frac{1}{n-n_\mathrm{p}} \sum_i \left(\frac{z_{i,\mathrm{CO_2,calc}} - z_{i,\mathrm{CO_2}}}{u(z_{i,\mathrm{CO_2}})} \right)^2 , \quad (19)$$

where n is the total number of experimental data points, and n_p is the number of parameters adjusted in the model fit.

It should be noted that by using Eq. (19), the data are only weighted according to their estimated uncertainty. Hence, more weight was put on regions with higher number of data points, which may skew the model since we are using an incomplete set of data. For the present purpose of interpreting the data, this simple approach was deemed sufficient.

In addition to the value of the objective function S, two statistics were used to describe the agreement between model and data, the absolute average deviation (AAD) and the bias (BIAS):

$$\mathrm{AAD} = \frac{100}{n} \sum_i \left| z_{i,\mathrm{CO_2}} - z_{i,\mathrm{CO_2,calc}} \right| , \quad (20)$$

and

$$\mathrm{BIAS} = \frac{100}{n} \sum_i \left(z_{i,\mathrm{CO_2}} - z_{i,\mathrm{CO_2,calc}} \right) . \quad (21)$$

The fitted models were compared with a selection of some of the high quality VLE data from the literature. An overview of these data is given in Table 8.

5.4.2. EOS-CG VLE

For EOS-CG [1, 2], two parameters in the reducing function for temperature in EOS-CG for CO_2 (1) + N_2 (2), $\beta_{T,12}$ and $\gamma_{T,12}$, were fitted. These two parameters were chosen for fitting as their main influence is on the shape of the VLE two-phase region, which is what we wanted to adjust to our data. The three remaining parameters in the reducing functions, and the 34 parameters of the departure function, were kept at the values given in [1, 2]. For details about these parameters and the structure of the EOS, see Gernert and Span [1] and Gernert [2].

The binary parameters for the reducing function for temperature in EOS-CG for CO_2 (1) + N_2 (2), $\beta_{T,12}$ and $\gamma_{T,12}$, were fitted against our VLE pressure, temperature and composition data for the temperatures 223.14, 298.17 and 303.16 K in Tables 4 and 5.

The fitted parameters of EOS-CG are shown in Table 7 together with the original parameter set from [1, 2, 7]. The values of the objective function S in Eq. (19) are also shown.

The VLE predictions of EOS-CG using the fitted parameters from Table 7 are shown in Figs. 7 to 10 together with relevant data and the uncertainty estimates of this work. The relative volatilities calculated from the fitted EOS-CG and the new data can be compared in Fig. 11.

The objective function value S decreased significantly by fitting the parameters, and it can be seen that the fitted model matched much better with our data in the critical region at 223.14 K than the original model, without causing significantly larger deviations at lower pressures. However, at 298.17 and 303.16 K, the fitted model matched slightly worse with our data in the critical region than the original model. This development can also be seen from the objective function values calculated for each temperature, shown in Table 8. The S value at 223.14 K decreases significantly, at expense of the slight increase in the S values at 298.17 and 303.16 K. This was probably caused by the inadequacy of the weighting of the model deviations in the objective function at the different temperatures, as mentioned in Section 5.4.1.

Table 7
Original and fitted parameters and objective function S value (Eq. (19)) for VLE calculation for CO_2 (1) + N_2 (2) in EOS-CG, valid for $T \in [223.15, 303.16]$ K.

	Original	Fitted
$\beta_{T,12}$	0.994140013	1.000800075
$\gamma_{T,12}$	1.107654104	1.110649656
$\beta_{v,12}$	1.022709642	
$\gamma_{v,12}$	1.047578256	
F_{12}	1	
S	36	14

Fig. 12a shows the deviations between our measured CO_2 mole fractions and those calculated by both the original and fitted version of EOS-CG at the same temperatures and pressures.

Fig. 13 shows the VLE predictions of the original and fitted model at a selection of temperatures different than those measured at in the present work. These temperatures were chosen on the basis of a selection of literature data used in the model fitting in Section 5.4.3, and an overview of the literature data is shown in Table 8.

With reference to these figures, it can be seen that the fitted model lowers the critical pressure significantly at the lower temperatures 218 to approximately 258 K, compared to the original model. At temperatures above this, the critical pressure started to shift from decrease to a slight increase. The critical composition changed very little compared to the original version of EOS-CG.

Fig. 12b shows the deviations between the measured CO_2 mole fractions in the literature data in Table 8 and those calculated by both the original and fitted version of EOS-CG at the same temperatures and pressures.

The figure shows that the fitted version of EOS-CG matched better than the original EOS-CG the data in the critical region at 240.00 K by Al-Sahhaf et al. [37] and at 243.15 K by Fandiño et al. [30]. For the remaining literature data, the fitted version of EOS-CG matches better than the original version of EOS-CG in some temperature regions, and somewhat worse at other temperatures. This is indicated by the AAD, BIAS and S values found in Table 8.

The fitted version of EOS-CG presented here, indicated a possibility to improve the description of the VLE in the critical region by EOS-CG. Only the VLE data measured at 223.15, 298.15 and 303.15 K in the present work was used

to perform the fit. Therefore, the model with the fitted parameters cannot be used to calculate other properties for the CO_2+N_2 binary system, such as density, heat capacity and others. For this, a complete new fit of the parameters is necessary, including the data for these properties, as well.

5.4.3. Peng-Robinson EOS

The alpha correction by Mathias and Copeman is given as [42]

$$\alpha_i(T) = \begin{cases} \left(1 + c_{1,i}h(T) + c_{2,i}h^2(T) + c_{3,i}h^3(T)\right)^2 & \text{if } T < T_{c,i}\,, \\ \left(1 + c_{1,i}h(T)\right)^2 & \text{if } T \geq T_{c,i}\,, \end{cases}$$
$$h(T) = 1 - \sqrt{T/T_{c,i}}\,, \qquad (22)$$

where $i = CO_2$ or N_2. The values for $c_{1,i}$, $c_{2,i}$, $c_{1,i}$, and the critical temperatures $T_{c,i}$ and pressures $p_{c,i}$, are given in Table 9.

The mixing rule by Wong and Sandler (WS) is given as [43]

$$b_m = \frac{\sum_i \sum_j x_i x_j \left(b - \frac{a}{RT}\right)_{ij}}{1 - \frac{A^E_\infty}{CRT} - \sum_i x_i \left(\frac{a_i}{b_i RT}\right)}\,, \qquad (23)$$

$$a_m = b_m RT - RT \sum_i \sum_j x_i x_j \left(b - \frac{a}{RT}\right)_{ij}\,, \qquad (24)$$

where a_m and b_m are the mixture parameters, and a_i and b_i are the pure component parameters, of the Peng-Robinson EOS. The cross second virial coefficient is given by [43]

$$\left(b - \frac{a}{RT}\right)_{ij} = \frac{\left(b_i - \frac{a_i}{RT}\right) + \left(b_j - \frac{a_j}{RT}\right)}{2}\left(1 - k_{ij}\right)\,, \qquad (25)$$

where k_{ij} is the Wong-Sandler binary interaction parameter.

The molar excess Helmholtz energy, A^E_∞, is modeled in the present work using the NRTL model [43]

$$\frac{A^E_\infty}{RT} = \sum_i x_i \left(\frac{\sum_j x_j \tau_{ji} \exp\left(-\alpha_{ji}\tau_{ji}\right)}{\sum_k x_k \exp\left(-\alpha_{ki}\tau_{ki}\right)}\right)\,, \qquad (26)$$

where α_{ij} are the non-randomness parameters and τ_{ij} are the binary interaction parameters of the NRTL model.

The following restrictions are put on the parameters:

$$\begin{aligned} k_{ij} &= k_{ji}\,, & k_{ii} &= 0\,, \\ \alpha_{ij} &= \alpha_{ji}\,, & \alpha_{ii} &= 0\,, \\ \tau_{ij} &\neq \tau_{ji}\,, & \tau_{ii} &= 0\,. \end{aligned} \qquad (27)$$

As in the work by Coquelet et al. [45], we have assumed a constant value for $\alpha_{12} = \alpha_{21} = 0.3$, based on the suggestions by Renon and Prausnitz [44] for a system of two non-polar components. This leaves 3 adjustable parameters in the PR-MC-WS-NRTL model: k_{12}, τ_{12} and τ_{21}. These parameters are assumed to be temperature dependent.

With temperature dependent parameters, it is of interest to fit the parameters to data at different temperatures, and try to determine a model for the temperature dependence of the parameters, enabling the use of the EOS at temperatures over the whole temperature range of the data.

To ensure some form of temperature dependency in the parameters, it was chosen to only perform parameter fitting for temperatures where measurements existed in the whole range from the vapor pressure of CO_2 up to the critical region. Our data contained measurements covering this region for the three temperatures 223, 298 and 303 K. These data were used to fit the three parameters k_{12}, τ_{12} and τ_{21} of the PR-MC-WS-NRTL EOS. In addition, these three parameters were fitted against literature data with measurements spanning the same pressure region for other temperatures. The selected literature data used for fitting the parameters are shown in Table 8.

The resulting parameter values for the different temperatures are shown in Table 10 and Figs. 6a and 6b, designated as Case 1.

With reference to Fig. 6a, the temperature dependencies of τ_{12} and τ_{21} could be described approximately by functions on the following form:

$$\tau_{12}(T) = a_{\tau_{12}} + b_{\tau_{12}}/(T - c_{\tau_{12}})\,, \qquad (28)$$

$$\tau_{21}(T) = a_{\tau_{21}} + b_{\tau_{21}}/(T - c_{\tau_{21}})\,. \qquad (29)$$

The optimal values of k_{12} seemed to be approximately constant up to 298.17 K. For the two data sets at 303 K, the optimal values were significantly higher. The reason for this seemed to be that the parameters of the EOS cannot be adjusted such as to simultaneously get a good fit of the data in the critical region at these higher temperatures and a good fit of the data below the critical region. The optimal parameters at these two temperatures gave a reasonable description of the data below the critical region, but predicted a significantly higher critical pressure than what was suggested by the data.

Based on this, the values of τ_{12} and τ_{21} were fitted again for these two temperature data sets, keeping k_{12} fixed at a value equal to the k_{12} optimal values at the lower temperature, approximately $k_{12} = 0.27$. This gave a significantly better match between the model prediction of the critical pressure and the critical pressure suggested by the data, at expense of the match of the model to the composition of the phases below the critical pressure.

To obtain an approximation to the temperature dependency of τ_{12} and τ_{21}, it was decided to fit τ_{12} and τ_{21} against the data sets in Table 8 using a constant value of $k_{12} = 0.266801$. The optimal values of τ_{12} and τ_{21} under this restriction are given in Table 10 as Case 2 and in Figs. 6a and 6b.

With $c_{\tau_{12}}$ fixed at 308 K, the coefficients $a_{\tau_{12}}$ and $b_{\tau_{12}}$ in Eq.(28) were fitted against the optimal values of τ_{12} for Case 2 for the temperatures where critical region data exist. Please refer to Table 8 for the data sets that were included. With $c_{\tau_{21}}$ fixed at 323 K, the coefficients $a_{\tau_{21}}$ and

Table 8
AAD and BIAS of the different EOSs, for data from the present work and data from literature.

ID	T (K)	EOS-CG Original AAD	BIAS	S	EOS-CG Fitted AAD	BIAS	S	PR-MC-WS-NRTL[a] AAD	BIAS	S	Data[b] p_{min} - p_{max} (MPa)	$n_{x_{CO_2}}$, $n_{y_{CO_2}}$	Source
1*	218.16	0.21	-0.14	5.73	0.38	-0.28	11.00	0.60	-0.09	15.93	0.97 - 15.03	11, 11	[30]
2	223.14	0.95	0.11	52.12	0.47	-0.08	16.86	0.78	0.03	25.81	1.94 - 18.22	16, 17	This work
3*	233.15	0.20	0.04	5.86	0.39	-0.11	11.90	0.64	-0.43	16.86	1.44 - 14.96	10, 10	[30]
4	240.00	1.03	-0.06	11.25	0.60	-0.25	6.38	1.07	-0.81	7.95	1.70 - 16.15	25, 21	[37, 48]
5	243.15	0.62	-0.15	23.78	0.38	-0.21	10.74	0.81	-0.67	19.86	1.51 - 15.21	11, 11	[30]
6	258.15	0.66	-0.46	18.49	0.63	-0.60	15.47	0.95	-0.95	23.24	2.79 - 13.64	13, 13	[30]
7*	270.00	0.22	0.05	11.57	0.24	-0.12	13.70	0.49	-0.40	N/A	9.56 - 9.58	1, 2	This work
8	270.00	0.39	-0.13	2.57	0.36	-0.26	2.21	0.53	-0.33	3.29	3.43 - 12.34	54, 63	[49, 28, 50, 48]
9	273.15	0.39	-0.14	11.05	0.38	-0.26	9.39	0.49	-0.13	14.10	3.54 - 11.79	11, 11	[30]
10	288.15	0.29	-0.27	7.91	0.29	-0.29	7.04	0.41	0.16	10.45	5.24 - 9.70	7, 7	[30]
11	288.30	0.51	-0.50	4.95	0.56	-0.54	5.20	0.35	-0.02	3.91	6.61 - 9.70	8, 8	[51]
12	293.30	0.32	0.06	2.81	0.38	0.03	2.92	0.63	0.39	10.03	6.00 - 9.11	10, 10	[51]
13	298.17	0.23	0.13	13.05	0.28	0.12	14.93	0.38	0.34	17.49	6.71 - 8.30	12, 12	This work
14	303.15	0.03	-0.02	1.04	0.04	-0.03	1.19	0.05	-0.04	1.41	7.31 - 7.57	6, 6	[30]
15	303.16	0.06	0.02	2.86	0.07	0.02	3.02	0.06	-0.05	2.83	7.40 - 7.56	7, 7	This work

[a] PR-MC-WS-NRTL Case 3. [b] Data pressure range p_{min} - p_{max}, number of liquid points $n_{x_{CO_2}}$ and vapor point $n_{y_{CO_2}}$. ID is a data set identifier. T is the mean temperature of the data set. * Not used for fitting the coefficients of Eqs. (28) and (29) since no data in the critical region.

$b_{\tau_{21}}$ in Eq. (29) were fitted in a similar way. The fit was performed using unweighted least squares.

The fitted coefficients are shown in Table 10 as Case 3, together with the calculated values of τ_{12} and τ_{21} from Eqs. (28) and (29).

The VLE predictions of PR-MC-WS-NRTL EOS model using the Case 3 parameters for the temperatures 223.14, 270.00, 298.17 and 303.16 K are shown in Figs. 7 to 10 with the measurement data, uncertainties, and other models considered in this work. The corresponding relative volatilities are shown in Fig. 11. The PR-MC-WS-NRTL EOS VLE predictions for the temperatures of the literature data in Table 8 are plotted in Fig. 13.

As it can be seen in Figs. 12c and 12d, the deviation between the model prediction of the composition of the phases and the experimental data was for most of the data points higher than for the fitted version of EOS-CG, shown in Figs. 12a and 12b. This was also reflected in the increased AAD and S values for the majority of the temperature data sets compared to the fitted version of EOS-CG, which can be found in Table 8. The loss in accuracy is augmented by the simpler formulation of the PR-MC-WS-NRTL model, compared to EOS-CG.

The prediction of the critical point from the PR-MC-WS-NRTL model (Case 3) was comparable with that of the fitted version of EOS-CG for the lower temperature range, except at 218.16 K. At temperatures above approximately 270 K, the critical pressure predicted by the PR-MC-WS-NRTL model agreed better with our experimental data than the fitted version of EOS-CG. However, the fitted version of EOS-CG gave a more accurate description of the composition of the phases below the critical region, as can be seen from Figs. 7 to 10.

The PR-MC-WS-NRTL EOS with $\alpha = 0.3$, $k_{12} = k_{21} = 0.266801$ and τ_{12} and τ_{21} described by Eqs. (28) and (29), respectively, provided an approximate description of the VLE of CO_2+N_2 over the temperature range 223.14 to 303.16 K. Although the model was less accurate than the fitted version of EOS-CG, it provided a fairly accurate description of the critical pressure at the different temperatures.

Table 9
Critical properties[a] and Mathias-Copeman coefficients[b] used in PR-MC-WS-NRTL EOS for CO_2 and N_2.

i	$T_{c,i}$ (K)	$p_{c,i}$ (MPa)	$c_{1,i}$	$c_{2,i}$	$c_{3,i}$
CO_2	304.2	7.3765	0.704606	-0.314862	1.89083
N_2	126.161	3.3944	0.404606	0.391057	-0.963495

[a] Values used by the in-house software. Slightly different from the values used in [6] and [22]: $T_{c,CO_2} = 304.1282$ K, $p_{c,CO_2} = 7.3773$ MPa, $T_{c,N_2} = 126.192$ K, $p_{c,N_2} = 3.3958$ MPa. [b] Parameters for CO_2 from [45]. Parameters for N_2 obtained by fitting the N_2 vapor pressure calculated using PR-MC against N_2 vapor pressures calculated by the N_2 reference EOS by Span et al. [22] over the temperature range between the N_2 triple point and the critical point.

Table 10
Optimal parameters k_{12}, τ_{12} and τ_{21} for the PR-MC-WS-NRTL model, fitted against data from the present work and literature data.

		Case 1[a]				Case 2[b]			Case 3[c]		
ID[d]	T (K)	k_{12}	τ_{12}	τ_{21}	S	τ_{12}	τ_{21}	S	τ_{12}	τ_{21}	S
1*	218.16	0.2900	1.3089	0.1064	4.6	1.0545	0.3482	6.5	1.5691	-0.0567	15.9
2	223.14	0.2689	1.5661	-0.0569	23.6	1.5478	-0.0432	23.6	1.5817	-0.0773	25.8
3*	233.15	0.2910	1.3736	-0.0553	8.1	1.0386	0.2261	9.9	1.6122	-0.1258	16.9
4	240.00	0.2805	1.9191	-0.3681	4.5	1.7554	-0.2797	4.7	1.6383	-0.1656	7.9
5	243.15	0.2630	1.5047	-0.1917	11.6	1.5545	-0.2235	11.6	1.6521	-0.1862	19.9
6	258.15	0.2844	1.7847	-0.4687	13.3	1.4619	-0.2874	13.7	1.7419	-0.3119	23.2
8	270.00	0.2824	2.2506	-0.6894	3.5	2.0062	-0.5610	3.4	1.8629	-0.4615	3.3
9	273.15	0.2643	2.0383	-0.5748	12.1	2.0802	-0.5959	12.1	1.9090	-0.5133	14.1
10	288.15	0.2567	1.8852	-0.5275	7.5	2.1554	-0.6901	7.5	2.3286	-0.8879	10.5
11	288.30	0.2541	2.0092	-0.7143	3.9	2.3286	-0.8882	3.9	2.3358	-0.8931	3.9
12	293.30	0.2529	2.2199	-0.6667	4.4	2.8110	-0.9317	4.2	2.6696	-1.1035	10.0
13	298.17	0.2669	3.3958	-1.2019	7.5	3.3919	-1.2001	7.5	3.3219	-1.3902	17.5
14	303.15	0.6231	7.7672	-2.7658	0.6	5.3201	-1.9738	1.5	5.3417	-1.8284	1.4
15	303.16	0.4235	6.1298	-2.2467	1.2	5.3199	-1.9738	3.5	5.3493	-1.8294	2.8

[a] $k_{12} = k_{21}$ varies freely, $\alpha = 0.3$ [b] $k_{12} = k_{21} = 0.266801$, $\alpha = 0.3$ [c] $k_{12} = k_{21} = 0.266801$, $\alpha = 0.3$. τ_{12} and τ_{21} calculated from Eqs. (28) and (29) respectively using $a_{\tau_{12}} = 1.35373$, $b_{\tau_{12}} = -19.3496$, $c_{\tau_{12}} = 308\,\mathrm{K}$, and $a_{\tau_{21}} = 0.357156$, $b_{\tau_{21}} = 43.3883$, $c_{\tau_{21}} = 323\,\mathrm{K}$.
[d] ID number corresponds to ID in Table 8. * Data set does not contain data in the critical region. Optimal values τ_{12} and τ_{21} for Case 2 not used for fitting coeffiecients of Eqs. (28) and (29).

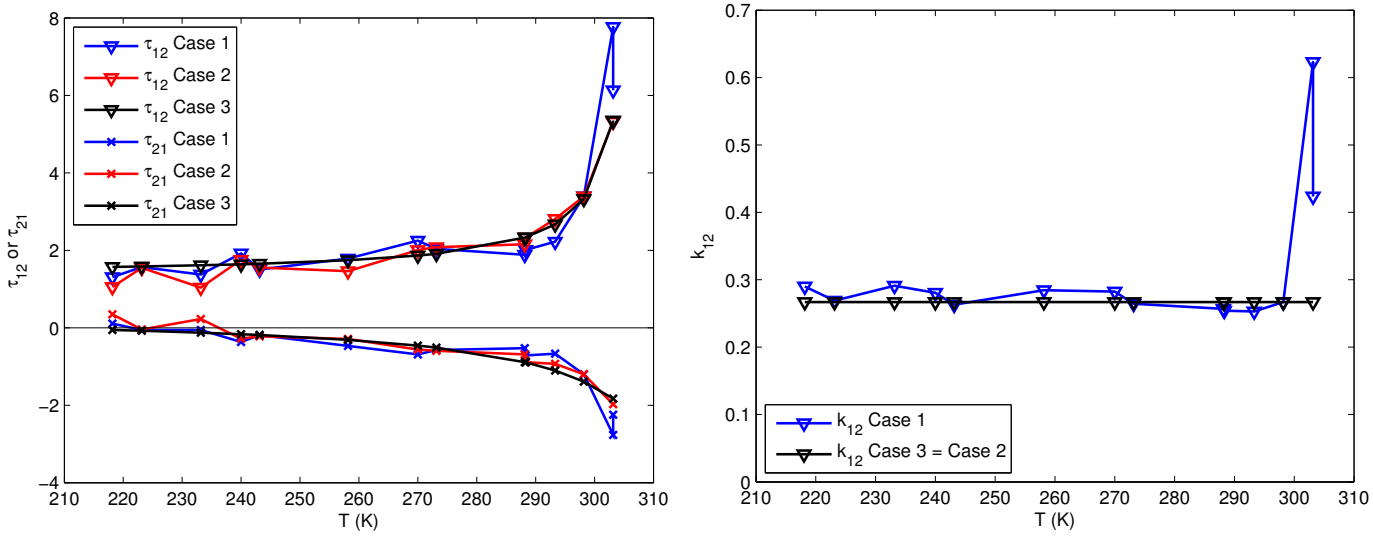

(a) Optimal values for τ_{12} and τ_{21} for the different temperature data sets in Table 8.

(b) Optimal values for k_{12} for the different temperature data sets in Table 8.

Fig. 6. Optimal values for τ_{12}, τ_{21} and k_{12} for the different temperature data sets in Table 8.

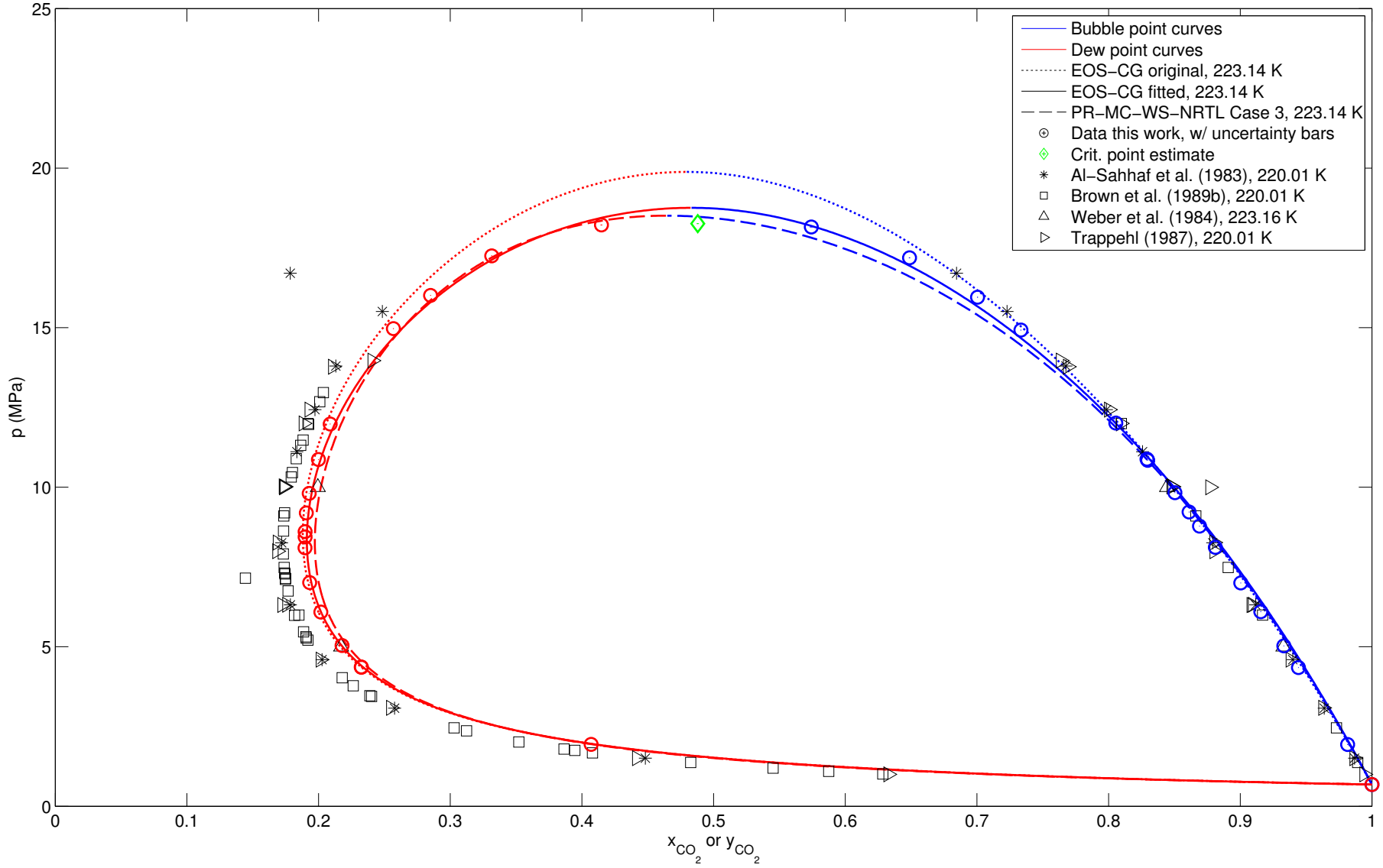

Fig. 7. Isothermal VLE data from literature [37, 28, 27, 52], EOS calculations at mean temperature $T = 223.14\,\mathrm{K}$, and measurements with estimated uncertainties from present work: $\bar{x}_{\mathrm{CO_2}}$, $\bar{y}_{\mathrm{CO_2}}$, $\bar{p}_{\mathrm{f}}$, $u_{\mathrm{c}}\left(\bar{x}_{\mathrm{CO_2}}\right)$, $u_{\mathrm{c}}\left(\bar{y}_{\mathrm{CO_2}}\right)$ and $u_{\mathrm{c}}\left(\bar{p}_{\mathrm{f}}\right)$ from Tables 4 and 5. Critical point estimation and its uncertainties are from Section 5.2.

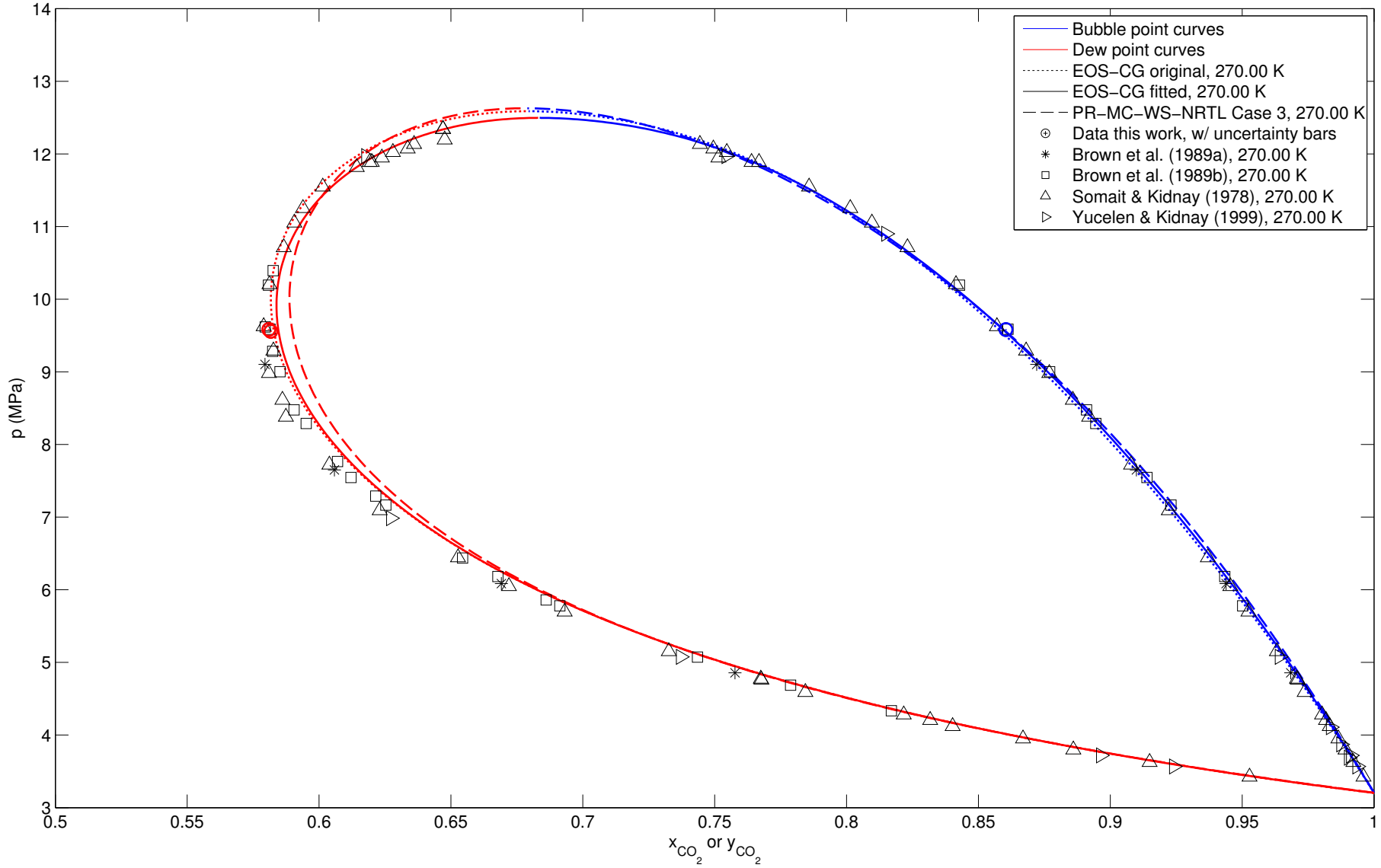

Fig. 8. Isothermal VLE data from literature [49, 28, 50, 48], EOS calculations at mean temperature $T = 270.00\,\mathrm{K}$, and measurements with estimated uncertainties from present work: $\bar{x}_{\mathrm{CO_2}}$, $\bar{y}_{\mathrm{CO_2}}$, $\bar{p}_{\mathrm{f}}$, $u_{\mathrm{c}}\left(\bar{x}_{\mathrm{CO_2}}\right)$, $u_{\mathrm{c}}\left(\bar{y}_{\mathrm{CO_2}}\right)$ and $u_{\mathrm{c}}\left(\bar{p}_{\mathrm{f}}\right)$ from Tables 4 and 5.

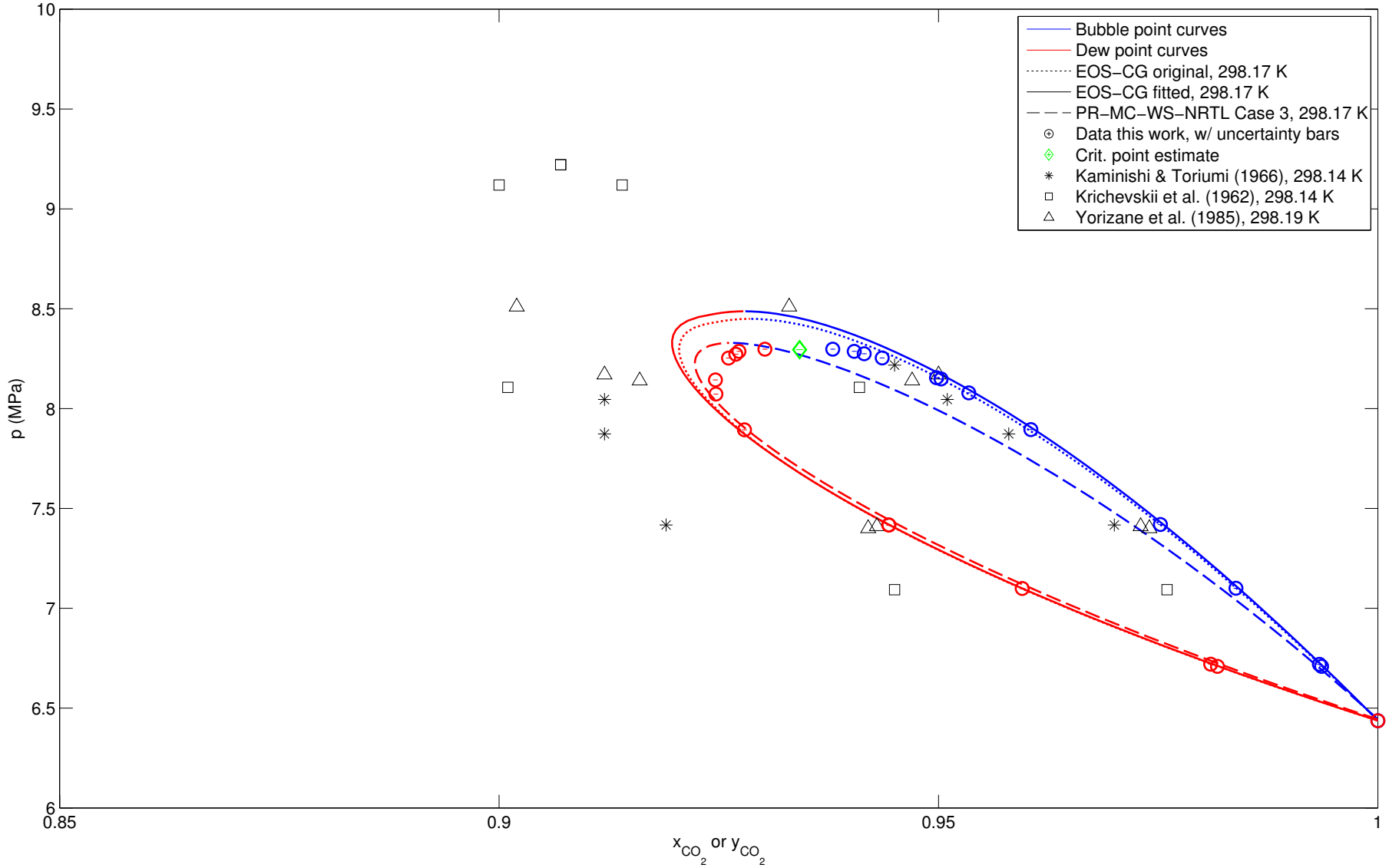

Fig. 9. Isothermal VLE data from literature [53, 54, 29], EOS calculations at mean temperature $T = 298.17\,\mathrm{K}$, and measurements with estimated uncertainties from present work: $\bar{x}_{\mathrm{CO_2}}$, $\bar{y}_{\mathrm{CO_2}}$, $\bar{p}_{\mathrm{f}}$, $u_{\mathrm{c}}\left(\bar{x}_{\mathrm{CO_2}}\right)$, $u_{\mathrm{c}}\left(\bar{y}_{\mathrm{CO_2}}\right)$ and $u_{\mathrm{c}}\left(\bar{p}_{\mathrm{f}}\right)$ from Tables 4 and 5. Critical point estimation and its uncertainties are from Section 5.2.

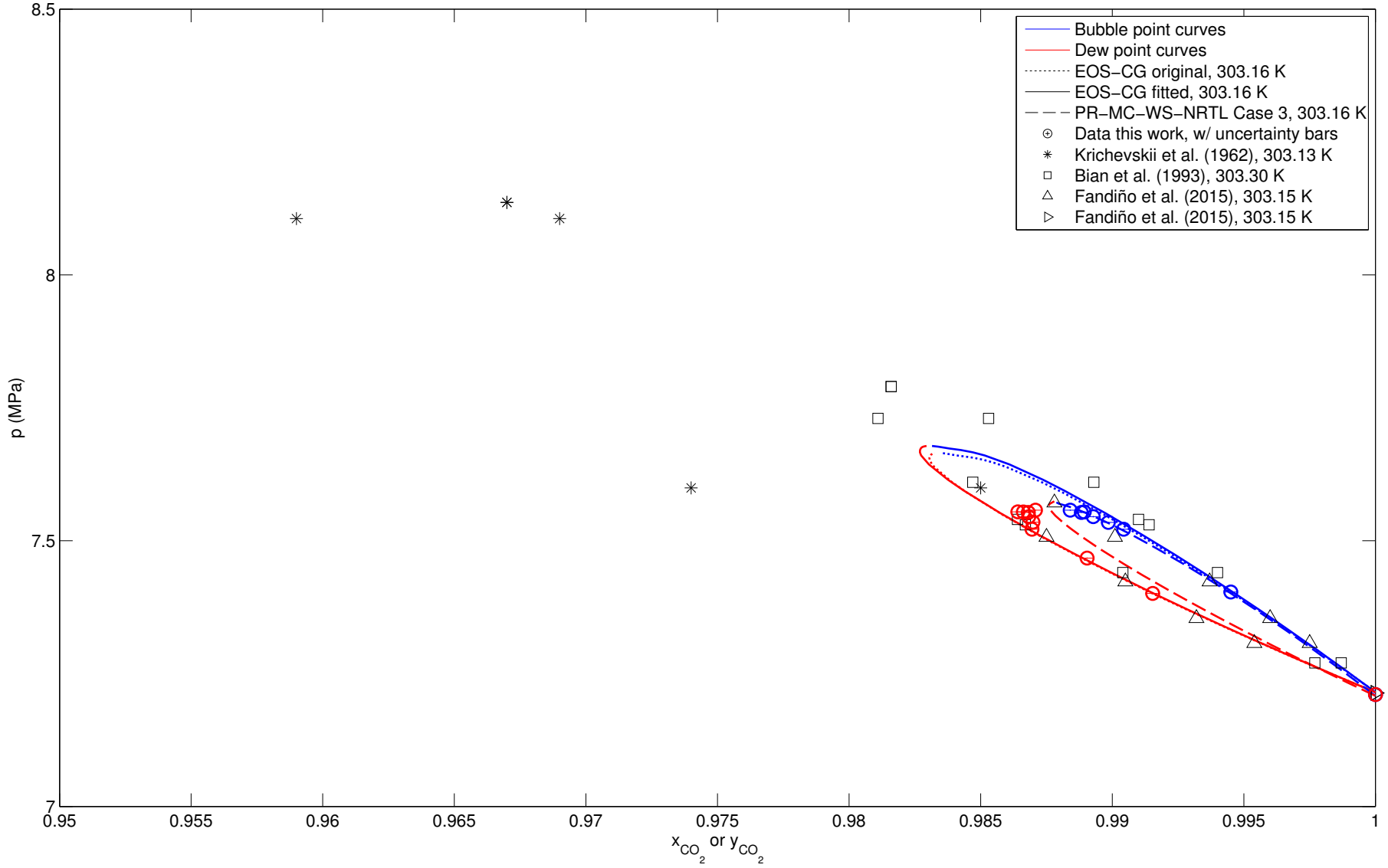

Fig. 10. Isothermal VLE data from literature [54, 55, 30], EOS calculations at mean temperature $T = 303.16\,\mathrm{K}$, and measurements with estimated uncertainties from present work: $\bar{x}_{\mathrm{CO_2}}$, $\bar{y}_{\mathrm{CO_2}}$, $\bar{p}_{\mathrm{f}}$, $u_{\mathrm{c}}\left(\bar{x}_{\mathrm{CO_2}}\right)$, $u_{\mathrm{c}}\left(\bar{y}_{\mathrm{CO_2}}\right)$ and $u_{\mathrm{c}}\left(\bar{p}_{\mathrm{f}}\right)$ from Tables 4 and 5.

6. Conclusions

This work describes a new facility for the measurement of vapor-liquid equilibria (VLE) of CO_2-rich mixtures, and reports the measurements of this setup on mixtures of CO_2 and N_2. More accurate VLE data will be required for a number of relevant mixtures in order to build better predictive models to be used in order to optimize the design and operation of various processes needed within CCS.

Our data covers a large range of VLE liquid and vapor phase CO_2 compositions, spanning from approximately 0.57 to 0.995 in the liquid phase, and from 0.19 to 0.992 in the vapor phase. Our measured CO_2 vapor pressures at the temperatures 223.14, 298.17 and 303.16 K are all within the values calculated from the Span-Wagner EOS. The agreement between our VLE data and high quality literature data is very good, the differences being within our and the literature data author's uncertainty estimates. The apparatus have shown that it is able to perform very stable measurements in the critical region, especially at the higher temperatures 298.17 and 303.16 K, where the two-phase region spans over very small pressure and composition ranges. It is reasonable to assume that our apparatus is working properly when it comes to performing VLE measurements of high quality in these temperature, pressure and composition ranges.

The VLE measurements in the critical region at 223.14 and 303.16 K, and the accurate measurements at 298.17 K are new contributions, as no data for these regions with the same accuracy could be found in the literature. These have been used to calculate estimates with low uncertainties for the critical points using a scaling law.

The equation of state (EOS) giving the current best description of the VLE of CO_2+N_2 system, the GERG-2008 EOS [7] (or EOS-CG [1, 2]), predicts a higher critical pressure than the measurements in this work suggests. At 223.14 K, this EOS predicts a critical pressure approximately 1.6 MPa higher than indicated by our data. The same behavior occurs at 298.17 and 303.16 K, with a predicted critical pressure 0.15 and 0.11 MPa higher than our data, respectively.

Two different EOSs have been fitted to our data and literature data. Two of the parameters of EOS-CG [1, 2] have been fitted. In addition, a fit has been made of the Peng-Robinson EOS [41] utilizing the alpha correction by Mathias and Copeman [42], the mixing rule by Wong and Sandler [43] and the NRTL excess Gibbs energy model [43]. These EOSs are able to describe the data in the present work quite accurately at the lower temperatures, especially in the critical region. However, at the higher temperatures, the description of the critical region is not so accurate. The EOSs also describe literature data quite accurately. Hence, this work illustrate the need to improve current models also with regards to a system which is relatively well known compared with other binary systems relevant for CCS.

Acknowledgements

This publication has been produced with support from the research program CLIMIT and the BIGCCS Centre, performed under the Norwegian research program Centres for Environment-friendly Energy Research (FME). The authors acknowledge the following partners for their contributions: Gassco, Shell, Statoil, TOTAL, ENGIE and the Research Council of Norway (193816/S60 and 200005/S60).

The research leading to these results has also received funding from the European Community's Seventh Framework Programme (*FP7-ENERGY-20121-1-2STAGE*) under *grant agreement* n° *308809* (The IMPACTS project). The authors acknowledge the project partners and the following funding partners for their contributions: Statoil Petroleum AS, Lundin Norway AS, Gas Natural Fenosa, MAN Diesel & Turbo SE and Vattenfall AB.

The authors would like to thank Dr. Morten Hammer, Dr. Geir Skaugen, Øivind Wilhelmsen, Eskil Aursand and Magnus Aashammer Gjennestad at SINTEF Energy Research for the in-house software used for VLE calculations and the model fitting. We would also like to thank Bjarne Malvik and Helge Johansen at SINTEF Energy Research and Håvard Rekstad and Reidar Tellebon of NTNU for their contributions.

Furthermore, the authors would like to thank Professor Roland Span of Ruhr-Universität Bochum and Dr. Eric W. Lemmon of NIST for suggesting parameters for fitting EOS-CG to the VLE data in the present work. Also, the authors would like to thank Dr. Johannes Gernert and Professor Span for the access to their literature data base [1].

Finally, the authors would like to thank the following summer interns at SINTEF Energy Research for their contributions: Asgeir Bjørgan, Petter Vollestad, Maximilian Schillings, Bjørn Holst Pettersen and Ingeborg Treu Røe.

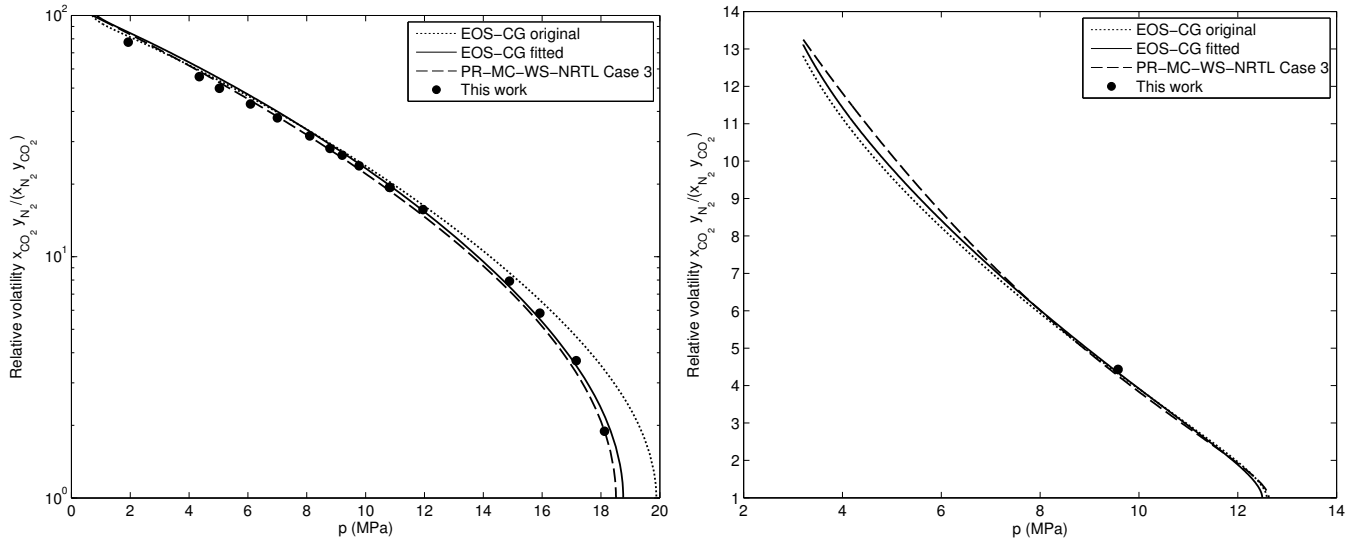

(a) 223.14 K

(b) 270.00 K

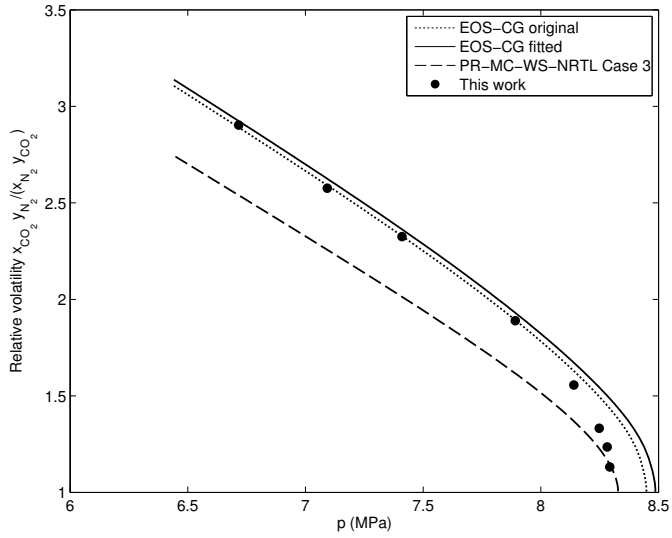

(c) 298.17 K

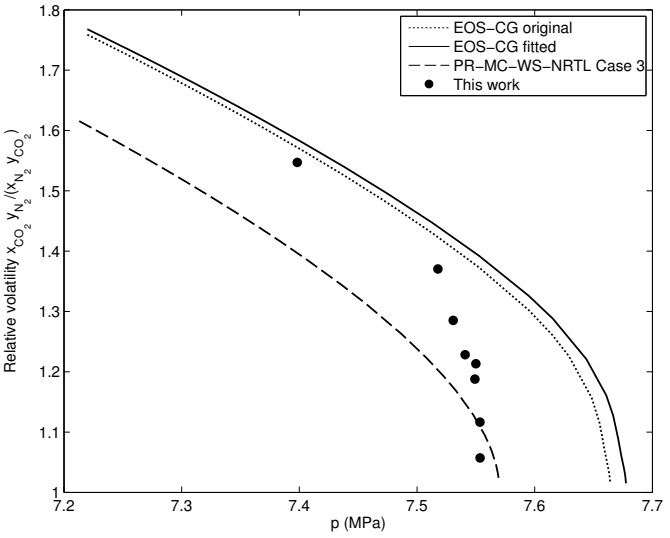

(d) 303.16 K

Fig. 11. Measured relative volatilities compared with different models.

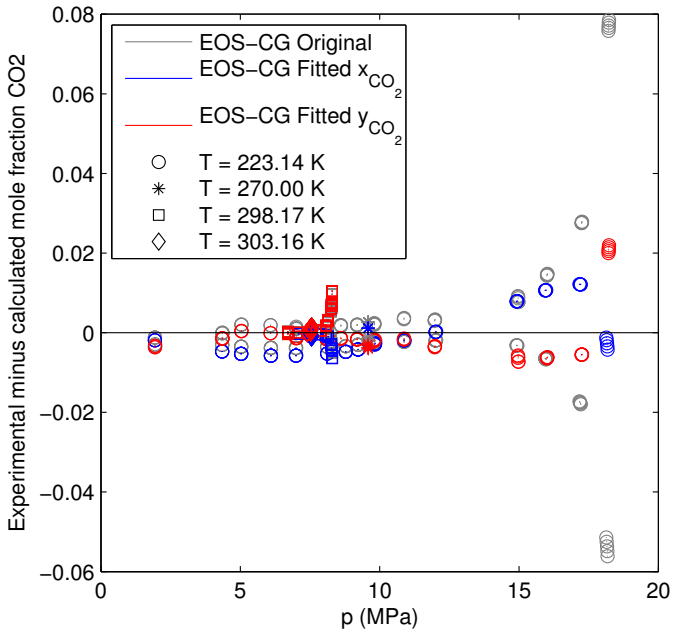

(a) VLE CO_2 mole fraction deviations between data in the present work and EOS-CG.

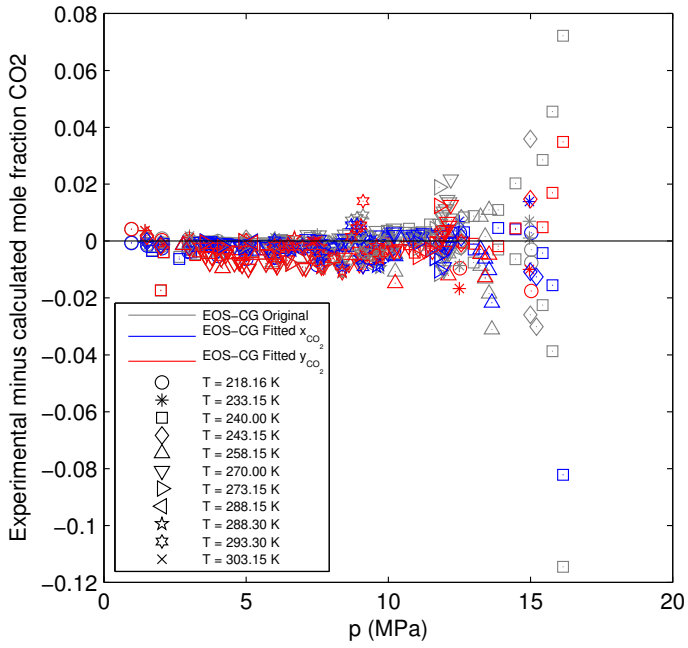

(b) VLE CO_2 mole fraction deviations between literature data and EOS-CG. Data listed in Table 8.

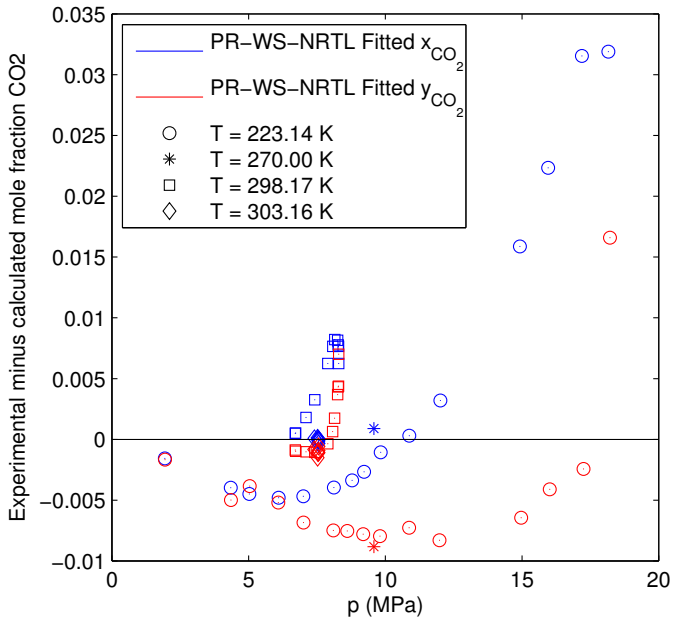

(c) VLE CO_2 mole fraction deviations between data in the present work and the PR-MC-WS-NRTL model.

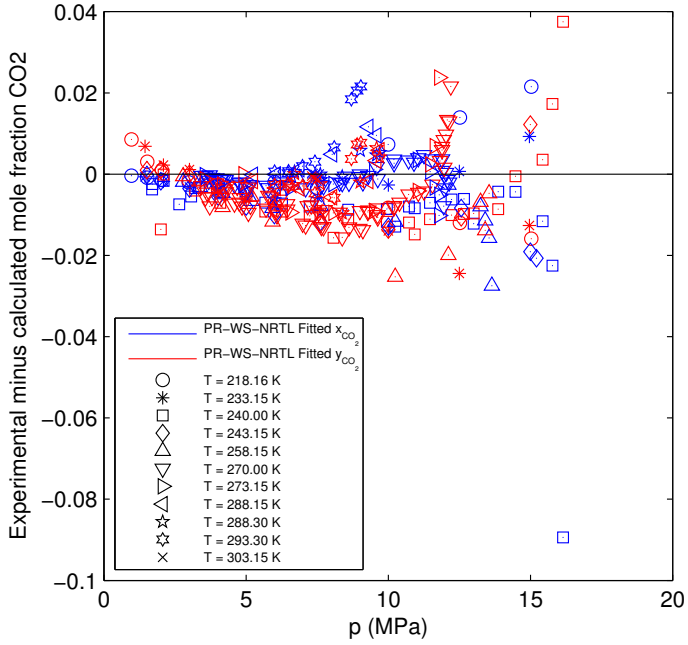

(d) VLE CO_2 mole fraction deviations between literature data and the PR-MC-WS-NRTL model. Data listed in Table 8.

Fig. 12. Mole fraction deviations between data and models.

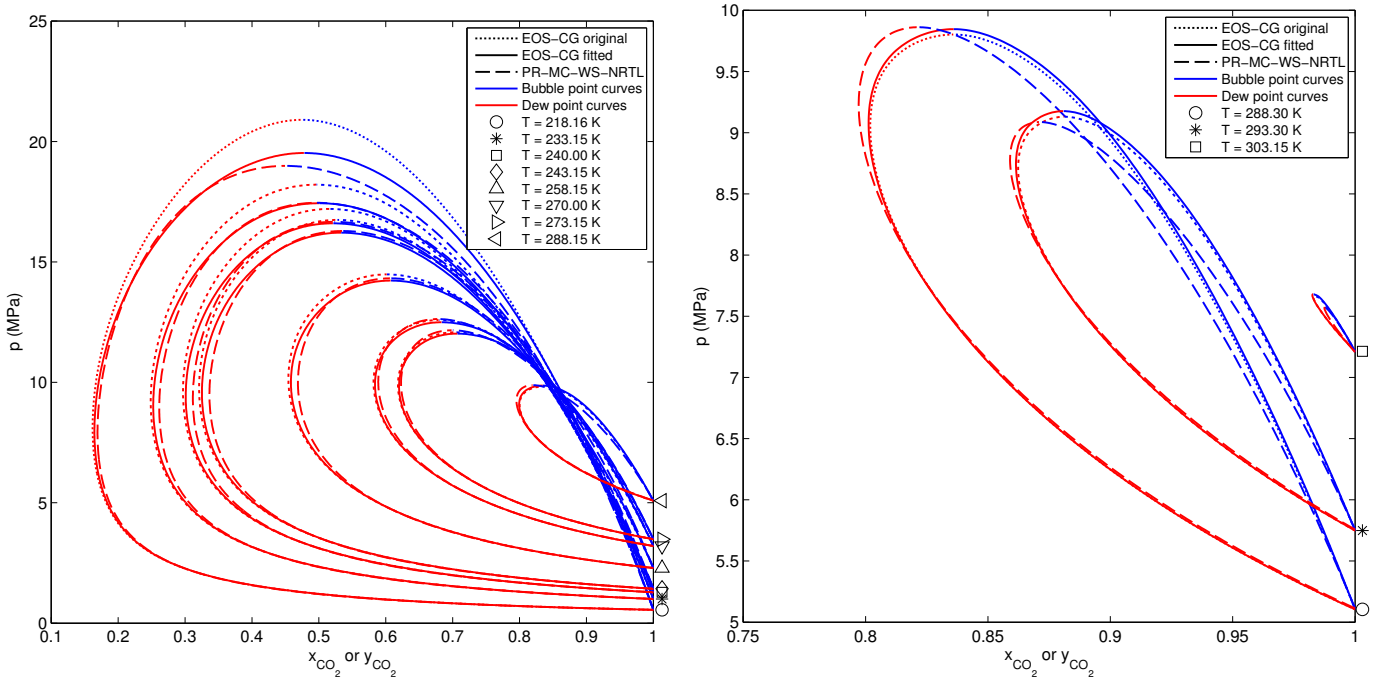

(a) Original and fitted EOS-CG and PR-MC-WS-NRTL EOS Case 3 plotted for the literature data temperatures T $\leq$ 288.15 K in Table 8.

(b) Original and fitted EOS-CG and PR-MC-WS-NRTL EOS Case 3 plotted for the literature data temperatures T $\geq$ 288.30 K in Table 8.

Fig. 13. Original and fitted versions of EOS-CG and PR-MC-WS-NRTL model for the literature data temperatures in Table 8.

List of symbols

a	half-width used to model uncertainties using a rectangular or triangular probability distribution (−)
a_i	Peng-Robinson pure component i parameter (−)
a_m	Peng-Robinson mixture parameter (−)
$\underline{A}^\mathrm{E}_\infty$	molar excess Helmholtz energy at infinite pressure ($\mathrm{J\,mol^{-1}}$)
b_i	Peng-Robinson pure component i parameter (−)
b_m	Peng-Robinson mixture parameter (−)
C	EOS-dependent constant in WS mixing rule. For PR, $C = \ln(\sqrt{2}-1)/\sqrt{2}$ (−)
$f_{i,\mathrm{L}}$	Section 5.4.1: Fugacity of component i in the liquid phase (MPa)
$f_{i,\mathrm{V}}$	Section 5.4.1: Fugacity of component i in the vapor phase (MPa)
F_{12}	EOS-CG weight parameter for CO_2+N_2 (−)
g_L	local acceleration of gravity ($\mathrm{m\,s^{-2}}$)
h_i	$i = 1,2,3,4$, liq. Distance used in p_hs calculation. See Section Appendix A.1. (m)
k_{ij}	WS binary interaction parameter between components i and j in Eq.(25) (−)
M	molar mass ($\mathrm{kg\,mol^{-1}}$)
p	pressure at VLE (MPa)
p_i	absolute pressure of sensor i, where $i = 1,2,3,4$ (MPa)
p_0	pressure at cell side of p_{11} (MPa)
p_{11}	differential pressure (MPa)
p_c	critical pressure
p_hs	hydrostatic pressure (MPa)
$\bar{p}$	pressure at VLE: mean pressure before one composition sample in Tables B.2 and B.3 (MPa)
$\bar{p}_\mathrm{f}$	pressure at VLE: mean of the pressures $\bar{p}$ for a series of composition samples in Tables 4 and 5 (MPa)
R	Resistance of SPRT at a temperature (Ω)
R	Universal gas constant = $8.3145\,\mathrm{J\,K^{-1}\,mol^{-1}}$
R_Ga	resistance of SPRT at T_Ga (Ω)
$R_{\mathrm{H_2O}}$	resistance of SPRT at $T_{\mathrm{H_2O}}$ (Ω)
R_Hg	resistance of SPRT at T_Hg (Ω)
R_ref	resistance of reference normal (Ω)
$s(z)$	sample standard deviation of variable z (−)
$s(\bar{z})$	sample standard deviation of the mean of variable z (−)
S	Model fitting objective function to be minimized (−)
T_{04}	ITS-90 temperature of top flange SPRT (K)
T_{05}	ITS-90 temperature of bottom flange SPRT (K)
T	ITS-90 temperature at VLE (K)
$\bar{T}$	ITS-90 temperature at VLE: mean temperature before one composition sample in Tables B.2 and B.3 (K)
$\bar{T}_\mathrm{f}$	ITS-90 temperature at VLE: mean of the temperatures $\bar{T}$ for a series of composition samples in Tables 4 and 5 (K)
T_Ga	ITS-90 temperature at gallium melting point (K)
$T_{\mathrm{H_2O}}$	ITS-90 temperature at water triple point (K)
T_Hg	ITS-90 temperature at mercury triple point (K)
$u(z)$	standard uncertainty of variable z (−)
$u_\mathrm{c}(z)$	combined standard uncertainty of variable z (−)
$u_\mathrm{tot}(z)$	total standard uncertainty of variable $z = x_{\mathrm{CO_2}}$ or $y_{\mathrm{CO_2}}$, from Eq. (A.33). (−)
W	ITS-90 ratio $R/R_{\mathrm{H_2O}}$ (−)
W_b	thermometry bridge ratio R/R_ref (−)
W_r	ITS-90 reference function (−)
$x_{\mathrm{CO_2}}$	liquid phase CO_2 mole fraction at VLE in Table B.2 (−)
$\bar{x}_{\mathrm{CO_2}}$	liquid phase CO_2 mole fraction at VLE: mean mole fraction a series of composition samples in Table 4 (−)

$x_{CO_2,calc}$	liquid phase CO_2 mole fraction at VLE, calculated from fitted EOS-CG. See Section 5.4.2. (−)
y_{CO_2}	vapor phase CO_2 mole fraction at VLE in Table B.3 (−)
$\bar{y}_{CO_2}$	vapor phase CO_2 mole fraction at VLE: mean mole fraction a series of composition samples in Table 5 (−)
$y_{CO_2,calc}$	vapor phase CO_2 mole fraction at VLE, calculated from fitted EOS-CG. See Section 5.4.2. (−)
z_{CO_2}	Liquid or vapor phase mole fraction at VLE
$z_{CO_2,c}$	Estimated critical composition in terms of CO_2 mole fraction, defined in Section 5.2.

Greek letters

α_{ij}	NRTL non-randomness parameter for binary interaction between components i and j in Eq. (26) (−)
β	Universal critical exponent of scaling law in Eq. (15)
$\beta_{T,12}$	EOS-CG parameter in temperature reducing function for CO_2+N_2 (−)
$\beta_{v,12}$	EOS-CG parameter in density reducing function for CO_2+N_2 (−)
$\gamma_{T,12}$	EOS-CG parameter in temperature reducing function for CO_2+N_2 (−)
$\gamma_{v,12}$	EOS-CG parameter in density reducing function for CO_2+N_2 (−)
λ_1	
λ_2	Parameters of scaling law in Eq. (15)
μ	
ρ	density ($kg\,m^{-3}$)
ρ_i	density in the four different regions $i = 1, 2, 3, 4$ used for calculation of p_{hs} ($kg\,m^{-3}$)
$\rho_{4,1}$	density of pure CO_2 in Region 4 used for calculation of p_{hs} ($kg\,m^{-3}$)
$\rho_{4,2}$	density of fluid in Region 4 used for calculation of p_{hs} ($kg\,m^{-3}$)
σ	standard deviation (−)
τ_{ij}	NRTL parameter for binary interaction between components i and j in Eq. (26) (−)

Subscripts

c	critical state

Superscripts

-	arithmetic mean

Abbreviations

ABBA	Weighing cycle of A and B comparisons
CAD	Computer-Aided Design
CCS	Carbon Capture, transport and Storage
EOS	Equation of State
EOS-CG	Equation of State for Combustion Gases and combustion gas like mixtures
GC	Gas Chromatograph
GUM	ISO Guide for the Estimation of Uncertainty in Measurement
MC	Mathias-Copeman alpha correction
NRTL	Non-Random Two-Liquid excess Gibbs energy model
OIML	Organisation Internationale de Métrologie Légale
PLC	Programmable logic controller
PR	Peng-Robinson EOS
SPRT	Standard Platinum Resistance Thermometer
SW	Span-Wagner EOS for CO_2
TCD	Thermal Conductivity Detector in GC
URL	Upper Range Limit for p_{11}
VLE	Vapor-Liquid Equilibrium
WS	Wong-Sandler mixing rule

References

[1] J. Gernert, R. Span, EOS-CG: A Helmholtz energy mixture model for humid gases and CCS mixtures, URL http://dx.doi.org/10.1016/j.jct.2015.05.015, in press, 2015.

[2] G. J. Gernert, A New Helmholtz Energy Model for Humid Gases and CCS Mixtures, PhD dissertation, Fakultät für Maschinenbau, Ruhr-Universität Bochum, Bochum, URL http://www-brs.ub.ruhr-uni-bochum.de/netahtml/HSS/Diss/GernertGeorgJohannes/diss.pdf, 2013.

[3] H. Li, J. P. Jakobsen, Ø. Wilhelmsen, J. Yan, PVTxy Properties of CO_2 Mixtures Relevant for CO_2 Capture, Transport and Storage: Review of Available Experimental Data and Theoretical Models, Appl. Energy 88 (11) (2011) 3567–3579, URL http://dx.doi.org/10.1016/j.apenergy.2011.03.052.

[4] S. W. Løvseth, G. Skaugen, H. G. J. Stang, J. P. Jakobsen, Ø. Wilhelmsen, R. Span, R. Wegge, CO_2 Mix Project: Experimental Determination of Thermo-Physical Properties of CO_2-Rich Mixtures, Energy Procedia 37 (2013) 7841–7849, URL http://dx.doi.org/10.1016/j.egypro.2014.09.001.

[5] S. W. Løvseth, H. G. J. Stang, S. F. Westman, I. Snustad, A. Austegard, Experimental Investigations of Impurity Impact on CO_2 Mixture Phase Equilibria, Energy Procedia 63 (2014) 2589–2595, URL http://dx.doi.org/10.1016/j.egypro.2014.11.281.

[6] R. Span, W. Wagner, A New Equation of State for Carbon Dioxide Covering the Fluid Region from the Triple-Point Temperature to 1100 K at Pressures up to 800 MPa, J. Phys. Chem. Ref. Data 25 (1996) 1509, URL http://dx.doi.org/10.1063/1.555991.

[7] O. Kunz, W. Wagner, The GERG-2008 Wide-Range Equation of State for Natural Gases and Other Mixtures: An Expansion of GERG-2004, J. Chem. Eng. Data 57 (11) (2012) 3032–3091, URL http://dx.doi.org/10.1021/je300655b.

[8] R. Span, J. Gernert, A. Jäger, Accurate Thermodynamic-Property Models for CO_2-Rich Mixtures, Energy Procedia 37 (2013) 2914–2922, URL http://dx.doi.org/10.1016/j.egypro.2013.06.177.

[9] E. De Visser, C. Hendriks, M. Barrio, M. J. Mølnvik, G. de Koeijer, S. Liljemark, Y. Le Gallo, Dynamis CO_2 Quality Recommendations, Int. J. Greenhouse Gas Control 2 (4) (2008) 478–484, URL http://dx.doi.org/10.1016/j.ijggc.2008.04.006.

[10] H. Li, Ø. Wilhelmsen, Y. Lv, W. Wang, J. Yan, Viscosities, Thermal Conductivities and Diffusion Coefficients of CO_2 Mixtures: Review of Experimental Data and Theoretical Models, Int. J. Greenhouse Gas Control 5 (5) (2011) 1119–1139, URL http://dx.doi.org/10.1016/j.ijggc.2011.07.009.

[11] R. D. Chirico, T. W. de Loos, J. Gmehling, A. R. H. Goodwin, S. Gupta, W. M. Haynes, K. N. Marsh, V. Rives, J. D. Olson, C. Spencer, J. F. Brennecke, J. P. M. Trusler, Guidelines for Reporting of Phase Equilibrium Measurements (IUPAC Recommendations 2012), Pure Appl. Chem. 84 (8) (2012) 1785–1813, URL http://dx.doi.org/10.1351/PAC-REC-11-05-02.

[12] BIPM, IEC, IFCC, ILAC, IUPAC, IUPAP, ISO, OIML, Evaluation of Measurement Data - Guide for the Expression of Uncertainty in Measurement. JCGM 100: 2008, 2008.

[13] M. Frenkel, R. D. Chirico, V. V. Diky, Q. Dong, S. Frenkel, P. R. Franchois, D. L. Embry, T. L. Teague, K. N. Marsh, R. C. Wilhoit, ThermoML - An XML-Based Approach for Storage and Exchange of Experimental and Critically Evaluated Thermophysical and Thermochemical Property Data. 1. Experimental data, J. Chem. Eng. Data 48 (1) (2003) 2–13, URL http://dx.doi.org/10.1021/je025645o.

[14] R. D. Chirico, M. Frenkel, V. V. Diky, K. N. Marsh, R. C. Wilhoit, ThermoML An XML-Based Approach for Storage and Exchange of Experimental and Critically Evaluated Thermophysical and Thermochemical Property Data. 2. Uncertainties, J. Chem. Eng. Data 48 (5) (2003) 1344–1359, URL http://dx.doi.org/10.1021/je034088i.

[15] M. Frenkel, R. D. Chirico, V. V. Diky, K. N. Marsh, J. H. Dymond, W. A. Wakeham, ThermoML An XML-Based Approach for Storage and Exchange of Experimental and Critically Evaluated Thermophysical and Thermochemical Property Data. 3. Critically Evaluated Data, Predicted Data, and Equation Representation, J. Chem. Eng. Data 49 (3) (2004) 381–393, URL http://dx.doi.org/10.1021/je049890e.

[16] R. D. Chirico, M. Frenkel, V. Diky, R. N. Goldberg, H. Heerklotz, J. E. Ladbury, D. P. Remeta, J. H. Dymond, A. R. Goodwin, K. N. Marsh, et al., ThermoML An XML-Based Approach for Storage and Exchange of Experimental and Critically Evaluated Thermophysical and Thermochemical Property Data. 4. Biomaterials, J. Chem. Eng. Data 55 (4) (2010) 1564–1572, URL http://dx.doi.org/10.1021/je900685d.

[17] S. F. Westman, H. G. J. Stang, S. Ø. Størset, H. Rekstad, A. Austegard, S. W. Løvseth, Accurate Phase Equilibrium Measurements of CO_2 Mixtures, Energy Procedia 51 (2014) 392–401, URL http://dx.doi.org/10.1016/j.egypro.2014.07.046.

[18] J. M. S. Fonseca, R. Dohrn, S. Peper, High-pressure fluid-phase equilibria: Experimental methods and systems investigated (2005–2008), Fluid Phase Equilib. 300 (1–2) (2011) 1–69, URL http://dx.doi.org/10.1016/j.fluid.2010.09.017.

[19] ARMINES, Patent n° FR 2 853 414, Procédé et dispositif pour prélever des micro-échantillons d'un fluide sous pression contenu dans un container, 2003.

[20] P. Guilbot, A. Valtz, H. Legendre, D. Richon, Rapid on-line sampler-injector: a reliable tool for HT-HP sampling and on-line GC analysis, Analusis 28 (5) (2000) 426–431, URL http://dx.doi.org/10.1051/analusis:2000128.

[21] S. Laugier, D. Richon, New apparatus to perform fast determinations of mixture vapor-liquid equilibria up to 10 MPa and 423 K, Rev. Sci. Instrum. 57 (3) (1986) 469–472, URL http://dx.doi.org/10.1063/1.1138909.

[22] R. Span, E. W. Lemmon, R. T. Jacobsen, W. Wagner, A. Yokozeki, A Reference Equation of State for the Thermodynamic Properties of Nitrogen for Temperatures from 63.151 to 1000 K and Pressures to 2200 MPa, J. Phys. Chem. Ref. Data 29 (6) (2000) 1361–1433, URL http://dx.doi.org/10.1063/1.1349047.

[23] H. Preston-Thomas, The International Temperature Scale of 1990 (ITS-90), Metrologia 27 (1) (1990) 3–10, URL http://dx.doi.org/10.1088/0026-1394/27/1/002.

[24] G. E. P. Box, G. M. Jenkins, G. C. Reinsel, Time series analysis : Forecasting and control, Wiley, ISBN 9780470272848, URL http://dx.doi.org/10.1002/9781118619193.oth3, 2008.

[25] A. M. Law, W. D. Kelton, Simulation modeling and analysis, McGraw-Hill, ISBN 0071008039, 1991.

[26] H. B. Callen, Thermodynamics and an Introduction to Thermostatistics, Wiley, 2 edn., ISBN 0471862568, 1985.

[27] W. Weber, S. Zeck, H. Knapp, Gas solubilities in liquid solvents at high pressures: apparatus and results for binary and ternary systems of N_2, CO_2 and CH_3OH, Fluid Phase Equilib. 18 (3) (1984) 253–278, URL http://dx.doi.org/10.1016/0378-3812(84)85011-6.

[28] T. S. Brown, E. D. Sloan, A. J. Kidnay, Vapor-liquid equilibria in the nitrogen+carbon dioxide+ethane system, Fluid Phase Equilib. 51 (1989) 299–313, URL http://dx.doi.org/10.1016/0378-3812(89)80372-3.

[29] M. Yorizane, S. Yoshimura, H. Masuoka, Y. Miyano, Y. Kakimoto, New Procedure for Vapor-Liquid Equilibria. Nitrogen+Carbon Dioxide, Methane+Freon 22, and Methane+Freon 12, J. Chem. Eng. Data 30 (2) (1985) 174–176, URL http://dx.doi.org/10.1021/je00040a012.

[30] O. Fandiño, J. P. M. Trusler, D. Vega-Maza, Phase behavior of (CO_2+H_2) and (CO_2+N_2) at temperatures between (218.15 and 303.15) K at pressures up to 15 MPa, Int. J. Greenhouse Gas Control 36 (2015) 78–92, URL http://dx.doi.org/10.1016/j.ijggc.2015.02.018.

[31] M. S. Green, M. Vicentini-Missoni, J. M. H. Levelt Sengers, Scaling-Law Equation of State for Gases in the Critical Region, Phys. Rev. Lett. 18 (1967) 1113–1117, URL http://dx.doi.org/10.1103/PhysRevLett.18.1113.

[32] L. P. Kadanoff, W. Götze, D. Hamblen, R. Hecht, E. A. S. Lewis, V. V. Palciauskas, M. Rayl, J. Swift, D. Aspnes, J. Kane, Static Phenomena Near Critical Points: Theory and Experiment, Rev. Mod. Phys. 39 (1967) 395–431, URL http://dx.doi.org/10.1103/RevModPhys.39.395.

[33] M. E. Fisher, The theory of equilibrium critical phenomena, Rep. Prog. Phys. 30 (2) (1967) 615, URL http://dx.doi.org/10.1088/0034-4885/30/2/306.

[34] P. Ungerer, B. Tavitian, A. Boutin, Applications of Molecular Simulation in the Oil and Gas Industry. Monte Carlo Methods, chap. 2, Editions Technip, Paris, France, note: Equation 2.100 is lacking the critical composition term, 2005.

[35] V. Lachet, T. de Bruin, P. Ungerer, C. Coquelet, A. Valtz, V. Hasanov, F. Lockwood, D. Richon, Thermodynamic behavior of the CO_2+SO_2 mixture: Experimental and Monte Carlo simulation studies, Energy Procedia 1 (1) (2009) 1641 – 1647, ISSN 1876-6102, URL http://dx.doi.org/10.1016/j.egypro.2009.01.215, greenhouse Gas Control Technologies 9Proceedings of the 9th International Conference on Greenhouse Gas Control Technologies (GHGT-9), 16-20 November 2008, Washington DC, {USA}.

[36] J. Sengers, J. Levelt Sengers, A universal representation of the thermodynamic properties of fluids in the critical region, Int. J. Thermophys. 5 (2) (1984) 195–208, ISSN 0195-928X, URL http://dx.doi.org/10.1007/BF00505500.

[37] T. A. Al-Sahhaf, A. J. Kidnay, E. D. Sloan, Liquid+Vapor Equilibria in the N_2+CO_2+ CH_4 System, Ind. Eng. Chem. Fundam. 22 (4) (1983) 372–380, URL http://dx.doi.org/10.1021/i100012a004.

[38] G. J. Esper, Direkte und indirekte pvT-Messungen an Fluiden, VDI-Verlag, 1987.

[39] G. J. Esper, D. M. Bailey, J. C. Holste, K. R. Hall, Volumetric behavior of near-equimolar mixtures for CO_2+CH_4 and CO_2+N_2, Fluid Phase Equilib. 49 (1989) 35–47, URL http://dx.doi.org/10.1016/0378-3812(89)80004-4.

[40] H. A. Duarte-Garza, J. C. Holste, K. R. Hall, K. N. Marsh, B. E. Gammon, Isochoric pVT and phase equilibrium measurements for carbon dioxide+ nitrogen, J. Chem. Eng. Data 40 (3) (1995) 704–711, URL http://dx.doi.org/10.1021/je00019a038.

[41] D.-Y. Peng, D. B. Robinson, A New Two-Constant Equation of State, Ind. Eng. Chem. Fundam. 15 (1) (1976) 59–64, URL http://dx.doi.org/10.1021/i160057a011.

[42] P. M. Mathias, T. W. Copeman, Extension of the Peng-Robinson equation of state to complex mixtures: Evaluation of the various forms of the local composition concept, Fluid Phase Equilib. 13 (1983) 91–108, URL http://dx.doi.org/10.1016/0378-3812(83)80084-3.

[43] D. S. H. Wong, S. I. Sandler, A Theoretically Correct Mixing Rule for Cubic Equations of State, AIChE J. 38 (5) (1992) 671–680, URL http://dx.doi.org/10.1002/aic.690380505.

[44] H. Renon, J. M. Prausnitz, Local compositions in thermodynamic excess functions for liquid mixtures, AIChE J. 14 (1) (1968) 135–144, URL http://dx.doi.org/10.1002/aic.690140124.

[45] C. Coquelet, A. Valtz, F. Dieu, D. Richon, P. Arpentinier, F. Lockwood, Isothermal P, x, y data for the argon+carbon dioxide system at six temperatures from 233.32 to 299.21 K and pressures up to 14 MPa, Fluid Phase Equilib. 273 (1-2) (2008) 38–43, URL http://dx.doi.org/10.1016/j.fluid.2008.08.010.

[46] B. E. Poling, J. M. Prausnitz, J. P. O'Connell, The properties of gases and liquids, vol. 5, McGraw-Hill New York, ISBN 0070116822, 2001.

[47] P. T. Boggs, R. H. Byrd, J. E. Rogers, R. B. Schnabel, User's Reference Guide for ODRPACK Version 2.01 Software for Weighted Orthogonal Distance Regression, URL http://docs.scipy.org/doc/external/odrpack_guide.pdf, 1992.

[48] B. Yucelen, A. J. Kidnay, Vapor-Liquid Equilibria in the Nitrogen+Carbon Dioxide+Propane System from 240 to 330 K at Pressures to 15 MPa, J. Chem. Eng. Data 44 (5) (1999) 926–931, URL http://dx.doi.org/10.1021/je980321e.

[49] T. S. Brown, V. G. Niesen, E. D. Sloan, A. J. Kidnay, Vapor-liquid equilibria for the binary systems of nitrogen, carbon dioxide, and n-butane at temperatures from 220 to 344 K., Fluid Phase Equilib. 53 (1989) 7–14, URL http://dx.doi.org/10.1016/0378-3812(89)80067-6.

[50] F. A. Somait, A. J. Kidnay, Liquid-Vapor Equilibria at 270.00 K for Systems Containing Nitrogen, Methane, and Carbon Dioxide, J. Chem. Eng. Data 23 (4) (1978) 301–305, URL http://dx.doi.org/10.1021/je60079a019.

[51] N. Xu, J. Dong, Y. Wang, J. Shi, High pressure vapor liquid equilibria at 293 K for systems containing nitrogen, methane and carbon dioxide, Fluid Phase Equilib. 81 (1992) 175–186, URL http://dx.doi.org/10.1016/0378-3812(92)85150-7.

[52] G. Trappehl, Experimentelle Untersuchung der Dampf-Flüssigkeits-Phasengleichgewichte und kalorischen Eigenschaften bei tiefen Temperaturen und hohen Drücken an Stoffgemischen bestehend aus N_2, CH_4, C_2H_6, C_3H_8 und CO_2, Ph.D. thesis, Technische Universität Berlin, 1987.

[53] G. Kaminishi, T. Toriumi, Vapor-Liquid Phase Equilibrium in the CO_2-H_2, CO_2-N_2 and CO_2-O_2 Systems [in Japanese], Kogyo Kagaku Zasshi 69 (1966) 175–178, URL http://doi.org/10.1246/nikkashi1898.69.2_175.

[54] I. R. Krichevskii, N. E. Khazanova, L. S. Lesnevskaya, L. Y. Sandalova, Equilibrium of Liquid-Gas at High Pressures in the System Nitrogen-Carbon Dioxide [in Russian], Khim. Prom-st. 3 (1962) 169–171.

[55] B. Bian, Y. Wang, J. Shi, E. Zhao, B. C.-Y. Lu, Simultaneous determination of vapor-liquid equilibrium and molar volumes for coexisting phases up to the critical temperature with a static method, Fluid Phase Equilib. 90 (1) (1993) 177–187, URL http://dx.doi.org/10.1016/0378-3812(93)85012-B.

[56] B. Mangum, G. Furukawa, Guidelines for Realizing the International Temperature Scale of 1990 (ITS-90), URL http://www.nist.gov/manuscript-publication-search.cfm?pub_id=905199, NIST Tech. Note 1265, 1990.

[57] M. S. L. of New Zealand, MSL Technical Guide 21 Using SPRT Calibration Certificates, URL https://www.msl.irl.cri.nz/training-and-resources/technical-guides, retrieved 2015-05-20, 2008.

[58] R. I. Veltcheva, J. V. Pearce, R. da Silva, G. Machin, R. L. Rusby, Strategies for Minimising the Uncertainty of the SPRT Self-Heating Correction, in: AIP Conf. Proc., vol. 1552, 433, URL http://dx.doi.org/10.1063/1.4821390, 2013.

[59] ISO, Gas analysis - Preparation of calibration gas mixtures - Gravimetric method, ISO 6142:2001, International Organization for Standardization, Geneva, Switzerland, 2001.

[60] M. E. Wieser, T. B. Coplen, Atomic weights of the elements 2009 (IUPAC Technical Report), Pure Appl. Chem. 83 (2) (2010) 359–396, URL http://dx.doi.org/10.1351/PAC-REP-10-09-14.

[61] M. E. Wieser, N. Holden, T. B. Coplen, J. K. Böhlke, M. Berglund, W. A. Brand, P. De Bièvre, M. Gröning, R. D. Loss, J. Meija, T. Hirata, T. Prohaska, R. Schoenberg, G. O'Connor, T. Walczyk, S. Yoneda, X.-K. Zhu, Atomic weights of the elements 2011 (IUPAC Technical Report), Pure Appl. Chem. 85 (5) (2013) 1047–1078, URL http://dx.doi.org/10.1351/PAC-REP-13-03-02.

[62] M. C. Leuenberger, M. F. Schibig, P. Nyfeler, Gas adsorption and desorption effects on cylinders and their importance for long-term gas records, Atmos. Chem. Phys. Discuss. 14 (13) (2014) 19293–19314, URL http://dx.doi.org/10.5194/acpd-14-19293-2014.

Appendix A. Detailed uncertainty analysis

Appendix A.1. Uncertainty analysis of pressure

As mentioned in Section 2.1, the equilibrium pressure at the vapor-liquid interface p was measured indirectly. The setup is shown in Fig. A.1. The absolute pressure sensor in use for a given experiment is designated p_i, where the index $i = 1, 2, 3, 4$ corresponds to the sensor in use, with increasing full scale pressure for increasing indices. The differential pressure transducer, designated p_{11}, was placed at the same elevation as the p_i sensors, to avoid a pressure difference due to a hydrostatic pressure. The differential pressure sensor and the tubing going down to the cell was heated to a temperature T_{10} above the cell temperature, to avoid condensation of the vapor phase in the tubing. Using these definitions, the pressure on the cell circuit side of the differential pressure sensor can be stated as $p_0 = p_i + p_{11}$.

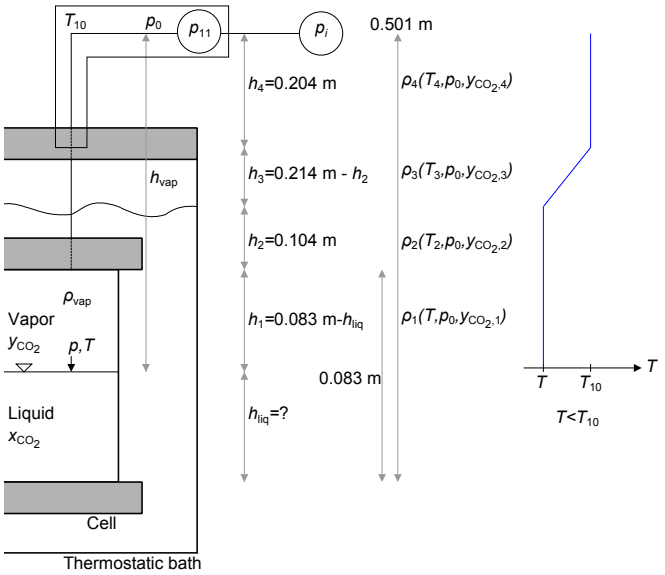

Fig. A.1. Sketch of pressure measurement system.

At thermodynamic equilibrium, the pressure at the vapor-liquid interface p is equal to p_0 plus the hydrostatic pressure of the fluid in the vertical distance between the position where p_0 is measured and the vapor-liquid interface. This hydrostatic pressure is designated p_{hs}. The pressure at the vapor-liquid interface can then be stated as

$$p = p_i + p_{11} + p_{\mathrm{hs}} \,. \tag{A.1}$$

Appendix A.1.1. Hydrostatic pressure p_{hs}

The hydrostatic pressure is in general equal to $\rho g_{\mathrm{L}} h$, that is, density times gravity times vertical height difference. This pressure will in most cases be very small compared to the cell pressure, as the fluid column is less than 0.5 m high, and, as the density of the fluid is approximately proportional to the cell pressure. The density of the fluid column ρ depends on the contents of the cell. The height depends on the liquid level in the cell h_{liq}, and can be measured quite accurately using a borescope to inspect the cell contents visually. The local gravity used, $g_{\mathrm{L}} = 9.821\,46\,\mathrm{m\,s^{-2}}$, was based on a measurement by the Geological Survey of Norway (NGU) in the room where the experimental setup is located. The hydrostatic pressure p_{hs} was calculated based on the mean absolute pressure value p_i over the time period of the VLE experiment, to obtain the equilibrium pressure p.

The tubing connecting the point where p_0 was calculated and the bulk contents of the cell was quite small in internal diameter (approximately 0.6 mm), and it was not certain that the contents of this tubing had the same composition and temperature as the bulk vapor phase in the cell, when the bulk contents of the cell had reached VLE. This made it difficult to calculate the density of the fluid very accurately.

In addition, the density of the fluid column will vary in the vertical region between p and p_0. As shown in Fig. A.1, the vertical region was divided into four different subregions, indicated with vertical distances h_i, with corresponding temperatures T_i, CO_2 mole fractions $y_{CO_2,i}$ and densities ρ_i, where $i = 1, 2, 3, 4$.

In Regions $i = 1, 2$ and 4, we could assume that the temperature, and thereby the composition, in the fluid column was approximately constant. Between the vapor-liquid interface and up to the thermostatic bath fluid surface, the temperature was assumed to be equal to T, as the bath fluid should keep a specified temperature given by the set point of the bath. The temperature in Regions 1 and 2 was therefore equal to T. In Region 4 the temperature was kept at T_{10}, and is assumed to be constant. We assumed that the temperature in Region 3, between the thermostatic bath liquid surface at T and the circuit kept at T_{10} was increasing linearly, as shown in Fig. A.1. This was not necessarily correct, as the region between the bath fluid surface and the bottom of the insulating lid was filled with air.

The pressure in these four regions was assumed to be equal to p_0, to be able to perform the calculation of the densities needed to calculate the hydrostatic pressure.

Based on the assumption of the temperature behavior in Region 3, we assumed that the density in Region 3 was decreasing linearly from the density in Regions 2 to 4 as we move up vertically. Assuming a vertical height datum $z = 0$ at the interface between Regions 2 and 3, the densities in this and the other regions could be expressed as

$$\begin{aligned} \rho_1 &= \rho_{vap}(T, p_0, y_{CO_2}) \,, \\ \rho_2 &= \rho_2(T, p_0, y_{CO_2,2}) \,, \\ \rho_3 &= \rho_2 + z(\rho_4 - \rho_2)/h_3 \,, \\ \rho_4 &= \rho_4(T_{10}, p_0, y_{CO_2,4}) \,. \end{aligned} \tag{A.2}$$

Under these assumptions, a general expression for the hy-

drostatic pressure could be written as

$$\begin{aligned} p_{\mathrm{hs}} &= f\left(\rho_1,\rho_2,\rho_4,h_1,h_2,h_3,h_4,g_{\mathrm{L}}\right) \\ &= \rho_1 g_{\mathrm{L}} h_1 + \rho_2 g_{\mathrm{L}} h_2 \\ &+ \int_{z=0}^{h_3} \rho_3(z) g_{\mathrm{L}} \mathrm{d}z + \rho_4 g_{\mathrm{L}} h_4 \\ &= \rho_1 g_{\mathrm{L}} h_1 + \rho_2 g_{\mathrm{L}} h_2 \\ &+ g_{\mathrm{L}}\left(\rho_2 h_3 + \frac{\rho_4-\rho_2}{2} h_3\right) + \rho_4 g_{\mathrm{L}} h_4 \,. \end{aligned} \tag{A.3}$$

During the experiments, T_{10} was kept at 313 K. At this temperature we were above the critical temperature of both N_2 (126.192 K [22]) and CO_2 (304.1282 K [6]), ensuring that the fluid in Region 4 was supercritical.

When making assumptions about the composition in the four different regions, we had several possibilities. In the current experimental procedure, CO_2 was filled into the cell first, and then the second component N_2. Regions 2-4 will therefore initially consist of pure CO_2, and the mixing of the contents of the cell using the stirrer did not affect the contents of these regions very much. Any mass transport from Region 1 to Regions 2-4 and back again, therefore, mainly relied on diffusion along the thin tubing.

As all our VLE experiments were carried out at temperatures above the critical temperature of N_2 and below the critical temperature of CO_2, vapor and liquid phases at equilibrium could only exist at pressures above the vapor pressure of CO_2. Based on this fact, the only place where pure CO_2 could exist at cell pressure p (above the vapor pressure of CO_2) was where the temperature was above the critical temperature of CO_2. This included Region 4 and the upper part of Region 3. For simplicity we assumed that only Region 4 was included. If we assumed that only the vapor phase of the cell had been in contact with the entrance of the tubing, the two extreme points for the possible total composition in Region 4, $y_{\mathrm{CO_2},4}$, were either pure CO_2 or the composition of the vapor phase with the lowest CO_2 content in the previous and current VLE measurements. Consequently, the difference in the calculated density in Region 4 was the largest during VLE measurements at low temperatures far from T_{10}, where the N_2 content of the vapor phase would increase.

The best solution to this would be to wait for a sufficiently long time after VLE has been reached in the cell, to ensure that the composition in Regions 2-4 is closer to that of the cell vapor phase. It was, however, difficult to determine what sufficient time would be.

Based on this discussion, the following assumptions were made about the contents of the fluid column: The density in Region 2 was assumed to be equal to that in Region 1, $\rho_2 = \rho_1(T, p_0, y_{\mathrm{CO_2}})$. The density and corresponding uncertainty in Region 4 were based on the most conservative estimate. It was assumed that the probability that the density in Region 4 is not included in the interval defined by the two density extremes (a_- and a_+) is equal to zero. A rectangular probability distribution was assumed, with the expected value of the density $\rho_4 = (a_+ + a_-)/2$. The standard uncertainty was then $u(\rho_4) = 0.5 \cdot |a_+ - a_-|/\sqrt{3}$. The two density extremes were designated $\rho_{4,1} = \rho_4(T_{10}, p_0, y_{\mathrm{CO_2},4} = 1)$ for pure CO_2, and $\rho_{4,2} = \rho_4(T_{10}, p_0, y_{\mathrm{CO_2},4} = y_{\mathrm{CO_2}})$ for CO_2 and N_2 with the composition equal to that of the cell vapor phase $y_{\mathrm{CO_2}}$. The density of supercritical pure CO_2 was calculated using the Span-Wagner EOS [6]. The density of the cell vapor phase was calculated using EOS-CG [1, 2]. The standard uncertainties in density for these EOSs at the relevant temperatures and pressures are given in Table 2.

Taking into the account the uncertainties in the densities calculated from the EOSs, the combined standard uncertainty $u_{\mathrm{c}}(\rho_4)$ is given by Eq. (3),

$$\begin{aligned} u_{\mathrm{c}}^2(\rho_4) = u^2(\rho_4) &+ \left[u(\rho_{4,1})\left(\partial\rho_4/\partial\rho_{4,1}\right)_{\rho_{4,2}}\right]^2 \\ &+ \left[u(\rho_{4,2})\left(\partial\rho_4/\partial\rho_{4,2}\right)_{\rho_{4,1}}\right]^2 \\ = u^2(\rho_4) &+ \left[u(\rho_{4,1})/2\right]^2 + \left[u(\rho_{4,2})/2\right]^2 . \end{aligned} \tag{A.4}$$

For specifying the height of the fluid column, there are two types of input variables. The first type are the numbers specified as constants in Fig. A.1 in the expressions for h_1, h_3 and h_4, which were taken from the CAD drawing of the apparatus and verified by manual measurements on the apparatus. The second type are the only two variables in the calculation of the fluid column height, h_{liq} and the distance from the bottom of the top flange to the thermostatic bath liquid surface, h_2.

The uncertainty in the liquid level h_{liq} can be significant, and this has two causes. The first is the uncertainty connected to measuring the level from a borescope picture, $u(h_{\mathrm{liq}}, 1)$. The second source for uncertainty is that the liquid level might change slightly from sample to sample, $u(h_{\mathrm{liq}}, 2)$. The current procedure is to sample a volume equal to the capillary sampler volume. The liquid sampler capillary had an internal volume of approximately $7.1 \cdot 10^{-3}\,\mathrm{cm}^3$, or 0.0071 % of the cell internal volume. For the vapor sampler capillary, the internal volume was $5.3 \cdot 10^{-3}\,\mathrm{cm}^3$, or 0.0053 % of the cell volume. Because of the relatively small volume of the samples withdrawn compared to the cell volume, the change in liquid level was found to be insignificant. The change in liquid level was calculated using an EOS, and checked using the borescope before and after the samples were taken. During the performed experiments, it was not possible to see a change in the liquid level before and after a series of liquid and vapor samples.

The standard uncertainty in the borescope determination of the liquid level was modeled using a rectangular distribution, with maximum bounds a estimated as 10 % of the maximum liquid level 0.083 m, $a = 0.0083$ m, yielding a standard uncertainty of $u(h_{\mathrm{liq}}, 1) = a/\sqrt{3} \approx 0.0048$ m. Since it was not possible to see a change in liquid level during the course of one experiment, the uncertainty contribution from this source was considered negligible compared to the borescope determination of the liquid level, and $u(h_{\mathrm{liq}}, 2) \approx 0$ m was assumed. Assuming independence of the two contributions, and using Eq. (5a), the total standard uncertainty was given as $u(h_{\mathrm{liq}}) = [u^2(h_{\mathrm{liq}}, 1) + u^2(h_{\mathrm{liq}}, 2)]^{0.5} = 0.0048$ m. The height h_2, determined by the fluid level in the thermo-

static bath, was subject to some variations. h_2 was also modeled using a rectangular distribution, with estimated $a = 0.010\,\mathrm{m}$, yielding $u(h_2) \approx 0.006\,\mathrm{m}$.

The uncertainty in the lengths obtained from the CAD drawing were assumed to be negligible compared to the uncertainty in h_{liq}. Using Eq. (3), this gave $u_c(h_1) = [1^2 \cdot u^2(\mathrm{CAD}) + (-1)^2 \cdot u^2(h_{\mathrm{liq}})]^{0.5} = 0.0048\,\mathrm{m}$ and $u_c(h_3) = [1^2 \cdot u^2(\mathrm{CAD}) + (-1)^2 \cdot u^2(h_2)]^{0.5} = 0.006\,\mathrm{m}$.

The variables of Eq. (A.3) are not independent, and as it is difficult to determine the correlations, the Type B evaluation of Eq. (4) was used for the combined standard uncertainty of p_{hs}:

$$\begin{aligned} u(p_{\mathrm{hs}}) &= \sum_{i=1,2} \left| u(\rho_i) \frac{\partial p_{\mathrm{hs}}}{\partial \rho_i} \right| + \left| u_c(\rho_4) \frac{\partial p_{\mathrm{hs}}}{\partial \rho_4} \right| \\ &+ \sum_{i=1,3} \left| u_c(h_i) \frac{\partial p_{\mathrm{hs}}}{\partial h_i} \right| + \sum_{i=2,4} \left| u(h_i) \frac{\partial p_{\mathrm{hs}}}{\partial h_i} \right| \\ &+ \left| u(g_{\mathrm{L}}) \frac{\partial p_{\mathrm{hs}}}{\partial g_{\mathrm{L}}} \right| . \end{aligned} \tag{A.5}$$

In the temperature range 223.15 to 303.15 K, the standard uncertainty $u(p_{\mathrm{hs}})$ was less than $10^{-4} \cdot p$. The main contributors were $u(\rho_4)$ and to a lesser extent $u_c(h_{\mathrm{liq}})$ and $u(h_2)$.

Appendix A.1.2. Differential pressure p_{11}

The differential pressure was measured using a Rosemount 3051S1CD differential pressure transmitter, in combination with a Rosemount 1199 remote mount seal/diaphragm. The transmitter can measure pressure differences over the diaphragm in the range $\pm 0.0623\,\mathrm{MPa}$. The transmitter was kept at a fairly constant temperature, as the room temperature was kept at around 22 °C by air-conditioning.

According to the specification of the transmitter, the measured value of the differential pressure is influenced by the temperature of the surroundings, the line pressure, the span of the measurements, how the transmitter is mounted, vibrations and changes in the voltage of the power supply. In addition, there is a discretization error due to the AD-conversion. Hence, in total 7 different uncertainty terms have been identified, with uncalibrated values given by:

$$u(p_{11},1) = 0.44\ \mathrm{Pa/K} \cdot \Delta T\ , \quad \text{Temperature} \tag{A.6a}$$

$$u(p_{11},2) = 7.6 \cdot 10^{-7} \cdot p_i\ , \quad \text{Line pressure} \tag{A.6b}$$

$$u(p_{11},3) = 4.9 \cdot 10^{-5}\,\mathrm{MPa}^{-1} \cdot p_i \cdot p_{11}\ , \quad \text{Span} \tag{A.6c}$$

$$u(p_{11},4) = 0.10\ \mathrm{MPa}\ , \quad \text{Mounting} \tag{A.6d}$$

$$u(p_{11},5) = 28\ \mathrm{Pa}\ , \quad \text{Vibrations} \tag{A.6e}$$

$$u(p_{11},6) = 2.1\,\mathrm{Pa\,V^{-1}} \cdot \Delta V\ , \quad \text{Voltage} \tag{A.6f}$$

$$u(p_{11},7) = 0.24\ \mathrm{kPa}\ . \quad \text{AD converter} \tag{A.6g}$$

In addition to these terms, a long term stability of 42 Pa was guaranteed for a period of 10 years. As the transmitter was bought 3 years ago, the stability should still be within this specification. The uncertainties were specified at $\pm 3\sigma$, and are functions of the calibrated URL and span. As nothing else was stated by the manufacturer, it was assumed that a normal probability distribution has been used in the estimation of the uncertainties. Hence, the specified uncertainties U were assumed to be three times the standard uncertainty u, $u = U/3$.

Some of the terms of Eq. (A.6) were reduced to insignificant levels through the design and procedures of the setup. The temperature dependent uncertainty $u(p_{11},1)$ was eliminated by controlling the ambient temperature. The line pressure $u(p_{11},2)$ and mounting dependent $u(p_{11},4)$ zero reading uncertainty were eliminated by physically connecting the two sides of the transmitter at different line pressures. Based on these measurements, an offset function using linear interpolation was constructed at T_{10}. The uncertainty caused by voltage variations, $u(p_{11},6)$, was negligible, leaving only the span error $u(p_{11},3)$, effect of vibrations, $u(p_{11},6)$, and AD-conversion error, $u(p_{11},7)$. The former term was in most measurements reduced, but not always completely eliminated, by controlling the pressure levels such that p_{11} was small. The transmitter was subjected to some small vibrations, especially from the motors powering the compressor in the cold thermostatic bath.

The largest contribution to uncertainty of p_{11} turned out to be the AD conversion. The specified accuracy of the used PLC was 0.3 % FS, where the full scale was 20 mA DC. Since nothing else was stated, this was assumed to be at $\pm 2\sigma$ calculated using a normal distribution, in accordance with the "GUM" [12]. This error can be reduced by decreasing the span or using an AD converter with higher resolution.

The contributing uncertainties in the differential pressure p_{11} are summarized in Table 2.

As the different contributions were independent we got

$$u(p_{11}) = \sqrt{u(p_{11},3)^2 + u(p_{11},5)^2 + u(p_{11},7)^2}\ . \tag{A.7}$$

It should be noted that the dominating source of uncertainty, $u(p_{11},7)$, was independent of line pressure, with a relative contribution of $3 - 4 \cdot 10^{-4}$ at the lowest measured line pressures around 0.7 MPa. Hence, for most of our data, the uncertainty contribution from the differential pressure measurements was insignificant.

Appendix A.1.3. Pressure transmitter p_i

The pressure transmitters p_i (Keller model PAA-33X) were delivered with certified "precision" stated as 0.01 % of the full scale pressure for the temperature range 10 to 40 °C, when the RS485 digital readout is used. The sensors had been calibrated in-situ before and after the VLE measurements were performed, against a dead weight tester that was calibrated by IKM Laboratorium in Norway in 2013 (Desgranges et Huot model 26000 M). It was not possible to see any drift in the response of the sensors from the first to the

second calibration. Based on the calibrations, the standard uncertainties of the sensor values were those given as $u(p_i)$ for $i = 1, 2, 3, 4$ in Table 2.

Appendix A.1.4. Total uncertainty in cell pressure p

As the hydrostatic pressure p_{hs} is a function of the absolute pressure p_i, and p_{11} changes when p_i changes, the three terms in Eq. (A.1) could not be assumed to be independent. Therefore, we had to use Eq. (4) to estimate the combined standard uncertainty in the cell pressure:

$$\begin{aligned} u_{\mathrm{c}}(p) &= \left|\frac{\partial p}{\partial p_i}\right| \left|u(p_i)\right| + \left|\frac{\partial p}{\partial p_{11}}\right| \left|u(p_{11})\right| + \left|\frac{\partial p}{\partial p_{\mathrm{hs}}}\right| \left|u(p_{\mathrm{hs}})\right| \\ &= \left|u(p_i)\right| + \left|u(p_{11})\right| + \left|u(p_{\mathrm{hs}})\right| . \end{aligned} \tag{A.8}$$

For the higher pressures between 10 and 20 MPa, the total uncertainty was dominated by the uncertainties in sensors p_3 and p_4, while for lower pressures below 10 MPa, the uncertainties in sensors p_1 and p_2 were of the same magnitude as the uncertainty caused by the A/D conversion in sensor p_{11}. For all pressures, the uncertainty in the hydrostatic pressure was small compared to these other sources.

Appendix A.2. Uncertainty analysis of temperature

The sensors T_{04} and T_{05} were standard platinum resistance thermometers (SPRT). The temperature of a SPRT is calculated by measuring the resistance of the SPRT at the unknown temperature and comparing this resistance to the measured resistance at other known temperatures. The framework used for doing this comparison was the International Temperature Scale of 1990 (ITS-90) [23]. As the VLE measurements were carried out in the temperature range 223.14 to 303.16 K, the ITS-90 calibrations were performed in the subrange defined by the triple point of mercury ($T_{90} \equiv 234.3156$ K), triple point of water ($T_{90} \equiv 273.16$ K) and the melting point of gallium ($T_{90} \equiv 302.9146$ K). The ITS-90 deviation function for this subrange (Section 3.3.3 in [23]) have been used together with the ITS-90 reference functions W_r (Eqs. 9a and 10a in [23]) to calculate the ITS-90 temperatures T_{90}. The extrapolation of this deviation function to 303.16 K, 0.24 K above the gallium melting point, was assumed to give negligible contribution to the temperature uncertainty. According to [56], the extrapolation of the deviation function to 223.14 K, 11 K below the mercury triple point is not advised when the utmost accurate temperature measurements are to be taken.

The resistance of the SPRT at a certain temperature was measured using an ASL F650AC Thermometry Bridge, together with a external Tinsley 5685A resistance normal placed inside a Tinsley 5648 temperature-controlled enclosure as reference. The measured input quantity was the bridge ratio:

$$W_b = \frac{R(T_{90})}{R_{ref}}\,, \tag{A.9}$$

where $R(T_{90})$ is the resistance of the SPRT at the unknown ITS-90 temperature T_{90}, and R_{ref} is the resistance of the Tinsley resistance normal. The resistance normal was calibrated inside the temperature-controlled enclosure by the Norwegian national metrology service Justervesenet on 2012-04-12. The calibration certificate stated $R_{ref} = 24.998\,982\,\Omega$ with a standard uncertainty of $u(R_{ref}, 1) = 6 \cdot 10^{-6}\,\Omega$. Taking into account the temperature stability of the enclosure and its effect on the resistance of the resistance normal, and the long term stability of the resistance, the total standard uncertainty at the time of use was estimated using Eq. (5a) to be $u(R_{ref}) = 8.5 \cdot 10^{-6}\,\Omega$.

The uncertainty $u(T_{90})$ in the calculated temperature T_{90} can be stated as

$$u(T_{90}) = \left| u(W_r(T_{90})) \cdot [\partial T_{90}/\partial W_r(T_{90})] \right|\,, \tag{A.10}$$

where $W_r(T_{90})$ is the ITS-90 reference function calculated based on the resistance of the SPRT at the calculated temperature and the resistance of the SPRT at the calibration points. Two reference functions were given in the ITS-90, and which one to use depends on the temperature. The derivative was obtained analytically as the inverse of $\partial W_r(T_{90})/\partial T_{90}$. For details, please refer to [23].

The simplified framework for uncertainty estimation of an ITS-90 temperature prepared by the Measurement Standards Laboratory of New Zealand [57] was used in the present work. To be able to use their simplified analysis, some requirements must be fulfilled.

The measurements on the calibration points should be performed using the same thermometry bridge. The calibrations were performed in-situ with the same bridge as used in the VLE measurements, so this requirement was fulfilled.

The uncertainty in the measurement of the ratio of Eq. (A.9) should be negligible. The ASL thermometry bridge specified accuracy in the ratio measurements was $6 \cdot 10^{-7}$. For the current value of R_{ref}, this corresponded to approximately 0.16 mK. Assuming a rectangular distribution gave $u(W_b) = 0.6 \cdot 10^{-6}/\sqrt{3} \approx 0.35 \cdot 10^{-6}$. The resolution of the ratio measurements was $1 \cdot 10^{-7}$, or approximately 0.025 mK, so the last digit should not be considered significant during the measurements. When uncertainties in the resistance measurements below 0.16 mK were considered to be negligible, this requirement was also satisfied.

The uncertainties in the ratio measurements at the triple point of water should be negligible. That is, the measured ratio of the SPRT when placed in the fixed point cell for the triple point of water was not significantly different from what it should have been if the SPRT was at the exact triple point temperature of water, defined in the ITS-90 to be 273.16 K. This offset can be caused by a number of reasons, which will be discussed here.

According to the calibration certificate of the water triple point cell, the standard uncertainty caused by the difference between the temperature of the water triple point cell and a reference cell at the National Physical Laboratory in England was 0.05 mK.

According to the specification of the cell, the temperature at the point where the SPRT is placed was approximately 0.2 mK lower than the true triple point temperature (273.16 K) due to the hydrostatic pressure effect.

The self-heating effect of the two SPRTs was checked at the triple point of water comparing the resistance at a measuring current of 1 mA and $1 \cdot \sqrt{2}$ mA according to the method of Veltcheva et al. [58], and the temperature at zero current was found to be approximately 0.6 mK lower than at the utilized measuring current 1 mA.

To ensure good heat transfer between the SPRT and the water triple point cell, the part of the cell well where the SPRT is placed was filled with distilled water during calibration.

Also, the temperature of the SPRT can be higher than the triple point temperature in the cell if heat is transferred from the surroundings down into the thermometer well. The triple point cell was placed inside an insulated dewar during calibration to minimize this effect.

The effect of both hydrostatic pressure and self-heating can be minimized by correcting the measured resistance. However, these effects were quite small, so the uncorrected resistances were used, and a rectangular distribution was assumed for these effects. The total standard uncertainty of the measurement of the water triple point temperature was estimated using Eq. (5b) as $u(T_{H_2O}) \approx 0.51$ mK.

The assumptions can be said to be fulfilled, and the standard uncertainty in the ITS-90 ratio $W(T_{90}) = R(T_{90})/R_{\mathrm{H_2O}}$ at an unknown temperature T_{90} could be expressed as [57]

$$\begin{aligned} u^2(W) &= f\left(u(R), u(R_{H_2O}), u(T,\mathrm{diff}), u(T_{H_2O})\right) \\ &= \left(\left.\frac{\partial W}{\partial R}\right|_{T_{90}} u(R)\right)^2 + \left(\left.\frac{\partial W}{\partial R_{H_2O}}\right|_{T_{90}} u(R_{H_2O})\right)^2 \\ &+ \left(\left.\frac{\partial W}{\partial T_{90}}\right|_{T_{90}} u(T,\mathrm{diff})\right)^2 + \left(\left.\frac{\partial W}{\partial T_{H_2O}}\right|_{T_{90}} u(T_{H_2O})\right)^2 \\ &\approx \left(\frac{1}{R_{H_2O}} u(R)\right)^2 + \left(\frac{W}{R_{H_2O}} u(R_{H_2O})\right)^2 \\ &+ \left(\left.\frac{\partial W_r}{\partial T_{90}}\right|_{T_{90}} u(T,\mathrm{diff})\right)^2 + \left(W \left.\frac{\partial W_r}{\partial T_{90}}\right|_{T_{90}} u(T_{H_2O})\right)^2 , \end{aligned} \tag{A.11}$$

where $u(R)$ and $u(R_{\mathrm{H_2O}})$ are the standard uncertainty in the resistance measurement at the unknown temperature and at the triple point of water. They were calculated as $u_R = \left|R_{\mathrm{ref}} \cdot u(W_{\mathrm{b}})\right| + \left|W_{\mathrm{b}} \cdot u(R_{\mathrm{ref}})\right|$.

$u(T,\mathrm{diff})$ is the uncertainty caused by the SPRT being at a temperature other than the one we want to measure, and this is usually the largest contribution to the total uncertainty in a temperature measurement. For the mercury triple point and the gallium melting point calibration points, this is equal to $u(T_{\mathrm{Hg}})$ and $u(T_{\mathrm{Ga}})$, and they were evaluated in the same way as for $u(T_{\mathrm{H_2O}})$. At an unknown temperature during the VLE experiments, this uncertainty was assumed to be equal to the difference between the measured temperatures of the two SPRTs and was modeled using a rectangular distribution: $u(T,\mathrm{diff}) = \left|T_{04} - T_{05}\right|/\sqrt{3}$.

The drift in the resistance can be controlled by performing regular calibration of the SPRT at the fixed points. The effect on the SPRT not being at the temperature we are trying to measure can only be controlled by ensuring the best possible heat transfer between the cell contents, which has the temperature we want to measure, and the SPRT. This can be ensured by, for example, avoiding having stagnant air surrounding the SPRT in the pocket in which it is placed. In the experimental setup, we had two SPRTs, one placed in the top flange and one in the bottom flange. Aluminium oxide powder was placed around the SPRTs in the pockets in which they were placed, to ensure good heat transfer to the titanium in the cell flanges. By having two sensors at these locations, we could be more certain that the temperatures measured by the SPRTs represented the temperature of the fluid inside the cell.

The standard uncertainty of the calculated reference function value is expressed as [57]

$$\begin{aligned} u^2(W_{\mathrm{r}}(T_{90})) &= u^2(W) \\ &+ u^2(W_{\mathrm{Hg}},\mathrm{tot}) + u^2(W_{\mathrm{Ga}},\mathrm{tot}) . \end{aligned} \tag{A.12}$$

Here,

$$u^2(W_{\mathrm{Hg}},\mathrm{tot}) = \left[\frac{(W-1)\cdot(W-W_{\mathrm{Ga}})}{(W_{\mathrm{Hg}}-1)\cdot(W_{\mathrm{Hg}}-W_{\mathrm{Ga}})}\right]^2 \cdot u^2(W_{\mathrm{Hg}}) , \tag{A.13}$$

and

$$u^2(W_{\mathrm{Ga}},\mathrm{tot}) = \left[\frac{(W-1)\cdot(W-W_{\mathrm{Hg}})}{(W_{\mathrm{Ga}}-1)\cdot(W_{\mathrm{Ga}}-W_{\mathrm{Hg}})}\right]^2 \cdot u^2(W_{\mathrm{Ga}}) , \tag{A.14}$$

where $u(W_{\mathrm{Hg}})$ and $u(W_{\mathrm{Ga}})$ were evaluated using Eq. (A.11).

Appendix A.2.1. Total uncertainty in cell temperature T

The discussion in the previous section concerns the uncertainty analysis of one of the two SPRTs used to measure the temperature, T_{04} and T_{05}. When the contents of the cell is at VLE, the temperature at the vapor/liquid interface, designated T, should be somewhere between the temperatures in the top flange, T_{04}, and in the bottom flange, T_{05}. This will be a reasonable assumption if the temperature of the thermostatic bath fluid is sufficiently uniform and stable in the heat transfer regions between the cell and the bath fluid. The uniformity and stability can be investigated by measuring the temperature around the perimeter of the cell seen from above and at different vertical positions ranging from the position of the top flange to the bottom flange.

Given that the uniformity and stability in these regions are sufficient, the VLE temperature can be approximated using the arithmetic mean of the two measured temperatures

$$T = \frac{T_{04} + T_{05}}{2} . \tag{A.15}$$

T_{04} and T_{05} can not be assumed to be independent, so the uncertainty in T must be expressed as

$$\begin{aligned} u(T) &= \left|u(T_{04})\frac{\partial T}{\partial T_{04}}\right| + \left|u(T_{05})\frac{\partial T}{\partial T_{05}}\right| \\ &= \left|u(T_{04})/2\right| + \left|u(T_{05})/2\right| . \end{aligned} \tag{A.16}$$

Appendix A.3. Uncertainty analysis of composition

The VLE composition analysis was performed using a GC, which was calibrated using gas mixtures with composition known to high accuracy. These mixtures were gravimetrically prepared using a custom-built rig in our laboratories at NTNU and SINTEF Energy Research [17], with adherence to the ISO standard [59]. The uncertainty of the VLE composition analysis has contributions from a range of sources, including the impurities of the gases used to prepare the calibration mixtures, the uncertainty in the molar masses, inaccuracies in the weighed masses, adsorption, repeatability / uncertainties of the sampling and GC analysis, and finally the consistency between the GC calibration function and data.

Appendix A.3.1. Composition calibration procedure

Each calibration gas was filled into the cell using the impurity pump shown in Fig. 1. The cell, pump and lines leading to the cell were kept at 313 K, to ensure that the calibration gas was in single phase. Using the same procedure as described in Section 2.3, the impurity pump and lines were first evacuated once, then flushed with the calibration gas to dilute any remaining impurities in the lines and pumps. This evacuation and flushing was repeated 5 times. After the final evacuation, the calibration gas was filled onto the impurity pump and connected lines, and maintained at a pressure of at least 0.5 MPa to prevent contamination of the gas.

The next step was to flush the cell with the calibration gas from the impurity pump and then evacuate. As with the pump, this process was repeated 5 times to remove most of the remaining impurities in the cell. After the final evacuation of the cell, the cell was flushed with the calibration gas once more, to minimize the effects of surface adsorption of the components in the calibration gas. The cell was then filled to different pressures in the range of 5 to 10 MPa.

Samples of varying sizes were withdrawn from the cell at various pressures. These samples formed the basis for the calibration of the composition analysis, giving a relation between the CO_2 mole fractions of the calibration gas mixtures and the GC detector response.

Appendix A.3.2. Source gas composition and molar mass

When preparing a calibration mixture gravimetrically, the composition and its uncertainty are affected by both the molar mass and purity of the source gases. According to [60, 61], the molar masses of monoatomic carbon C, monoatomic oxygen O in commercial tank gas CO_2 and monoatomic nitrogen N in commercial tank gas N_2 generally lie within ranges of width 0.6, 0.15, and 0.05 mg mol^{-1}, respectively. The arithmetic mean values of these ranges were used as the molar masses of the atomic elements, and, as a conservative estimate, the half width of the ranges used as standard uncertainties in the atomic element molar masses. The standard uncertainty in the molecular molar masses of CO_2 and N_2 were calculated using Eq. (3). The molar masses M_{CO_2}, M_{N_2} and uncertainties are summarized in Table A.1. As can be seen, the relative uncertainties of M_{CO_2} and M_{N_2} were of the order of 10 and 1 ppm, respectively. The minimum certified purities of the CO_2 and N_2 gas sources used to prepare the calibration gas mixtures are provided in Table 1. Moreover, the maximum content of certain impurities were specified by the providers of the CO_2 and N_2 gas. Due to impurities, the molar masses of these gases were not exactly equal to the molar masses of CO_2 and N_2, respectively. For the CO_2 gas, the maximum specified impurity content by volume was less than 2 ppm H_2O, 1 ppm O_2, 5 ppm N_2, 1 ppm hydrocarbons C_nH_m and 1 ppm H_2. For the N_2 gas, less than 0.5 ppm H_2O, 0.1 ppm O_2, 0.1 ppm hydrocarbons C_nH_m and 0.5 ppm CO_2 and CO have been specified.

Table A.1
Molar masses of atomic elements and compounds. Data from [60, 61].

Component i	M_i	$u(M_i)$	Unit
C	0.0120108	0.0000003	kg mol^{-1}
O	0.01599938	0.00000007	kg mol^{-1}
N	0.01400673	0.00000002	kg mol^{-1}
CO_2	0.0440096	0.0000003	kg mol^{-1}
N_2	0.02801345	0.00000005	kg mol^{-1}
CO_2+imp	0.0440094		kg mol^{-1}
N_2+imp	0.02801345		kg mol^{-1}

Since the composition of the CO_2 and N_2 source gases was not known, but only their minimum purities and maximum concentrations of some impurities, it was assumed that completely pure gases and maximum impurity were equally probable. More specifically, it was assumed that the standard uncertainty of the purity of the source gases equaled half the maximum certified impurity fraction and estimated that the actual purity level was the minimum purity plus this standard uncertainty. Furthermore, it was assumed that the concentration of each impurity component was proportional to its maximum fraction provided in the gas specifications. With the mole fractions of the different components set, the molar mass of the sample of component $i = CO_2$ or N_2 could be estimated as

$$M_{i+\text{imp}} = y_{i,\text{ in sample}} \cdot M_i + \sum_{j=\text{impurities}} y_{j,\text{ in sample}} \cdot M_j \,. \quad \text{(A.17)}$$

The molar mass M_j of each impurity j was calculated using data from Wieser et al. [61], assuming methane CH_4 for the hydrocarbon impurity specification, and the mean value of the molar mass of CO_2 and CO for the impurity specification was used where these two components were combined. The calculated molar masses $M_{CO_2+\text{imp}}$ and $M_{N_2+\text{imp}}$ of the gas samples are shown in Table A.1. The effective molar mass of each component $i = CO_2$ or N_2 could be written as

$$M_{i,\text{eff}} = \frac{M_{i+\text{imp}}}{y_{i,\text{ in sample}}} = M_i + \frac{\left(1 - y_{i,\text{ in sample}}\right) M_{\text{imp}}}{y_{i,\text{ in sample}}} \,, \quad \text{(A.18)}$$

where

$$M_{\text{imp}} = \frac{\sum_{j=\text{impurities}} y_{j,\text{ in sample}} \cdot M_j}{1 - y_{i,\text{ in sample}}} \,. \quad \text{(A.19)}$$

Appendix A.3.3. Gravimetric preparation

As described in [17], the calibration gas mixtures were prepared by injecting CO_2 and N_2 consecutively into the calibration gas cylinder and weighing the cylinder accurately using a comparator with certified weights before and after each gas injection. Based on the discussion in Appendix A.3.2 above, the resulting masses of each component, $i = CO_2$ and N_2, with impurities were converted into moles, excluding impurities, using Eq. (A.18):

$$n_i = m_{i+\text{imp}}/M_{i,\text{eff}} \,. \tag{A.20}$$

Both the numerator and denominator in Eq. (A.20) contribute to uncertainty. The uncertainty in mass $m_{i+\text{imp}}$ was a function of a range of factors, including the repeatability of the ABBA mass comparisons, the uncertainty in the buoyancy correction, the uncertainty in the OIML masses, where the repeatability was the dominating contributor. Using the fact that $y_{CO_2\text{ in sample}}$ was close to unity, it can be shown that the uncertainty term from the effective molar mass, $M_{i,\text{eff}}$, to the first order can be estimated by

$$u\left(n_i, \mathrm{M_{eff}}\right) = n_i \cdot \frac{\sqrt{4u^2(y_{i,\text{ in sample}})M_{\text{imp}}^2 + u^2(M_i)}}{M_i} \,, \tag{A.21}$$

where

$$u(y_{i,\text{ in sample}}) = 1 - y_{i,\text{ in sample}} \,. \tag{A.22}$$

Note that the definition in Eq. (A.22) is a formalization of the assumptions made with regards to source gas purity uncertainty discussed in Appendix A.3.2.

Appendix A.3.4. Sampling and estimated composition uncertainty

As discussed in Appendix A.3.1, each of the calibration gas mixtures was filled onto the cell to calibrate the GC. The cell was kept at 313.15 K to ensure that the contents of the cell were in a uniform supercritical state. Samples were taken from the VLE cell using both the liquid and vapor Rolsi$^{\text{TM}}$ samplers with different opening times to get samples which spanned the expected sample size during VLE experiments. 7 samples were taken for each selected combination of calibration gas mixture, sampler, and sampler opening time. The first 2 samples were discarded as flushing samples, leaving 5 valid samples. The uncertainty of the calibration mixture uncertainty reaching the GC could be estimated as

$$u_c(y_{CO_2,\text{cal}}) = \sqrt{u^2(y_{CO_2,\text{cal}}, m) + u^2(y_{CO_2,\text{cal}}, M_{\text{eff}}) + u^2(y_{CO_2,\text{cal}}, \text{ads.})} \,, \tag{A.23}$$

where

$$u(y_{CO_2,\text{cal}}, m) = \frac{u(n_{CO_2}, m) \cdot n_{CO_2} + u(n_{N_2}, m) \cdot n_{N_2}}{\left(n_{CO_2} + n_{N_2}\right)^2} \tag{A.24}$$

$$u(y_{CO_2,\text{cal}}, M_{\text{eff}}) = \frac{\sqrt{u^2(n_{CO_2}, M_{\text{eff}}) \cdot n_{CO_2}^2 + u^2(n_{N_2}, M_{\text{eff}}) \cdot n_{N_2}^2}}{\left(n_{CO_2} + n_{N_2}\right)^2} \,. \tag{A.25}$$

Note that due to the measurement procedure, where the value readings of the scale between the two gas component fillings are used both to calculate the mass of N_2 and CO_2, the deviations in the measured masses of the two components can be negatively correlated, leading to a positive correlation with respect to the impact mole fractions. With reference to Section 3.1, Eq. (A.24) provides a conservative estimate.

The third term in Eq. (A.23), $u(y_{CO_2,\text{cal}}, \text{ads.})$, was the contribution to uncertainty from adsorption. It is expected that CO_2 should be adsorbed by metallic surfaces to a small degree, but higher than N_2, but little work has been dedicated to quantify this effect. Leuenberger et al. [62] performed experiments with mixtures including CO_2 on commercial steel and aluminium gas cylinders. No polishing was performed in the experiments. Their measurements indicated that CO_2 formed at most a molecular monolayer on steel bottles using a model ignoring surface roughness. In our case, the pump and most of the piping were sulfinert treated and were expected to have minimum adsorption. Also the cell was expected to have little adsorption. Nevertheless, it was assumed monolayer adsorption in both the cylinders where the calibration mixtures were prepared and in the cell, and the maximum estimated adsorption of CO_2 in the gas cylinder and cell became:

$$\Delta n_{CO_2,\text{max.ads.,cyl.}} = \frac{A_{\text{cyl.}}}{A_{CO_2} \cdot N_A} \,, \tag{A.26}$$

$$\Delta n_{CO_2,\text{max.ads.,cell}} = \frac{A_{\text{cell}}}{A_{CO_2} \cdot N_A} \,. \tag{A.27}$$

Here, $A_{CO_2} \cdot N_A$ is the surface area of a monolayer of one mole of CO_2. $A_{\text{cyl.}}$ and A_{cell} are the inner surface areas of the gas cylinder and VLE cell, respectively. The adsorption will vary depending on unknown experimental conditions, in particular the unknown surface roughness of the gas cylinder. For simplicity, the uncertainty was here estimated based on the adsorption level provided by Eqs. (A.26) and (A.27):

$$u(y_{CO_2,\text{cal}}, \text{ads.}) = \frac{\Delta n_{CO_2,\text{max.ads.,cyl.}} \cdot n_{CO_2,\text{cyl.}}}{\left(n_{CO_2,\text{cyl.}} + n_{N_2,\text{cyl.}}\right)^2} + \frac{\Delta n_{CO_2,\text{max.ads.,cell}} \cdot n_{CO_2,\text{cell}}}{\left(n_{CO_2,\text{cell}} + n_{N_2,\text{cell}}\right)^2} \,, \tag{A.28}$$

where $n_{i,j}$ is the number of mole of component i in vessel j. The mole values in the cell were calculated using the GERG-2008 at 5 bar pressure. As seen in Table A.2, this estimate for adsorption uncertainty contribution was of the same order as the other uncertainties for the calibration gas, and, as will be seen later, the adsorption would have to be order of magnitudes larger than assumed in order to be of significance for the final VLE data.

Appendix A.3.5. GC integration and calibration function

The areas under the CO_2 and N_2 peaks in the GC response curve, designated A_{CO_2} and A_{N_2}, were obtained for each sample by careful numerical integration. If the detector response

were ideal, the area of each component should be proportional to the number of moles of each component having passed through the detector. However, because of nonlinearities in the detector response, the following model consisting of a linear and a nonlinear term was found to give an adequate description of the relation between moles of each component in the sample to the area of each component:

$$\hat{n}_{\mathrm{CO_2}} \cdot k = A_{\mathrm{CO_2}} + c_2 \cdot (A_{\mathrm{CO_2}})^{c_4} \,, \tag{A.29}$$

$$\hat{n}_{\mathrm{N_2}} \cdot k = c_1 \cdot A_{\mathrm{N_2}} + c_3 \cdot (A_{\mathrm{N_2}})^{c_5} \,, \tag{A.30}$$

$$\hat{y}_{\mathrm{CO_2,cal}} = \frac{\hat{n}_{\mathrm{CO_2}}}{\hat{n}_{\mathrm{CO_2}} + \hat{n}_{\mathrm{N_2}}} \,. \tag{A.31}$$

where the $\hat{y}_{\mathrm{CO_2,cal}}$ is the estimator of the CO_2 mole fraction for a calibration gas mixture given the areas for the current sample, and c_i for $i = 1$ through 5 are the parameters of the model. k is an unknown factor relating the areas to the number of moles. However, this factor was not of interest, as only the mole fraction was of interest. For each series of 5 valid samples, the mean value and sample standard deviation of the estimator, $\bar{\hat{y}}_{\mathrm{CO_2,cal}}$ and $s(\bar{\hat{y}}_{\mathrm{CO_2,cal}})$, were calculated.

The parameters c_i were fitted by performing the following weighted least squares minimization of the objective function S:

$$\min_{c_i} S(c_i) = \sum_{\text{series}} \left(\frac{y_{\mathrm{CO_2,cal}} - \bar{\hat{y}}_{\mathrm{CO_2,cal}}}{\sqrt{u_c^2(y_{\mathrm{CO_2,cal}}) + s^2(\bar{\hat{y}}_{\mathrm{CO_2,cal}})}} \right)^2 . \tag{A.32}$$

The model was fitted against a total of $n = 47$ series (each series consisting of 5 samples), giving the parameter estimates found in Table A.3. As shown in Fig. A.2, the errors between the calibration gas CO_2 mole fractions and the model predictions, $e = y_{\mathrm{CO_2,cal}} - \bar{\hat{y}}_{\mathrm{CO_2,cal}}$, were randomly scattered around zero over the composition range $y_{\mathrm{CO_2,cal}}$, which indicated an appropriate model structure. The sample standard deviation of the errors, $s(e)$, are also given in Table A.3. This model was used to convert the areas resulting from the analysis of a composition sample taken during a VLE experiment into a CO_2 mole fraction.

Since $s(e)$ was about 20 to 40 times larger than the standard uncertainties of the CO_2 mole fractions of the calibration gases, given in Table A.2, it was assumed that $s(e)$ gave an estimate of the standard uncertainty of the CO_2 mole fraction arising from the composition analysis, $u(x_{\mathrm{CO_2}}) = u(y_{\mathrm{CO_2}})$. To be precise, $u(x_{\mathrm{CO_2}}) = u(y_{\mathrm{CO_2}})$ was the standard uncertainty of the CO_2 mole fraction of a composition sample taken from the cell, caused by the *analysis alone*, excluding all uncertainties caused by factors such as that the sample taken had a composition different from the VLE composition of the phase sampled at the current temperature and pressure. Factors such as these, and their influence, could in most cases not be known exactly, and could only be minimized by measures such as sufficient stirring of the cell contents until equilibrium had been reached, sufficient time for the phases to settle after stirring was completed, waiting for some time to let pressure and temperature gradients even out, taking

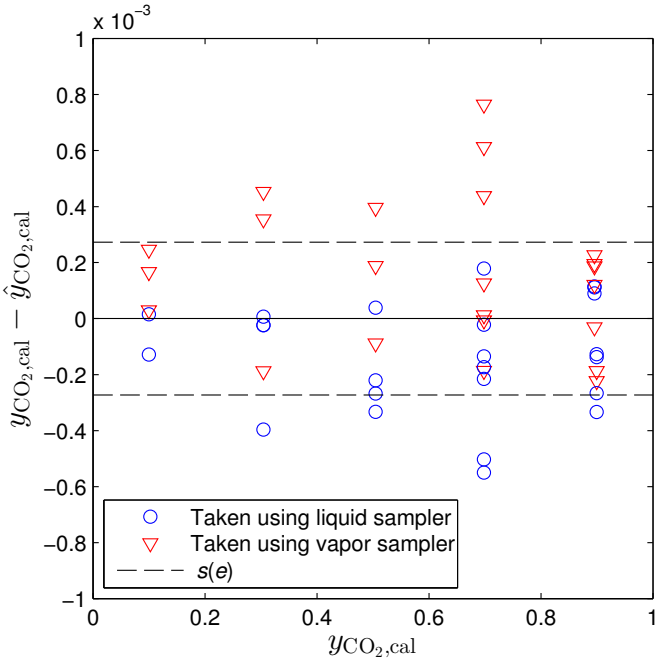

Fig. A.2. Composition calibration: Error between actual compositions in Table A.2 and composition model in Eq. (A.31), given as $y_{\mathrm{CO_2,cal}} - \hat{y}_{\mathrm{CO_2,cal}}$ versus $y_{\mathrm{CO_2,cal}}$. Composition analysis uncertainty $u(x_{\mathrm{CO_2}}) = u(y_{\mathrm{CO_2}}) = s(e)$ from Table A.3.

Table A.2
CO_2+N_2 calibration gas mixtures

$y_{\mathrm{CO_2,cal}}$	$u(y_{\mathrm{CO_2,cal}}, m)$	$u(y_{\mathrm{CO_2,cal}}, M_{\mathrm{eff}})$	$u(y_{\mathrm{CO_2,cal}}, \mathrm{ads.})$	$u_c(y_{\mathrm{CO_2,cal}})$
0.099737	$3.3 \cdot 10^{-6}$	$6.7 \cdot 10^{-6}$	$1.1 \cdot 10^{-6}$	$7.6 \cdot 10^{-6}$
0.304099	$4.8 \cdot 10^{-6}$	$4.1 \cdot 10^{-6}$	$3.4 \cdot 10^{-6}$	$7.2 \cdot 10^{-6}$
0.504479	$6.9 \cdot 10^{-6}$	$3.1 \cdot 10^{-6}$	$5.7 \cdot 10^{-6}$	$9.5 \cdot 10^{-6}$
0.698094	$6.9 \cdot 10^{-6}$	$4.5 \cdot 10^{-6}$	$7.8 \cdot 10^{-6}$	$11.4 \cdot 10^{-6}$
0.899263	$7.2 \cdot 10^{-6}$	$7.4 \cdot 10^{-6}$	$9.8 \cdot 10^{-6}$	$14.3 \cdot 10^{-6}$
0.895405	$4.4 \cdot 10^{-6}$	$7.4 \cdot 10^{-6}$	$9.8 \cdot 10^{-6}$	$13.0 \cdot 10^{-6}$

dummy samples to flush the contents of the Rolsi™ samplers before samples were assumed to represent the composition of the bulk of the phase sampled inside the cell, and the other measures described in Section 2.3.

Appendix A.3.6. Total uncertainty in liquid and vapor phase mole fractions $x_{\mathrm{CO_2}}$ and $y_{\mathrm{CO_2}}$

As described in Section 2.1, the composition of the phases at VLE was a function of T and p. Therefore, for a given set of measured T, p, $x_{\mathrm{CO_2}}$ and $y_{\mathrm{CO_2}}$ at VLE, the uncertainty of T and p contributed to additional uncertainty in the compositions, giving the following total standard uncertainty of the composition:

$$u_{\mathrm{tot}}(z_{\mathrm{CO_2}}) = \sqrt{u^2(z_{\mathrm{CO_2}}) + \left(u_c(\bar{T}) \cdot \frac{\partial z_{\mathrm{CO_2}}}{\partial T} \right)^2 + \left(u_c(\bar{p}) \cdot \frac{\partial z_{\mathrm{CO_2}}}{\partial p} \right)^2} , \tag{A.33}$$

where z_{CO_2} was equal to either x_{CO_2} or y_{CO_2}, and $u_c(\bar{T})$ and $u_c(\bar{p})$ were the experimental standard deviations of the mean of the temperature and pressure measurements taken before the composition sample was taken. The derivatives in Eq. (A.33) were calculated numerically from EOS-CG fitted to our data. Details about this is explained in Section 5.4.2.

Table A.3
Fitted parameters of the $\bar{\bar{y}}_{CO_2,cal}$ model and standard uncertainty of composition analysis $u(x_{CO_2}) = u(y_{CO_2})$.

Variable	Value
c_1	1.138 315
c_2	$6.799\,039 \cdot 10^{-5}$
c_3	$5.775\,209 \cdot 10^{-3}$
c_4	1.830 740
c_5	1.398 399
$u(x_{CO_2}) = u(y_{CO_2}) = s(e)$	$2.7269 \cdot 10^{-4}$
n	47

Appendix B. Detailed experimental data

Detailed VLE data for the liquid phase samples are given in Table B.2, and for the vapor phase samples in Table B.3. Each row in the tables corresponds to one composition sample. A series of samples taken at the same VLE experiment is identified by the same ID.

For ease of reading, a summary of the symbols used in the tables will be given in Table B.1. The descriptions can also be found in the list of symbols.

Table B.1
Summary of symbols used in Tables B.2 and B.3.

Symbol	Description
ID	Identifier for a series of samples. L, V and P corresponds to liquid, vapor and CO_2 vapor pressure series, respectively.
$\bar{T}$	Mean temperature before the sample is withdrawn from the cell. See Section 3.5.
$\bar{p}$	Mean pressure before the sample is withdrawn from the cell. See Section 3.5.
x_{CO_2}	Liquid phase CO_2 mole fraction of the sample.
y_{CO_2}	Vapor phase CO_2 mole fraction of the sample.
$s(T)$	Sample standard deviation of the measured temperatures used to calculate $\bar{T}$. See Eq. (7).
$s(\bar{T})$	Standard random uncertainty of $\bar{T}$. See Eq. (6).
$\bar{u}(T)$	Standard systematic uncertainty of $\bar{T}$. See Section 3.5.
$u_c(\bar{T})$	Combined standard uncertainty of $\bar{T}$. See Eq. (10).
$s(p)$	Sample standard deviation of the measured pressures used to calculate $\bar{p}$. See Eq. (7).
$s(\bar{p})$	Standard random uncertainty of $\bar{p}$. See Eq. (6).
$\bar{u}(p)$	Standard systematic uncertainty of $\bar{p}$. See Section 3.5.
$u_c(\bar{p})$	Combined standard uncertainty of $\bar{p}$. See Eq. (10).
$u(z_{CO_2})$[1]	Standard uncertainty of a sample from composition analysis alone. See Sections 3.4 and Appendix A.3.
$u_{tot}(z_{CO_2})$[1]	Total standard uncertainty of a sample, caused by additional contribution from the uncertainty in temperature and pressure. See Eq. (A.33).
$z_{CO_2,calc}$[1]	VLE CO_2 mole fraction at $(\bar{T}, \bar{p})$, calculated using the fitted version of EOS-CG. See Section 5.4.2.
$\partial z_{CO_2}/\partial T$[1]	Partial derivative of phase composition at VLE with respect to temperature. Used in Eq. (A.33).
$\partial z_{CO_2}/\partial p$[1]	Partial derivative of phase composition at VLE with respect to pressure. Used in Eq. (A.33).

[1] z_{CO_2} equal to either x_{CO_2} or y_{CO_2}.

Table B.2
Liquid phase: Experimental VLE data for $CO_2 + N_2$ at mean temperature $\bar{T}$, mean pressure $\bar{p}$, and sample liquid phase mole fraction x_{CO_2}.

	Data			Temperature				Pressure				Composition			Composition derivatives	
ID	$\bar{T}$	$\bar{p}$	x_{CO_2}	$s(T)$	$s(\bar{T})$	$\bar{u}(T)$	$u_c(\bar{T})$	$s(p)$	$s(\bar{p})$	$\bar{u}(p)$	$u_c(\bar{p})$	$u(x_{CO_2})$	$u_{tot}(x_{CO_2})$	$x_{CO_2,calc}$	$\partial x_{CO_2}/\partial T$	$\partial x_{CO_2}/\partial p$
	(K)	(MPa)	(-)	(K)	(K)	(K)	(K)	(MPa)	(MPa)	(MPa)	(MPa)	(-)	(-)	(-)	(K^{-1})	(MPa^{-1})
P1	223.138	0.6829	0.99999	5.8e-4	5.3e-5	2.5e-3	2.5e-3	1.5e-5	2.5e-6	5.0e-4	5.0e-4					
L1	223.140	1.9355	0.98155	1.1e-3	7.6e-5	2.4e-3	2.4e-3	4.3e-5	3.9e-6	5.2e-4	5.2e-4	2.7e-4	2.7e-4	0.98346	0.00025	-0.01359
	223.139	1.9354	0.98158	9.2e-4	9.6e-5	2.4e-3	2.4e-3	3.6e-5	5.5e-6	5.2e-4	5.2e-4	2.7e-4	2.7e-4	0.98347	0.00025	-0.01359
	223.140	1.9353	0.98156	5.3e-4	3.7e-5	2.5e-3	2.5e-3	2.4e-5	1.9e-6	5.2e-4	5.2e-4	2.7e-4	2.7e-4	0.98347	0.00025	-0.01359
L2	223.138	4.3474	0.94421	6.9e-4	9.6e-5	2.6e-3	2.6e-3	6.8e-5	2.0e-5	1.1e-3	1.1e-3	2.7e-4	2.7e-4	0.94894	0.00000	-0.01510
	223.138	4.3470	0.94421	8.0e-4	8.4e-5	2.6e-3	2.6e-3	7.7e-5	1.9e-5	1.1e-3	1.1e-3	2.7e-4	2.7e-4	0.94895	0.00000	-0.01510
	223.138	4.3466	0.94423	7.7e-4	9.6e-5	2.6e-3	2.6e-3	8.1e-5	2.7e-5	1.1e-3	1.1e-3	2.7e-4	2.7e-4	0.94895	0.00000	-0.01510
	223.138	4.3462	0.94422	1.4e-3	2.5e-4	2.6e-3	2.6e-3	6.6e-5	1.4e-5	1.1e-3	1.1e-3	2.7e-4	2.7e-4	0.94896	0.00000	-0.01510
L3	223.139	5.0305	0.93311	6.3e-4	7.0e-5	3.4e-3	3.4e-3	7.0e-5	1.4e-5	1.1e-3	1.1e-3	2.7e-4	2.7e-4	0.93846	-0.00008	-0.01560
	223.139	5.0296	0.93313	5.2e-4	3.9e-5	3.3e-3	3.3e-3	5.4e-5	4.7e-6	1.1e-3	1.1e-3	2.7e-4	2.7e-4	0.93847	-0.00008	-0.01559
	223.140	5.0287	0.93314	4.7e-4	6.2e-5	3.5e-3	3.5e-3	7.4e-5	2.0e-5	1.1e-3	1.1e-3	2.7e-4	2.7e-4	0.93849	-0.00008	-0.01559
	223.140	5.0278	0.93315	4.4e-4	1.9e-5	3.2e-3	3.2e-3	9.2e-5	3.4e-5	1.1e-3	1.1e-3	2.7e-4	2.7e-4	0.93850	-0.00008	-0.01559
	223.139	5.0270	0.93316	4.3e-4	2.3e-5	3.5e-3	3.5e-3	7.5e-5	2.3e-5	1.1e-3	1.1e-3	2.7e-4	2.7e-4	0.93851	-0.00008	-0.01559
L4	223.143	6.0998	0.91555	4.7e-4	2.8e-5	5.4e-3	5.4e-3	1.0e-4	1.7e-5	1.1e-3	1.1e-3	2.7e-4	2.7e-4	0.92134	-0.00022	-0.01644
	223.143	6.0987	0.91555	5.4e-4	1.3e-4	5.5e-3	5.5e-3	1.1e-4	3.6e-5	1.1e-3	1.1e-3	2.7e-4	2.7e-4	0.92135	-0.00022	-0.01644
	223.142	6.0976	0.91557	4.4e-4	1.1e-4	5.6e-3	5.6e-3	9.2e-5	1.9e-5	1.1e-3	1.1e-3	2.7e-4	2.7e-4	0.92137	-0.00022	-0.01645
	223.142	6.0965	0.91560	4.0e-4	2.8e-5	5.4e-3	5.4e-3	1.1e-4	2.5e-5	1.1e-3	1.1e-3	2.7e-4	2.7e-4	0.92139	-0.00022	-0.01644
	223.142	6.0954	0.91558	4.8e-4	6.7e-5	5.6e-3	5.6e-3	9.2e-5	1.7e-5	1.1e-3	1.1e-3	2.7e-4	2.7e-4	0.92141	-0.00022	-0.01646
L5	223.141	7.0010	0.90034	5.3e-4	5.2e-5	5.4e-3	5.4e-3	1.1e-4	2.5e-5	1.1e-3	1.1e-3	2.7e-4	2.7e-4	0.90617	-0.00035	-0.01723
	223.142	6.9995	0.90037	5.2e-4	5.1e-5	5.6e-3	5.6e-3	1.3e-4	4.0e-5	1.1e-3	1.1e-3	2.7e-4	2.7e-4	0.90619	-0.00035	-0.01723
	223.141	6.9979	0.90042	4.8e-4	3.9e-5	5.4e-3	5.4e-3	1.2e-4	2.8e-5	1.1e-3	1.1e-3	2.7e-4	2.7e-4	0.90622	-0.00035	-0.01723
	223.141	6.9963	0.90045	4.6e-4	4.1e-5	5.3e-3	5.3e-3	1.8e-4	6.9e-5	1.1e-3	1.2e-3	2.7e-4	2.7e-4	0.90625	-0.00035	-0.01723
	223.141	6.9949	0.90046	6.8e-4	1.2e-4	5.3e-3	5.3e-3	1.3e-4	4.1e-5	1.1e-3	1.1e-3	2.7e-4	2.7e-4	0.90627	-0.00035	-0.01723
L6	223.139	8.1168	0.88107	9.3e-4	6.4e-5	4.6e-3	4.6e-3	1.6e-4	5.5e-5	1.2e-3	1.2e-3	2.7e-4	2.7e-4	0.88634	-0.00053	-0.01833
	223.139	8.1152	0.88108	1.3e-3	4.0e-4	5.1e-3	5.1e-3	1.4e-4	2.9e-5	1.2e-3	1.2e-3	2.7e-4	2.7e-4	0.88637	-0.00053	-0.01833
	223.140	8.1132	0.88110	8.2e-4	2.1e-4	5.5e-3	5.5e-3	1.9e-4	6.8e-5	1.2e-3	1.2e-3	2.7e-4	2.7e-4	0.88641	-0.00053	-0.01833
L7	223.140	8.7875	0.86896	1.2e-3	1.0e-4	3.4e-3	3.4e-3	1.9e-4	6.5e-5	1.3e-3	1.3e-3	2.7e-4	2.7e-4	0.87380	-0.00065	-0.01903
	223.140	8.7845	0.86901	9.9e-4	1.2e-4	3.3e-3	3.3e-3	1.4e-4	1.9e-5	1.3e-3	1.3e-3	2.7e-4	2.7e-4	0.87386	-0.00065	-0.01906
	223.140	8.7814	0.86907	8.8e-4	2.5e-4	3.3e-3	3.3e-3	1.6e-4	3.2e-5	1.3e-3	1.3e-3	2.7e-4	2.7e-4	0.87392	-0.00065	-0.01906
	223.140	8.7784	0.86913	5.6e-4	7.7e-5	3.3e-3	3.3e-3	1.2e-4	1.6e-5	1.3e-3	1.3e-3	2.7e-4	2.7e-4	0.87397	-0.00065	-0.01906
	223.140	8.7756	0.86920	5.4e-4	6.5e-5	3.3e-3	3.3e-3	1.4e-4	3.3e-5	1.3e-3	1.3e-3	2.7e-4	2.7e-4	0.87403	-0.00065	-0.01905
L8	223.139	9.2282	0.86102	1.0e-3	4.1e-4	6.2e-3	6.2e-3	2.0e-4	8.3e-5	1.4e-3	1.4e-3	2.7e-4	2.7e-4	0.86529	-0.00074	-0.01959
	223.140	9.2257	0.86108	6.3e-4	1.3e-4	6.0e-3	6.0e-3	2.3e-4	9.7e-5	1.4e-3	1.4e-3	2.7e-4	2.7e-4	0.86533	-0.00074	-0.01958
	223.140	9.2232	0.86113	7.4e-4	1.2e-4	5.9e-3	5.9e-3	2.1e-4	8.7e-5	1.4e-3	1.4e-3	2.7e-4	2.7e-4	0.86538	-0.00074	-0.01958
	223.140	9.2208	0.86118	1.1e-3	1.5e-4	5.9e-3	5.9e-3	1.9e-4	4.9e-5	1.4e-3	1.4e-3	2.7e-4	2.7e-4	0.86543	-0.00074	-0.01958
	223.140	9.2182	0.86120	5.9e-4	9.9e-5	5.8e-3	5.8e-3	2.3e-4	9.9e-5	1.4e-3	1.4e-3	2.7e-4	2.7e-4	0.86548	-0.00074	-0.01957
L9	223.141	9.8378	0.85046	6.2e-4	9.4e-5	5.1e-3	5.1e-3	1.4e-4	1.2e-5	2.7e-3	2.7e-3	2.7e-4	2.8e-4	0.85311	-0.00087	-0.02036
	223.141	9.8334	0.85046	6.0e-4	9.7e-5	5.2e-3	5.2e-3	1.5e-4	1.5e-5	2.7e-3	2.7e-3	2.7e-4	2.8e-4	0.85320	-0.00087	-0.02035
	223.141	9.8290	0.85043	4.1e-4	6.8e-5	5.3e-3	5.3e-3	1.2e-4	1.7e-5	2.7e-3	2.7e-3	2.7e-4	2.8e-4	0.85329	-0.00087	-0.02035
	223.142	9.8249	0.85042	4.9e-4	7.9e-5	5.3e-3	5.3e-3	1.1e-4	1.0e-5	2.7e-3	2.7e-3	2.7e-4	2.8e-4	0.85338	-0.00087	-0.02034
	223.141	9.8207	0.85040	6.3e-4	7.1e-5	5.3e-3	5.3e-3	1.4e-4	1.5e-5	2.7e-3	2.7e-3	2.7e-4	2.8e-4	0.85346	-0.00087	-0.02034
L10	223.140	10.8526	0.82961	5.0e-4	7.4e-5	3.6e-3	3.6e-3	1.6e-4	3.3e-5	2.7e-3	2.7e-3	2.7e-4	2.8e-4	0.83173	-0.00112	-0.02181
	223.140	10.8476	0.82965	5.5e-4	3.4e-5	3.7e-3	3.7e-3	1.4e-4	4.3e-5	2.7e-3	2.7e-3	2.7e-4	2.8e-4	0.83184	-0.00112	-0.02181
	223.140	10.8429	0.82978	5.0e-4	4.1e-5	3.6e-3	3.6e-3	1.8e-4	6.2e-5	2.7e-3	2.7e-3	2.7e-4	2.8e-4	0.83194	-0.00112	-0.02180
	223.140	10.8383	0.82979	6.2e-4	6.8e-5	3.6e-3	3.6e-3	1.4e-4	3.6e-5	2.7e-3	2.7e-3	2.7e-4	2.8e-4	0.83205	-0.00112	-0.02179
	223.140	10.8337	0.82986	6.1e-4	8.5e-5	3.6e-3	3.6e-3	1.3e-4	3.1e-5	2.7e-3	2.7e-3	2.7e-4	2.8e-4	0.83215	-0.00111	-0.02178
L11	223.142	10.8855	0.82906	5.0e-4	1.2e-4	5.5e-3	5.5e-3	3.4e-4	1.5e-4	2.7e-3	2.7e-3	2.7e-4	2.8e-4	0.83101	-0.00113	-0.02187
	223.142	10.8817	0.82913	5.3e-4	4.8e-5	5.3e-3	5.3e-3	4.0e-4	1.8e-4	2.7e-3	2.7e-3	2.7e-4	2.8e-4	0.83110	-0.00113	-0.02186

	223.142	10.8778	0.82920	4.9e-4	7.4e-5	5.5e-3	5.5e-3	3.3e-4	1.5e-4	2.7e-3	2.7e-3	2.7e-4	2.8e-4	0.83118	-0.00113	-0.02185
	223.142	10.8740	0.82927	7.0e-4	1.7e-4	5.3e-3	5.3e-3	3.6e-4	1.6e-4	2.7e-3	2.7e-3	2.7e-4	2.8e-4	0.83127	-0.00113	-0.02185
	223.142	10.8703	0.82937	5.3e-4	2.4e-5	5.5e-3	5.5e-3	4.3e-4	2.1e-4	2.7e-3	2.7e-3	2.7e-4	2.8e-4	0.83135	-0.00112	-0.02184
L12	223.142	12.0229	0.80523	4.8e-4	6.8e-5	5.6e-3	5.6e-3	2.6e-4	1.0e-4	2.7e-3	2.7e-3	2.7e-4	2.8e-4	0.80506	-0.00147	-0.02384
	223.143	12.0164	0.80533	6.2e-4	1.7e-4	5.6e-3	5.6e-3	1.9e-4	2.1e-5	2.7e-3	2.7e-3	2.7e-4	2.8e-4	0.80522	-0.00146	-0.02380
	223.143	12.0104	0.80544	4.9e-4	3.3e-5	5.4e-3	5.4e-3	1.8e-4	3.6e-5	2.7e-3	2.7e-3	2.7e-4	2.8e-4	0.80536	-0.00146	-0.02381
	223.143	12.0046	0.80558	4.7e-4	3.2e-5	5.5e-3	5.5e-3	2.0e-4	3.9e-5	2.7e-3	2.7e-3	2.7e-4	2.8e-4	0.80550	-0.00146	-0.02380
	223.143	11.9989	0.80570	9.0e-4	2.2e-4	5.4e-3	5.4e-3	2.2e-4	7.5e-5	2.7e-3	2.7e-3	2.7e-4	2.8e-4	0.80563	-0.00146	-0.02375
L13	223.137	14.9391	0.73298	1.2e-3	2.7e-4	3.2e-3	3.2e-3	1.4e-4	2.3e-5	2.8e-3	2.8e-3	2.7e-4	2.9e-4	0.72512	-0.00286	-0.03207
	223.138	14.9309	0.73320	1.3e-3	3.6e-4	3.1e-3	3.1e-3	1.4e-4	1.7e-5	2.8e-3	2.8e-3	2.7e-4	2.9e-4	0.72538	-0.00286	-0.03206
	223.138	14.9227	0.73343	8.0e-4	2.7e-4	2.9e-3	3.0e-3	1.8e-4	2.6e-5	2.8e-3	2.8e-3	2.7e-4	2.9e-4	0.72564	-0.00285	-0.03203
	223.137	14.9146	0.73365	1.3e-3	3.3e-4	2.9e-3	2.9e-3	1.5e-4	1.9e-5	2.8e-3	2.8e-3	2.7e-4	2.9e-4	0.72590	-0.00285	-0.03198
	223.138	14.9066	0.73389	1.1e-3	2.0e-4	2.9e-3	2.9e-3	1.8e-4	2.8e-5	2.8e-3	2.8e-3	2.7e-4	2.9e-4	0.72616	-0.00284	-0.03195
L14	223.140	15.9750	0.69976	4.9e-4	6.6e-5	2.9e-3	2.9e-3	1.6e-4	2.6e-5	2.8e-3	2.8e-3	2.7e-4	2.9e-4	0.68920	-0.00377	-0.03772
	223.140	15.9653	0.70011	5.1e-4	3.9e-5	2.9e-3	2.9e-3	1.5e-4	1.4e-5	2.8e-3	2.8e-3	2.7e-4	2.9e-4	0.68957	-0.00376	-0.03764
	223.140	15.9554	0.70043	7.2e-4	2.7e-5	2.8e-3	2.8e-3	1.9e-4	3.2e-5	2.8e-3	2.8e-3	2.7e-4	2.9e-4	0.68994	-0.00375	-0.03753
	223.140	15.9457	0.70082	4.7e-4	3.8e-5	2.9e-3	2.9e-3	2.1e-4	5.8e-5	2.8e-3	2.8e-3	2.7e-4	2.9e-4	0.69031	-0.00374	-0.03748
	223.140	15.9358	0.70117	4.6e-4	4.4e-5	2.8e-3	2.8e-3	1.9e-4	2.3e-5	2.8e-3	2.8e-3	2.7e-4	2.9e-4	0.69067	-0.00373	-0.03741
L15	223.137	17.2137	0.64760	9.5e-4	1.6e-4	2.9e-3	2.9e-3	3.1e-4	7.1e-5	2.8e-3	2.8e-3	2.7e-4	3.1e-4	0.63566	-0.00577	-0.05066
	223.138	17.2024	0.64820	1.2e-3	3.9e-4	2.9e-3	2.9e-3	3.1e-4	7.0e-5	2.8e-3	2.8e-3	2.7e-4	3.1e-4	0.63623	-0.00574	-0.05048
	223.137	17.1910	0.64881	1.5e-3	3.4e-4	2.8e-3	2.8e-3	1.7e-4	3.6e-5	2.8e-3	2.8e-3	2.7e-4	3.1e-4	0.63681	-0.00571	-0.05029
	223.137	17.1799	0.64938	1.4e-3	3.0e-4	2.8e-3	2.8e-3	2.9e-4	1.1e-4	2.8e-3	2.8e-3	2.7e-4	3.1e-4	0.63737	-0.00569	-0.05012
	223.138	17.1687	0.64996	1.2e-3	4.8e-4	2.7e-3	2.7e-3	2.8e-4	1.1e-4	2.8e-3	2.8e-3	2.7e-4	3.1e-4	0.63793	-0.00566	-0.04991
L16	223.138	18.1797	0.57071	7.6e-4	1.3e-4	2.7e-3	2.8e-3	2.4e-4	6.0e-5	2.8e-3	2.8e-3	2.7e-4	3.6e-4	0.57516	-0.01029	-0.08178
	223.139	18.1679	0.57251	5.3e-4	1.3e-4	2.6e-3	2.6e-3	2.2e-4	7.8e-5	2.8e-3	2.8e-3	2.7e-4	3.5e-4	0.57612	-0.01018	-0.08100
	223.139	18.1560	0.57425	6.5e-4	9.5e-5	2.7e-3	2.7e-3	1.9e-4	5.6e-5	2.8e-3	2.8e-3	2.7e-4	3.5e-4	0.57708	-0.01007	-0.08023
	223.139	18.1442	0.57594	7.2e-4	1.1e-4	2.9e-3	2.9e-3	2.1e-4	4.9e-5	2.8e-3	2.8e-3	2.7e-4	3.5e-4	0.57802	-0.00996	-0.07949
	223.138	18.1323	0.57755	8.1e-4	1.6e-4	2.6e-3	2.6e-3	2.7e-4	6.7e-5	2.8e-3	2.8e-3	2.7e-4	3.5e-4	0.57897	-0.00985	-0.07876
L17	269.996	9.5887	0.86031	1.1e-3	6.0e-5	6.1e-3	6.1e-3	3.7e-4	1.7e-4	1.4e-3	1.4e-3	2.7e-4	2.8e-4	0.85917	0.00078	-0.03037
	269.996	9.5855	0.86039	1.0e-3	1.0e-4	5.6e-3	5.6e-3	3.1e-4	1.3e-4	1.4e-3	1.4e-3	2.7e-4	2.8e-4	0.85927	0.00078	-0.03036
	269.996	9.5824	0.86047	1.0e-3	1.4e-4	5.7e-3	5.7e-3	2.3e-4	9.7e-5	1.4e-3	1.4e-3	2.7e-4	2.8e-4	0.85936	0.00078	-0.03034
	269.996	9.5793	0.86050	1.2e-3	1.1e-4	5.8e-3	5.8e-3	3.6e-4	1.6e-4	1.4e-3	1.4e-3	2.7e-4	2.8e-4	0.85946	0.00079	-0.03033
	269.996	9.5761	0.86061	1.3e-3	9.4e-5	5.5e-3	5.5e-3	3.7e-4	1.8e-4	1.4e-3	1.4e-3	2.7e-4	2.8e-4	0.85955	0.00079	-0.03031
P2	298.174	6.4369	0.99999	2.1e-4	1.9e-5	1.6e-3	1.6e-3	8.5e-5	8.0e-6	1.2e-3	1.2e-3					
L18	298.157	6.7092	0.99359	5.2e-4	7.9e-5	1.4e-3	1.4e-3	1.0e-4	2.9e-5	1.1e-3	1.1e-3	2.7e-4	2.7e-4	0.99370	0.00333	-0.02357
	298.158	6.7091	0.99358	7.6e-4	1.8e-4	1.4e-3	1.4e-3	1.0e-4	9.9e-6	1.1e-3	1.1e-3	2.7e-4	2.7e-4	0.99371	0.00333	-0.02357
	298.158	6.7089	0.99359	6.7e-4	2.6e-4	1.5e-3	1.5e-3	1.1e-4	2.1e-5	1.1e-3	1.1e-3	2.7e-4	2.7e-4	0.99372	0.00333	-0.02357
	298.158	6.7087	0.99359	5.7e-4	2.2e-4	1.5e-3	1.5e-3	1.1e-4	1.3e-5	1.1e-3	1.1e-3	2.7e-4	2.7e-4	0.99372	0.00333	-0.02357
L19	298.160	6.7192	0.99334	3.8e-4	3.1e-5	1.4e-3	1.4e-3	1.3e-4	2.2e-5	1.1e-3	1.1e-3	2.7e-4	2.7e-4	0.99348	0.00333	-0.02362
	298.160	6.7193	0.99334	3.4e-4	2.9e-5	1.4e-3	1.4e-3	8.6e-4	1.5e-4	1.1e-3	1.1e-3	2.7e-4	2.7e-4	0.99347	0.00333	-0.02362
L20	298.160	7.1004	0.98384	3.7e-4	5.2e-5	1.6e-3	1.6e-3	1.1e-4	1.7e-5	1.1e-3	1.1e-3	2.7e-4	2.7e-4	0.98411	0.00331	-0.02566
	298.160	7.1001	0.98385	4.8e-4	4.9e-5	1.6e-3	1.6e-3	1.8e-4	2.7e-5	1.1e-3	1.1e-3	2.7e-4	2.7e-4	0.98411	0.00331	-0.02566
	298.161	7.1005	0.98385	5.9e-4	1.5e-4	1.5e-3	1.5e-3	6.9e-4	1.0e-4	1.1e-3	1.1e-3	2.7e-4	2.7e-4	0.98410	0.00331	-0.02566
	298.161	7.1000	0.98384	5.2e-4	1.2e-4	1.6e-3	1.6e-3	1.6e-4	1.3e-5	1.1e-3	1.1e-3	2.7e-4	2.7e-4	0.98412	0.00331	-0.02566
	298.162	7.1005	0.98384	3.4e-4	5.2e-5	1.6e-3	1.6e-3	3.6e-4	4.7e-5	1.1e-3	1.1e-3	2.7e-4	2.7e-4	0.98411	0.00331	-0.02566
L21	298.162	7.4190	0.97525	3.0e-4	1.1e-4	1.5e-3	1.5e-3	1.9e-4	4.0e-5	1.2e-3	1.2e-3	2.7e-4	2.7e-4	0.97557	0.00325	-0.02807
	298.162	7.4186	0.97526	3.1e-4	1.1e-4	1.4e-3	1.4e-3	1.9e-4	2.1e-5	1.1e-3	1.1e-3	2.7e-4	2.7e-4	0.97558	0.00325	-0.02807
	298.162	7.4197	0.97524	3.1e-4	9.8e-5	1.4e-3	1.4e-3	1.0e-3	1.1e-4	1.2e-3	1.2e-3	2.7e-4	2.7e-4	0.97555	0.00325	-0.02808
	298.162	7.4193	0.97524	2.4e-4	2.4e-5	1.4e-3	1.4e-3	4.0e-4	6.7e-5	1.2e-3	1.2e-3	2.7e-4	2.7e-4	0.97557	0.00325	-0.02808
	298.163	7.4191	0.97525	3.8e-4	4.9e-5	1.5e-3	1.5e-3	2.5e-4	3.3e-5	1.2e-3	1.2e-3	2.7e-4	2.7e-4	0.97557	0.00325	-0.02808
	298.162	7.4187	0.97525	5.7e-4	8.7e-5	1.6e-3	1.6e-3	2.1e-4	2.7e-5	1.2e-3	1.2e-3	2.7e-4	2.7e-4	0.97558	0.00325	-0.02807
L22	298.173	7.8939	0.96051	3.6e-4	3.9e-5	1.4e-3	1.4e-3	1.4e-4	3.1e-5	1.2e-3	1.2e-3	2.7e-4	2.8e-4	0.96094	0.00288	-0.03463
	298.174	7.8953	0.96050	8.9e-4	3.6e-4	1.5e-3	1.5e-3	5.0e-4	6.8e-5	1.2e-3	1.2e-3	2.7e-4	2.8e-4	0.96089	0.00288	-0.03467
	298.175	7.8947	0.96050	3.6e-4	2.8e-5	1.5e-3	1.5e-3	1.4e-4	1.6e-5	1.2e-3	1.2e-3	2.7e-4	2.8e-4	0.96092	0.00288	-0.03465

	298.175	7.8945	0.96050	3.6e-4	1.7e-5	1.5e-3	1.5e-3	1.3e-4	1.1e-5	1.2e-3	1.2e-3	2.7e-4	2.8e-4	0.96092	0.00288	-0.03465
L23	298.174	8.0782	0.95343	2.5e-4	1.7e-5	1.6e-3	1.6e-3	2.5e-4	4.2e-5	1.2e-3	1.2e-3	2.7e-4	2.8e-4	0.95414	0.00248	-0.03964
	298.174	8.0783	0.95345	2.6e-4	8.8e-5	1.6e-3	1.6e-3	2.4e-4	7.7e-5	1.2e-3	1.2e-3	2.7e-4	2.8e-4	0.95413	0.00248	-0.03965
	298.174	8.0782	0.95344	3.1e-4	5.5e-5	1.5e-3	1.5e-3	3.5e-4	5.2e-5	1.2e-3	1.2e-3	2.7e-4	2.8e-4	0.95413	0.00248	-0.03964
	298.173	8.0783	0.95344	2.5e-4	2.9e-5	1.6e-3	1.6e-3	2.9e-4	8.7e-5	1.2e-3	1.2e-3	2.7e-4	2.8e-4	0.95413	0.00248	-0.03965
L24	298.171	8.1485	0.95025	3.8e-4	9.3e-5	1.3e-3	1.3e-3	1.5e-4	1.6e-5	1.2e-3	1.2e-3	2.7e-4	2.8e-4	0.95125	0.00224	-0.04233
	298.171	8.1479	0.95028	2.9e-4	7.1e-5	1.5e-3	1.5e-3	1.7e-4	2.9e-5	1.2e-3	1.2e-3	2.7e-4	2.8e-4	0.95127	0.00224	-0.04231
	298.171	8.1471	0.95031	5.6e-4	2.1e-4	1.4e-3	1.4e-3	1.6e-4	4.2e-5	1.3e-3	1.3e-3	2.7e-4	2.8e-4	0.95131	0.00224	-0.04228
	298.171	8.1480	0.95031	4.9e-4	3.3e-5	1.4e-3	1.4e-3	1.4e-3	2.4e-4	1.2e-3	1.3e-3	2.7e-4	2.8e-4	0.95127	0.00224	-0.04232
	298.171	8.1480	0.95029	3.8e-4	4.6e-5	1.4e-3	1.4e-3	3.6e-4	4.7e-5	1.2e-3	1.2e-3	2.7e-4	2.8e-4	0.95127	0.00224	-0.04231
L25	298.173	8.1552	0.94976	4.5e-4	1.0e-4	1.4e-3	1.4e-3	1.5e-4	1.6e-5	1.2e-3	1.2e-3	2.7e-4	2.8e-4	0.95097	0.00221	-0.04263
	298.174	8.1543	0.94977	6.6e-4	1.1e-4	1.5e-3	1.5e-3	2.4e-4	3.3e-5	1.2e-3	1.2e-3	2.7e-4	2.8e-4	0.95101	0.00221	-0.04260
	298.173	8.1538	0.94976	2.5e-4	4.6e-5	1.5e-3	1.5e-3	1.9e-4	3.5e-5	1.2e-3	1.2e-3	2.7e-4	2.8e-4	0.95103	0.00222	-0.04257
L26	298.175	8.2543	0.94368	2.8e-4	5.7e-5	1.5e-3	1.5e-3	1.0e-3	2.5e-4	1.2e-3	1.2e-3	2.7e-4	2.8e-4	0.94650	0.00169	-0.04793
	298.175	8.2532	0.94366	2.2e-4	2.3e-5	1.5e-3	1.5e-3	1.8e-4	4.0e-5	1.2e-3	1.2e-3	2.7e-4	2.8e-4	0.94656	0.00170	-0.04786
	298.173	8.2540	0.94344	6.3e-4	1.7e-4	1.4e-3	1.5e-3	2.2e-4	4.4e-5	1.2e-3	1.2e-3	2.7e-4	2.8e-4	0.94651	0.00169	-0.04790
	298.173	8.2532	0.94353	6.0e-4	2.1e-4	1.5e-3	1.5e-3	2.1e-4	3.6e-5	1.2e-3	1.2e-3	2.7e-4	2.8e-4	0.94655	0.00170	-0.04785
	298.173	8.2526	0.94358	5.8e-4	5.7e-5	1.5e-3	1.5e-3	2.4e-4	6.3e-5	1.2e-3	1.2e-3	2.7e-4	2.8e-4	0.94658	0.00170	-0.04781
	298.174	8.2523	0.94362	4.6e-4	9.7e-5	1.5e-3	1.5e-3	1.8e-4	4.0e-5	1.2e-3	1.2e-3	2.7e-4	2.8e-4	0.94660	0.00171	-0.04779
	298.174	8.2521	0.94364	2.4e-4	1.3e-5	1.5e-3	1.5e-3	1.7e-4	3.3e-5	1.2e-3	1.2e-3	2.7e-4	2.8e-4	0.94660	0.00171	-0.04778
L27	298.173	8.2748	0.94151	4.0e-4	1.2e-4	1.4e-3	1.4e-3	2.2e-3	2.5e-4	1.3e-3	1.3e-3	2.7e-4	2.8e-4	0.94550	0.00154	-0.04938
	298.173	8.2743	0.94153	2.4e-4	7.3e-5	1.5e-3	1.5e-3	1.2e-4	2.5e-5	1.3e-3	1.3e-3	2.7e-4	2.8e-4	0.94553	0.00154	-0.04933
	298.173	8.2742	0.94155	2.1e-4	1.6e-5	1.5e-3	1.5e-3	4.8e-4	1.2e-4	1.3e-3	1.3e-3	2.7e-4	2.8e-4	0.94553	0.00154	-0.04933
	298.174	8.2743	0.94162	9.8e-4	4.3e-4	1.5e-3	1.5e-3	1.4e-4	1.8e-5	1.3e-3	1.3e-3	2.7e-4	2.8e-4	0.94553	0.00154	-0.04934
	298.175	8.2740	0.94154	9.8e-5	1.5e-5	1.5e-3	1.5e-3	2.4e-4	5.0e-5	1.2e-3	1.3e-3	2.7e-4	2.8e-4	0.94555	0.00154	-0.04932
L28	298.174	8.2862	0.94039	4.7e-4	4.0e-5	1.5e-3	1.5e-3	1.9e-4	3.0e-5	1.3e-3	1.3e-3	2.7e-4	2.8e-4	0.94494	0.00144	-0.05027
	298.174	8.2863	0.94041	1.9e-4	2.3e-5	1.5e-3	1.5e-3	1.7e-4	3.4e-5	1.3e-3	1.3e-3	2.7e-4	2.8e-4	0.94493	0.00144	-0.05027
	298.174	8.2863	0.94042	2.2e-4	2.1e-5	1.5e-3	1.5e-3	1.2e-4	1.1e-5	1.3e-3	1.3e-3	2.7e-4	2.8e-4	0.94493	0.00144	-0.05027
	298.174	8.2862	0.94042	1.8e-4	2.2e-5	1.5e-3	1.5e-3	1.1e-4	1.5e-5	1.3e-3	1.3e-3	2.7e-4	2.8e-4	0.94494	0.00144	-0.05027
	298.175	8.2863	0.94042	1.5e-4	1.5e-5	1.5e-3	1.5e-3	1.5e-4	3.9e-5	1.3e-3	1.3e-3	2.7e-4	2.8e-4	0.94493	0.00144	-0.05028
L29	298.175	8.2975	0.93795	2.6e-4	3.0e-5	1.6e-3	1.6e-3	1.9e-4	4.1e-5	1.2e-3	1.2e-3	2.7e-4	2.8e-4	0.94437	0.00134	-0.05124
	298.175	8.2972	0.93794	1.6e-4	1.1e-5	1.6e-3	1.6e-3	1.0e-4	2.7e-5	1.2e-3	1.2e-3	2.7e-4	2.8e-4	0.94438	0.00134	-0.05121
	298.175	8.2969	0.93795	1.7e-4	1.3e-5	1.6e-3	1.6e-3	1.5e-4	4.3e-5	1.2e-3	1.2e-3	2.7e-4	2.8e-4	0.94439	0.00134	-0.05119
	298.176	8.2967	0.93802	2.0e-4	1.5e-5	1.6e-3	1.6e-3	1.6e-4	1.7e-5	1.2e-3	1.2e-3	2.7e-4	2.8e-4	0.94441	0.00134	-0.05117
P3	303.158	7.2105	0.99999	3.2e-4	9.5e-6	2.0e-3	2.0e-3	1.4e-4	3.0e-5	1.1e-3	1.1e-3					
L30	303.156	7.4036	0.99451	2.6e-4	5.8e-5	1.9e-3	1.9e-3	2.1e-4	4.4e-5	1.1e-3	1.1e-3	2.7e-4	2.7e-4	0.99457	0.00440	-0.03049
	303.155	7.4035	0.99450	3.4e-4	8.4e-5	1.9e-3	1.9e-3	2.1e-4	3.6e-5	1.1e-3	1.1e-3	2.7e-4	2.7e-4	0.99457	0.00440	-0.03048
	303.156	7.4034	0.99450	2.7e-4	2.8e-5	1.9e-3	1.9e-3	1.2e-4	1.8e-5	1.1e-3	1.1e-3	2.7e-4	2.7e-4	0.99457	0.00440	-0.03048
	303.158	7.4035	0.99450	3.0e-4	4.1e-5	2.0e-3	2.0e-3	1.7e-4	2.6e-5	1.1e-3	1.1e-3	2.7e-4	2.7e-4	0.99458	0.00440	-0.03049
	303.158	7.4036	0.99451	2.1e-4	1.5e-5	2.0e-3	2.0e-3	1.0e-4	1.5e-5	1.1e-3	1.1e-3	2.7e-4	2.7e-4	0.99458	0.00440	-0.03049
L31	303.156	7.5215	0.99044	6.1e-4	1.4e-4	1.7e-3	1.7e-3	1.7e-4	3.5e-5	1.1e-3	1.1e-3	2.7e-4	2.8e-4	0.99079	0.00417	-0.03400
	303.155	7.5217	0.99043	4.6e-4	1.1e-4	1.7e-3	1.7e-3	1.8e-4	3.3e-5	1.1e-3	1.1e-3	2.7e-4	2.8e-4	0.99078	0.00417	-0.03401
	303.155	7.5216	0.99044	3.9e-4	2.1e-5	1.7e-3	1.7e-3	1.8e-4	2.9e-5	1.1e-3	1.1e-3	2.7e-4	2.8e-4	0.99078	0.00417	-0.03400
	303.154	7.5217	0.99044	2.5e-4	2.1e-5	1.7e-3	1.7e-3	1.7e-4	2.8e-5	1.1e-3	1.1e-3	2.7e-4	2.8e-4	0.99078	0.00417	-0.03401
L32	303.157	7.5344	0.98985	3.4e-4	2.2e-5	1.7e-3	1.7e-3	1.0e-4	1.2e-5	1.1e-3	1.1e-3	2.7e-4	2.8e-4	0.99035	0.00412	-0.03456
	303.157	7.5345	0.98986	3.8e-4	2.6e-5	1.7e-3	1.7e-3	1.3e-4	1.2e-5	1.1e-3	1.1e-3	2.7e-4	2.8e-4	0.99035	0.00412	-0.03456
	303.157	7.5345	0.98985	2.3e-4	1.5e-5	1.7e-3	1.7e-3	9.5e-5	7.3e-6	1.1e-3	1.1e-3	2.7e-4	2.8e-4	0.99035	0.00412	-0.03456
	303.157	7.5346	0.98984	5.0e-4	9.6e-5	1.7e-3	1.7e-3	1.3e-4	2.5e-5	1.1e-3	1.1e-3	2.7e-4	2.8e-4	0.99034	0.00412	-0.03457
L33	303.157	7.5452	0.98928	6.5e-4	5.2e-5	1.7e-3	1.7e-3	1.3e-4	2.5e-5	1.2e-3	1.2e-3	2.7e-4	2.8e-4	0.98997	0.00407	-0.03508
	303.157	7.5451	0.98928	5.0e-4	1.8e-5	1.7e-3	1.7e-3	1.4e-4	2.6e-5	1.2e-3	1.2e-3	2.7e-4	2.8e-4	0.98998	0.00407	-0.03507
	303.157	7.5452	0.98928	3.3e-4	2.9e-5	1.7e-3	1.7e-3	1.2e-4	2.2e-5	1.2e-3	1.2e-3	2.7e-4	2.8e-4	0.98998	0.00407	-0.03507
	303.157	7.5451	0.98926	4.1e-4	4.0e-5	1.7e-3	1.7e-3	1.3e-4	1.6e-5	1.2e-3	1.2e-3	2.7e-4	2.8e-4	0.98998	0.00407	-0.03507
L34	303.157	7.5531	0.98883	2.2e-4	2.2e-5	1.8e-3	1.8e-3	1.1e-4	6.7e-6	1.2e-3	1.2e-3	2.7e-4	2.8e-4	0.98970	0.00403	-0.03548
	303.157	7.5531	0.98883	4.1e-4	1.9e-5	1.8e-3	1.8e-3	1.1e-4	1.6e-5	1.2e-3	1.2e-3	2.7e-4	2.8e-4	0.98970	0.00403	-0.03548

	303.157	7.5531	0.98882	3.4e-4	3.6e-5	1.8e-3	1.8e-3	1.2e-4	1.7e-5	1.2e-3	1.2e-3	2.7e-4	2.8e-4	0.98970	0.00403	-0.03548
	303.157	7.5531	0.98883	4.3e-4	3.4e-5	1.8e-3	1.8e-3	1.2e-4	4.2e-5	1.2e-3	1.2e-3	2.7e-4	2.8e-4	0.98970	0.00403	-0.03549
	303.157	7.5532	0.98883	2.2e-4	1.9e-5	1.8e-3	1.8e-3	1.6e-4	2.2e-5	1.2e-3	1.2e-3	2.7e-4	2.8e-4	0.98969	0.00403	-0.03549
L35	303.156	7.5538	0.98893	6.5e-4	1.5e-4	1.7e-3	1.8e-3	1.2e-4	1.1e-5	1.1e-3	1.1e-3	2.7e-4	2.8e-4	0.98967	0.00403	-0.03552
	303.157	7.5539	0.98894	5.3e-4	6.4e-5	1.7e-3	1.7e-3	1.2e-4	1.3e-5	1.1e-3	1.1e-3	2.7e-4	2.8e-4	0.98967	0.00403	-0.03552
	303.157	7.5540	0.98894	4.0e-4	4.7e-5	1.7e-3	1.7e-3	1.1e-4	1.9e-5	1.1e-3	1.1e-3	2.7e-4	2.8e-4	0.98966	0.00403	-0.03553
	303.157	7.5541	0.98894	4.3e-4	3.0e-5	1.7e-3	1.7e-3	1.4e-4	1.1e-5	1.1e-3	1.1e-3	2.7e-4	2.8e-4	0.98966	0.00403	-0.03554
L36	303.157	7.5573	0.98839	4.2e-4	2.5e-5	1.7e-3	1.7e-3	9.8e-5	9.5e-6	1.1e-3	1.1e-3	2.7e-4	2.8e-4	0.98954	0.00401	-0.03572
	303.157	7.5574	0.98840	9.7e-5	1.2e-5	1.7e-3	1.7e-3	1.4e-4	2.5e-5	1.1e-3	1.1e-3	2.7e-4	2.8e-4	0.98954	0.00401	-0.03573
	303.157	7.5575	0.98841	2.0e-4	2.2e-5	1.8e-3	1.8e-3	1.1e-4	7.4e-6	1.1e-3	1.1e-3	2.7e-4	2.8e-4	0.98954	0.00401	-0.03573
	303.157	7.5576	0.98840	4.6e-4	8.0e-5	1.7e-3	1.7e-3	1.1e-4	1.0e-5	1.1e-3	1.1e-3	2.7e-4	2.8e-4	0.98954	0.00401	-0.03573
	303.158	7.5576	0.98842	4.3e-4	8.4e-5	1.8e-3	1.8e-3	1.4e-4	1.7e-5	1.1e-3	1.1e-3	2.7e-4	2.8e-4	0.98954	0.00401	-0.03574

Table B.3
Vapor phase: Experimental VLE data for $CO_2 + N_2$ at mean temperature $\bar{T}$, mean pressure $\bar{p}$, and sample vapor phase mole fraction y_{CO_2}.

	Data			Temperature				Pressure				Composition			Composition derivatives	
ID	$\bar{T}$	$\bar{p}$	y_{CO_2}	$s(T)$	$s(\bar{T})$	$\bar{u}(T)$	$u_c(\bar{T})$	$s(p)$	$s(\bar{p})$	$\bar{u}(p)$	$u_c(\bar{p})$	$u(y_{CO_2})$	$u_{tot}(y_{CO_2})$	$y_{CO_2,calc}$	$\partial y_{CO_2}/\partial T$	$\partial y_{CO_2}/\partial p$
	(K)	(MPa)	(-)	(K)	(K)	(K)	(K)	(MPa)	(MPa)	(MPa)	(MPa)	(-)	(-)	(-)	(K^{-1})	(MPa^{-1})
P1	223.138	0.6829	0.99999	5.8e-4	5.3e-5	2.5e-3	2.5e-3	1.5e-5	2.5e-6	5.0e-4	5.0e-4					
V1	223.139	1.9390	0.40681	6.1e-4	4.4e-5	2.6e-3	2.6e-3	4.3e-5	1.7e-5	5.2e-4	5.2e-4	2.7e-4	2.9e-4	0.41039	0.01519	-0.16961
	223.139	1.9383	0.40723	5.3e-4	6.6e-5	2.5e-3	2.5e-3	3.8e-5	1.5e-5	5.2e-4	5.2e-4	2.7e-4	2.9e-4	0.41050	0.01519	-0.16972
	223.139	1.9377	0.40697	6.9e-4	1.1e-4	2.5e-3	2.5e-3	3.0e-5	1.0e-5	5.2e-4	5.2e-4	2.7e-4	2.9e-4	0.41060	0.01520	-0.16983
V2	223.139	4.3569	0.23252	4.0e-4	2.1e-5	2.5e-3	2.5e-3	6.6e-5	9.1e-6	1.1e-3	1.1e-3	2.7e-4	2.8e-4	0.23389	0.00808	-0.02909
	223.139	4.3551	0.23239	4.8e-4	3.1e-5	2.6e-3	2.6e-3	5.8e-5	4.9e-6	1.1e-3	1.1e-3	2.7e-4	2.8e-4	0.23394	0.00808	-0.02912
	223.139	4.3534	0.23260	4.8e-4	5.2e-5	2.6e-3	2.6e-3	7.4e-5	1.7e-5	1.1e-3	1.1e-3	2.7e-4	2.8e-4	0.23399	0.00808	-0.02915
	223.139	4.3518	0.23256	4.3e-4	2.1e-5	2.5e-3	2.5e-3	6.4e-5	7.8e-6	1.1e-3	1.1e-3	2.7e-4	2.8e-4	0.23404	0.00809	-0.02918
	223.139	4.3502	0.23258	5.5e-4	6.3e-5	2.5e-3	2.5e-3	7.2e-5	1.8e-5	1.1e-3	1.1e-3	2.7e-4	2.8e-4	0.23408	0.00809	-0.02920
V3	223.138	4.3683	0.23235	8.3e-4	5.9e-5	2.6e-3	2.6e-3	7.5e-5	9.6e-6	1.1e-3	1.1e-3	2.7e-4	2.8e-4	0.23355	0.00806	-0.02890
	223.139	4.3668	0.23262	7.7e-4	2.5e-4	2.5e-3	2.6e-3	6.8e-5	1.6e-5	1.1e-3	1.1e-3	2.7e-4	2.8e-4	0.23360	0.00807	-0.02892
	223.139	4.3652	0.23248	5.6e-4	1.9e-4	2.4e-3	2.5e-3	7.7e-5	2.5e-5	1.1e-3	1.1e-3	2.7e-4	2.8e-4	0.23365	0.00807	-0.02895
	223.138	4.3637	0.23228	5.9e-4	3.2e-5	2.5e-3	2.5e-3	8.7e-5	2.2e-5	1.1e-3	1.1e-3	2.7e-4	2.8e-4	0.23368	0.00807	-0.02898
	223.139	4.3622	0.23224	5.7e-4	1.3e-4	2.5e-3	2.5e-3	7.3e-5	1.1e-5	1.1e-3	1.1e-3	2.7e-4	2.8e-4	0.23373	0.00807	-0.02900
V4	223.139	5.0396	0.21776	4.3e-4	3.5e-5	3.4e-3	3.4e-3	7.6e-5	2.0e-5	1.1e-3	1.1e-3	2.7e-4	2.7e-4	0.21741	0.00732	-0.01979
	223.139	5.0378	0.21786	4.1e-4	4.2e-5	3.4e-3	3.4e-3	7.3e-5	1.6e-5	1.1e-3	1.1e-3	2.7e-4	2.7e-4	0.21745	0.00732	-0.01981
	223.139	5.0360	0.21793	4.2e-4	4.6e-5	3.5e-3	3.5e-3	8.5e-5	2.8e-5	1.1e-3	1.1e-3	2.7e-4	2.7e-4	0.21749	0.00733	-0.01983
V5	223.141	6.0871	0.20170	8.9e-4	2.5e-4	5.3e-3	5.3e-3	1.3e-4	4.5e-5	1.1e-3	1.1e-3	2.7e-4	2.8e-4	0.20183	0.00652	-0.01073
	223.141	6.0835	0.20179	9.4e-4	2.6e-4	4.9e-3	4.9e-3	1.6e-4	6.6e-5	1.1e-3	1.1e-3	2.7e-4	2.7e-4	0.20187	0.00652	-0.01075
V6	223.140	7.0153	0.19315	1.2e-3	3.5e-4	4.8e-3	4.8e-3	1.9e-4	7.9e-5	1.1e-3	1.2e-3	2.7e-4	2.7e-4	0.19446	0.00604	-0.00543
	223.139	7.0072	0.19323	1.8e-3	3.6e-4	4.9e-3	4.9e-3	2.0e-1	3.1e-3	1.1e-3	3.3e-3	2.7e-4	2.7e-4	0.19450	0.00604	-0.00547
	223.139	7.0108	0.19318	1.8e-3	3.2e-4	5.0e-3	5.0e-3	1.5e-4	5.6e-5	1.1e-3	1.1e-3	2.7e-4	2.7e-4	0.19448	0.00604	-0.00545
	223.140	7.0087	0.19365	1.3e-3	4.7e-4	4.7e-3	4.7e-3	1.9e-4	8.0e-5	1.1e-3	1.2e-3	2.7e-4	2.7e-4	0.19450	0.00604	-0.00546
	223.139	7.0065	0.19311	1.6e-3	3.7e-4	4.9e-3	4.9e-3	1.3e-4	4.4e-5	1.1e-3	1.1e-3	2.7e-4	2.7e-4	0.19451	0.00605	-0.00547
V7	223.141	8.1033	0.18991	6.3e-4	3.1e-5	5.6e-3	5.6e-3	1.3e-4	1.1e-5	1.2e-3	1.2e-3	2.7e-4	2.7e-4	0.19118	0.00565	-0.00083
	223.141	8.1011	0.18977	7.7e-4	5.3e-5	5.8e-3	5.8e-3	1.4e-4	3.3e-5	1.2e-3	1.2e-3	2.7e-4	2.7e-4	0.19118	0.00565	-0.00084
	223.141	8.0989	0.18972	6.3e-4	8.1e-5	5.7e-3	5.7e-3	1.5e-4	3.6e-5	1.2e-3	1.2e-3	2.7e-4	2.7e-4	0.19118	0.00565	-0.00085
	223.141	8.0967	0.18957	1.0e-3	1.2e-4	5.8e-3	5.8e-3	1.5e-4	2.6e-5	1.2e-3	1.2e-3	2.7e-4	2.7e-4	0.19118	0.00566	-0.00086
	223.141	8.0947	0.18956	1.0e-3	1.0e-4	5.8e-3	5.8e-3	1.5e-4	3.2e-5	1.2e-3	1.2e-3	2.7e-4	2.7e-4	0.19118	0.00566	-0.00086
V8	223.141	8.4451	0.18984	4.3e-4	1.7e-5	3.6e-3	3.6e-3	1.2e-4	9.8e-6	1.3e-3	1.3e-3	2.7e-4	2.7e-4	0.19110	0.00556	0.00040
	223.141	8.4427	0.18977	5.5e-4	1.1e-4	3.6e-3	3.6e-3	1.4e-4	1.3e-5	1.3e-3	1.3e-3	2.7e-4	2.7e-4	0.19110	0.00556	0.00039
	223.141	8.4402	0.18983	5.6e-4	4.3e-5	3.6e-3	3.6e-3	1.3e-4	2.9e-5	1.3e-3	1.3e-3	2.7e-4	2.7e-4	0.19110	0.00556	0.00038
	223.142	8.4378	0.18980	5.3e-4	5.5e-5	3.6e-3	3.6e-3	1.0e-4	1.6e-5	1.3e-3	1.3e-3	2.7e-4	2.7e-4	0.19111	0.00556	0.00037
	223.142	8.4354	0.18981	4.9e-4	3.7e-5	3.6e-3	3.6e-3	1.1e-4	1.5e-5	1.3e-3	1.3e-3	2.7e-4	2.7e-4	0.19111	0.00556	0.00036
V9	223.143	8.6114	0.18970	1.4e-3	3.7e-4	4.2e-3	4.2e-3	1.8e-4	4.1e-5	1.3e-3	1.3e-3	2.7e-4	2.7e-4	0.19123	0.00552	0.00097
	223.142	8.6090	0.18970	1.2e-3	4.8e-4	4.1e-3	4.1e-3	1.5e-4	5.3e-5	1.3e-3	1.3e-3	2.7e-4	2.7e-4	0.19122	0.00552	0.00097
	223.142	8.6068	0.18989	9.8e-4	2.0e-4	4.1e-3	4.1e-3	1.2e-4	2.9e-5	1.3e-3	1.3e-3	2.7e-4	2.7e-4	0.19122	0.00552	0.00096
	223.141	8.6045	0.18990	1.6e-3	2.0e-4	4.2e-3	4.2e-3	1.2e-4	1.4e-5	1.3e-3	1.3e-3	2.7e-4	2.7e-4	0.19121	0.00552	0.00095
V10	223.140	9.1958	0.19076	8.5e-4	1.0e-4	5.4e-3	5.4e-3	2.6e-4	9.4e-5	1.4e-3	1.4e-3	2.7e-4	2.7e-4	0.19235	0.00540	0.00290
	223.140	9.1939	0.19077	8.9e-4	2.0e-4	5.6e-3	5.6e-3	2.2e-4	8.5e-5	1.4e-3	1.4e-3	2.7e-4	2.7e-4	0.19234	0.00540	0.00289
	223.140	9.1920	0.19071	1.3e-3	2.4e-4	5.3e-3	5.3e-3	3.0e-4	1.3e-4	1.4e-3	1.4e-3	2.7e-4	2.7e-4	0.19234	0.00540	0.00289
	223.141	9.1902	0.19061	1.0e-3	1.9e-4	5.4e-3	5.4e-3	2.6e-4	1.1e-4	1.4e-3	1.4e-3	2.7e-4	2.7e-4	0.19234	0.00540	0.00288
	223.141	9.1883	0.19059	6.0e-4	5.0e-5	5.3e-3	5.3e-3	2.3e-4	8.8e-5	1.4e-3	1.4e-3	2.7e-4	2.7e-4	0.19233	0.00540	0.00287
V11	223.141	9.8106	0.19262	6.0e-4	1.1e-4	5.4e-3	5.4e-3	1.0e-4	2.8e-5	2.6e-3	2.6e-3	2.7e-4	2.7e-4	0.19473	0.00530	0.00481
	223.141	9.8078	0.19301	6.1e-4	7.1e-5	5.3e-3	5.3e-3	1.4e-4	3.3e-5	2.6e-3	2.6e-3	2.7e-4	2.7e-4	0.19472	0.00530	0.00480
	223.141	9.8050	0.19280	4.2e-4	3.3e-5	5.1e-3	5.1e-3	1.4e-4	4.0e-5	2.6e-3	2.6e-3	2.7e-4	2.7e-4	0.19471	0.00530	0.00479
	223.141	9.8022	0.19276	7.1e-4	5.7e-5	5.1e-3	5.1e-3	1.2e-4	2.3e-5	2.6e-3	2.6e-3	2.7e-4	2.7e-4	0.19469	0.00530	0.00479
	223.141	9.7995	0.19294	5.9e-4	6.2e-5	5.3e-3	5.3e-3	1.4e-4	4.4e-5	2.6e-3	2.6e-3	2.7e-4	2.7e-4	0.19468	0.00530	0.00478

V12	223.139	10.8727	0.20008	7.2e-4	1.8e-4	3.2e-3	3.2e-3	1.4e-4	2.5e-5	2.7e-3	2.7e-3	2.7e-4	2.7e-4	0.20154	0.00519	0.00802
	223.139	10.8693	0.19989	1.0e-3	2.7e-4	3.2e-3	3.2e-3	1.3e-4	3.7e-5	2.7e-3	2.7e-3	2.7e-4	2.7e-4	0.20151	0.00519	0.00801
	223.138	10.8661	0.19973	1.1e-3	1.4e-4	3.2e-3	3.2e-3	1.6e-4	3.1e-5	2.7e-3	2.7e-3	2.7e-4	2.7e-4	0.20148	0.00519	0.00800
V13	223.142	11.9841	0.20903	8.7e-4	2.1e-4	4.7e-3	4.7e-3	3.7e-4	1.3e-4	2.7e-3	2.7e-3	2.7e-4	2.8e-4	0.21237	0.00516	0.01149
	223.141	11.9814	0.20890	1.1e-3	1.7e-4	5.0e-3	5.0e-3	3.5e-4	1.4e-4	2.7e-3	2.7e-3	2.7e-4	2.8e-4	0.21234	0.00516	0.01148
	223.140	11.9761	0.20861	1.5e-3	2.9e-4	5.3e-3	5.3e-3	4.1e-4	1.4e-4	2.7e-3	2.7e-3	2.7e-4	2.8e-4	0.21228	0.00516	0.01147
	223.140	11.9733	0.20870	1.2e-3	2.5e-4	5.1e-3	5.1e-3	4.0e-4	1.6e-4	2.7e-3	2.7e-3	2.7e-4	2.8e-4	0.21224	0.00516	0.01146
V14	223.136	14.9794	0.25628	1.6e-3	3.4e-4	3.2e-3	3.2e-3	1.2e-4	9.3e-6	2.8e-3	2.8e-3	2.7e-4	2.8e-4	0.26355	0.00568	0.02379
	223.138	14.9746	0.25617	8.8e-4	2.1e-4	3.0e-3	3.0e-3	1.3e-4	2.4e-5	2.8e-3	2.8e-3	2.7e-4	2.8e-4	0.26345	0.00568	0.02376
	223.138	14.9699	0.25704	1.1e-3	2.4e-4	2.9e-3	2.9e-3	1.7e-4	3.4e-5	2.8e-3	2.8e-3	2.7e-4	2.8e-4	0.26334	0.00568	0.02373
	223.138	14.9652	0.25728	9.4e-4	1.7e-4	2.9e-3	2.9e-3	1.4e-4	2.0e-5	2.8e-3	2.8e-3	2.7e-4	2.8e-4	0.26323	0.00568	0.02371
	223.138	14.9605	0.25740	1.3e-3	2.4e-4	3.0e-3	3.0e-3	1.2e-4	1.2e-5	2.8e-3	2.8e-3	2.7e-4	2.8e-4	0.26311	0.00567	0.02368
V15	223.137	16.0198	0.28550	9.7e-4	2.5e-4	2.8e-3	2.8e-3	1.7e-4	2.2e-5	2.8e-3	2.8e-3	2.7e-4	2.9e-4	0.29163	0.00629	0.03059
	223.138	16.0148	0.28524	7.5e-4	1.2e-4	2.8e-3	2.8e-3	2.1e-4	4.5e-5	2.8e-3	2.8e-3	2.7e-4	2.9e-4	0.29148	0.00628	0.03056
	223.137	16.0098	0.28512	1.0e-3	3.1e-4	2.7e-3	2.7e-3	2.0e-4	5.6e-5	2.8e-3	2.8e-3	2.7e-4	2.9e-4	0.29133	0.00628	0.03051
	223.138	16.0048	0.28489	1.0e-3	3.2e-4	2.8e-3	2.8e-3	1.8e-4	2.9e-5	2.8e-3	2.8e-3	2.7e-4	2.9e-4	0.29118	0.00627	0.03048
	223.138	16.0000	0.28458	8.9e-4	2.0e-4	3.0e-3	3.0e-3	1.9e-4	6.8e-5	2.8e-3	2.8e-3	2.7e-4	2.9e-4	0.29103	0.00627	0.03044
V16	223.139	17.2601	0.33191	1.1e-3	2.8e-4	3.0e-3	3.0e-3	4.0e-4	1.4e-4	2.8e-3	2.8e-3	2.7e-4	3.0e-4	0.33739	0.00794	0.04523
	223.138	17.2552	0.33174	1.5e-3	3.4e-4	2.8e-3	2.8e-3	4.9e-4	2.0e-4	2.8e-3	2.8e-3	2.7e-4	3.0e-4	0.33717	0.00793	0.04514
	223.138	17.2520	0.33148	1.2e-3	3.1e-4	2.8e-3	2.9e-3	2.3e-4	6.8e-5	2.8e-3	2.8e-3	2.7e-4	3.0e-4	0.33702	0.00792	0.04508
	223.139	17.2465	0.33121	1.2e-3	3.2e-4	2.8e-3	2.8e-3	1.5e-4	1.7e-5	2.8e-3	2.8e-3	2.7e-4	3.0e-4	0.33678	0.00791	0.04498
	223.139	17.2414	0.33105	8.2e-4	8.2e-5	2.8e-3	2.8e-3	2.6e-4	5.1e-5	2.8e-3	2.8e-3	2.7e-4	3.0e-4	0.33655	0.00790	0.04488
V17	223.138	18.2267	0.41654	1.0e-3	2.6e-4	2.8e-3	2.8e-3	3.0e-4	5.9e-5	2.8e-3	2.8e-3	2.7e-4	3.6e-4	0.39455	0.01284	0.08223
	223.138	18.2220	0.41566	1.1e-3	2.0e-4	2.6e-3	2.6e-3	2.7e-4	1.2e-4	2.8e-3	2.8e-3	2.7e-4	3.6e-4	0.39416	0.01279	0.08185
	223.138	18.2172	0.41477	1.3e-3	3.1e-4	2.7e-3	2.7e-3	2.3e-4	4.5e-5	2.8e-3	2.8e-3	2.7e-4	3.6e-4	0.39377	0.01273	0.08146
	223.138	18.2126	0.41396	9.5e-4	2.0e-4	2.8e-3	2.8e-3	2.0e-4	6.3e-5	2.8e-3	2.8e-3	2.7e-4	3.6e-4	0.39340	0.01268	0.08108
	223.138	18.2080	0.41307	1.1e-3	1.7e-4	2.8e-3	2.8e-3	2.2e-4	3.2e-5	2.8e-3	2.8e-3	2.7e-4	3.5e-4	0.39302	0.01263	0.08065
V18	269.997	9.5760	0.58157	1.2e-3	8.0e-5	5.0e-3	5.0e-3	6.6e-4	3.2e-4	1.4e-3	1.4e-3	2.7e-4	2.8e-4	0.58456	0.01120	-0.00414
	269.997	9.5703	0.58194	8.8e-4	3.4e-5	4.8e-3	4.8e-3	8.6e-4	4.3e-4	1.4e-3	1.5e-3	2.7e-4	2.8e-4	0.58459	0.01120	-0.00421
	269.997	9.5647	0.58216	1.0e-3	1.0e-4	4.6e-3	4.6e-3	6.6e-4	3.1e-4	1.4e-3	1.4e-3	2.7e-4	2.8e-4	0.58462	0.01120	-0.00428
	269.997	9.5595	0.58144	9.8e-4	9.4e-5	4.7e-3	4.7e-3	7.0e-4	3.4e-4	1.4e-3	1.4e-3	2.7e-4	2.8e-4	0.58464	0.01120	-0.00434
	269.997	9.5541	0.58112	8.9e-4	3.8e-5	4.8e-3	4.8e-3	6.8e-4	3.3e-4	1.4e-3	1.4e-3	2.7e-4	2.8e-4	0.58466	0.01120	-0.00440
	269.997	9.5491	0.58109	9.7e-4	8.1e-5	4.7e-3	4.7e-3	5.9e-4	2.8e-4	1.4e-3	1.4e-3	2.7e-4	2.8e-4	0.58468	0.01120	-0.00446
	269.997	9.5440	0.58106	1.0e-3	8.7e-5	4.8e-3	4.8e-3	6.1e-4	3.0e-4	1.4e-3	1.4e-3	2.7e-4	2.8e-4	0.58470	0.01120	-0.00453
	269.997	9.5393	0.58315	8.9e-4	7.6e-5	4.7e-3	4.7e-3	6.0e-4	2.8e-4	1.4e-3	1.4e-3	2.7e-4	2.8e-4	0.58473	0.01120	-0.00458
V19	269.995	9.5912	0.58057	1.4e-3	7.1e-5	6.1e-3	6.1e-3	2.5e-4	9.8e-5	1.4e-3	1.4e-3	2.7e-4	2.8e-4	0.58449	0.01121	-0.00396
	269.996	9.5876	0.58046	1.2e-3	9.9e-5	5.7e-3	5.7e-3	2.8e-4	1.1e-4	1.4e-3	1.4e-3	2.7e-4	2.8e-4	0.58451	0.01120	-0.00400
	269.996	9.5840	0.58169	1.3e-3	6.1e-5	6.3e-3	6.3e-3	3.7e-4	1.7e-4	1.4e-3	1.4e-3	2.7e-4	2.8e-4	0.58452	0.01120	-0.00404
	269.995	9.5802	0.58124	9.5e-4	7.8e-5	6.0e-3	6.0e-3	3.6e-4	1.7e-4	1.4e-3	1.4e-3	2.7e-4	2.8e-4	0.58453	0.01120	-0.00409
	269.996	9.5766	0.58080	1.0e-3	1.1e-4	5.7e-3	5.7e-3	2.9e-4	1.3e-4	1.4e-3	1.4e-3	2.7e-4	2.8e-4	0.58455	0.01120	-0.00413
P2	298.174	6.4369	0.99999	2.1e-4	1.9e-5	1.6e-3	1.6e-3	8.5e-5	8.0e-6	1.2e-3	1.2e-3					
V20	298.159	6.7086	0.98156	2.0e-4	1.9e-5	1.5e-3	1.5e-3	1.1e-4	2.1e-5	1.1e-3	1.1e-3	2.7e-4	2.8e-4	0.98182	0.01031	-0.06269
	298.159	6.7089	0.98206	4.4e-4	4.0e-5	1.5e-3	1.5e-3	1.1e-4	3.1e-5	1.1e-3	1.1e-3	2.7e-4	2.8e-4	0.98180	0.01031	-0.06269
	298.159	6.7088	0.98205	6.8e-4	4.1e-5	1.5e-3	1.5e-3	1.3e-4	3.6e-5	1.1e-3	1.1e-3	2.7e-4	2.8e-4	0.98181	0.01031	-0.06269
	298.159	6.7090	0.98161	4.3e-4	2.4e-5	1.5e-3	1.5e-3	1.4e-4	2.8e-5	1.1e-3	1.1e-3	2.7e-4	2.8e-4	0.98180	0.01031	-0.06268
	298.159	6.7090	0.98197	3.2e-4	4.8e-5	1.5e-3	1.5e-3	1.1e-4	1.8e-5	1.1e-3	1.1e-3	2.7e-4	2.8e-4	0.98180	0.01031	-0.06268
	298.159	6.7088	0.98153	3.5e-4	1.7e-5	1.5e-3	1.5e-3	1.1e-4	1.6e-5	1.1e-3	1.1e-3	2.7e-4	2.8e-4	0.98181	0.01031	-0.06269
	298.159	6.7088	0.98142	3.1e-4	4.0e-5	1.5e-3	1.5e-3	1.1e-4	2.4e-5	1.1e-3	1.1e-3	2.7e-4	2.8e-4	0.98181	0.01031	-0.06269
	298.159	6.7087	0.98170	1.9e-4	1.5e-5	1.5e-3	1.5e-3	1.1e-4	2.6e-5	1.1e-3	1.1e-3	2.7e-4	2.8e-4	0.98182	0.01031	-0.06269
V21	298.158	6.7192	0.98099	3.4e-4	6.7e-5	1.5e-3	1.5e-3	2.1e-4	8.6e-5	1.1e-3	1.1e-3	2.7e-4	2.8e-4	0.98114	0.01030	-0.06240
	298.158	6.7190	0.98096	3.7e-4	5.0e-5	1.5e-3	1.5e-3	2.4e-4	1.0e-4	1.1e-3	1.1e-3	2.7e-4	2.8e-4	0.98116	0.01030	-0.06240
	298.158	6.7196	0.98098	4.0e-4	8.2e-5	1.4e-3	1.4e-3	1.2e-4	4.9e-5	1.1e-3	1.1e-3	2.7e-4	2.8e-4	0.98112	0.01030	-0.06238
	298.158	6.7197	0.98095	2.3e-4	2.7e-5	1.5e-3	1.5e-3	8.4e-5	7.4e-6	1.1e-3	1.1e-3	2.7e-4	2.8e-4	0.98112	0.01030	-0.06238
	298.158	6.7195	0.98097	1.8e-4	3.6e-5	1.5e-3	1.5e-3	7.9e-5	6.4e-6	1.1e-3	1.1e-3	2.7e-4	2.8e-4	0.98113	0.01030	-0.06239

V22	298.162	7.0988	0.95950	3.9e-4	5.4e-5	1.6e-3	1.6e-3	2.3e-4	8.3e-5	1.2e-3	1.2e-3	2.7e-4	2.8e-4	0.95950	0.01014	-0.05193
	298.162	7.0989	0.95953	4.3e-4	4.1e-5	1.4e-3	1.4e-3	1.1e-4	1.3e-5	1.1e-3	1.1e-3	2.7e-4	2.8e-4	0.95949	0.01014	-0.05193
V23	298.162	7.4165	0.94445	3.8e-4	2.7e-5	1.4e-3	1.4e-3	2.2e-4	6.1e-5	1.1e-3	1.1e-3	2.7e-4	2.8e-4	0.94438	0.01006	-0.04314
	298.161	7.4163	0.94444	3.8e-4	4.8e-5	1.3e-3	1.3e-3	1.7e-4	1.2e-5	1.1e-3	1.1e-3	2.7e-4	2.8e-4	0.94438	0.01006	-0.04315
	298.161	7.4161	0.94432	3.9e-4	2.2e-5	1.5e-3	1.5e-3	1.9e-4	1.5e-5	1.1e-3	1.1e-3	2.7e-4	2.8e-4	0.94440	0.01006	-0.04315
	298.162	7.4160	0.94421	1.7e-4	3.1e-5	1.5e-3	1.5e-3	1.9e-4	2.6e-5	1.1e-3	1.1e-3	2.7e-4	2.8e-4	0.94440	0.01006	-0.04316
V24	298.162	7.4185	0.94444	4.7e-4	9.0e-5	1.4e-3	1.4e-3	2.9e-4	2.5e-5	1.1e-3	1.1e-3	2.7e-4	2.8e-4	0.94430	0.01006	-0.04308
	298.163	7.4179	0.94414	3.1e-4	3.2e-5	1.6e-3	1.6e-3	2.1e-4	5.2e-5	1.1e-3	1.1e-3	2.7e-4	2.8e-4	0.94434	0.01006	-0.04310
	298.163	7.4182	0.94441	3.0e-4	1.3e-5	1.4e-3	1.4e-3	6.4e-4	1.4e-4	1.1e-3	1.1e-3	2.7e-4	2.8e-4	0.94433	0.01006	-0.04310
	298.163	7.4183	0.94437	3.4e-4	5.8e-5	1.5e-3	1.5e-3	6.4e-4	1.2e-4	1.1e-3	1.1e-3	2.7e-4	2.8e-4	0.94432	0.01006	-0.04309
	298.163	7.4175	0.94443	1.1e-4	1.4e-5	1.5e-3	1.5e-3	2.3e-4	7.0e-5	1.1e-3	1.1e-3	2.7e-4	2.8e-4	0.94435	0.01006	-0.04311
	298.163	7.4169	0.94439	1.5e-4	1.9e-5	1.5e-3	1.5e-3	1.7e-4	2.3e-5	1.1e-3	1.1e-3	2.7e-4	2.8e-4	0.94438	0.01006	-0.04313
	298.163	7.4165	0.94429	3.4e-4	3.0e-5	1.5e-3	1.5e-3	1.9e-4	5.3e-5	1.1e-3	1.2e-3	2.7e-4	2.8e-4	0.94440	0.01006	-0.04314
	298.163	7.4163	0.94423	2.4e-4	1.3e-5	1.5e-3	1.5e-3	1.6e-4	3.6e-5	1.2e-3	1.2e-3	2.7e-4	2.8e-4	0.94441	0.01006	-0.04315
V25	298.175	7.8941	0.92785	3.3e-4	4.1e-5	1.5e-3	1.5e-3	1.8e-4	3.3e-5	1.2e-3	1.2e-3	2.7e-4	2.8e-4	0.92734	0.01019	-0.02817
	298.175	7.8939	0.92790	2.7e-4	2.8e-5	1.4e-3	1.4e-3	1.3e-4	2.1e-5	1.2e-3	1.2e-3	2.7e-4	2.8e-4	0.92735	0.01019	-0.02818
	298.175	7.8937	0.92788	3.8e-4	3.0e-5	1.5e-3	1.5e-3	1.5e-4	2.3e-5	1.2e-3	1.2e-3	2.7e-4	2.8e-4	0.92735	0.01019	-0.02819
	298.175	7.8935	0.92785	2.5e-4	1.9e-5	1.5e-3	1.5e-3	1.3e-4	2.1e-5	1.2e-3	1.2e-3	2.7e-4	2.8e-4	0.92736	0.01019	-0.02820
	298.175	7.8934	0.92797	3.4e-4	3.7e-5	1.5e-3	1.5e-3	1.4e-4	3.1e-5	1.2e-3	1.2e-3	2.7e-4	2.8e-4	0.92736	0.01019	-0.02821
	298.175	7.8932	0.92798	2.1e-4	3.5e-5	1.5e-3	1.5e-3	1.3e-4	2.1e-5	1.2e-3	1.2e-3	2.7e-4	2.8e-4	0.92736	0.01019	-0.02821
	298.175	7.8930	0.92803	1.9e-4	4.0e-5	1.5e-3	1.5e-3	1.7e-4	2.9e-5	1.2e-3	1.2e-3	2.7e-4	2.8e-4	0.92737	0.01019	-0.02821
	298.175	7.8928	0.92790	1.8e-4	1.2e-5	1.5e-3	1.5e-3	1.5e-4	4.8e-5	1.2e-3	1.2e-3	2.7e-4	2.8e-4	0.92738	0.01019	-0.02822
V26	298.174	8.0737	0.92445	2.7e-4	9.9e-5	1.6e-3	1.6e-3	1.7e-4	4.1e-5	1.2e-3	1.2e-3	2.7e-4	2.7e-4	0.92290	0.01046	-0.02074
	298.174	8.0731	0.92481	2.5e-4	1.6e-5	1.6e-3	1.6e-3	1.4e-4	5.0e-5	1.2e-3	1.2e-3	2.7e-4	2.7e-4	0.92292	0.01046	-0.02077
	298.174	8.0728	0.92463	2.0e-4	2.4e-5	1.6e-3	1.6e-3	1.6e-4	2.4e-5	1.2e-3	1.2e-3	2.7e-4	2.7e-4	0.92292	0.01046	-0.02079
	298.174	8.0726	0.92468	1.6e-4	1.5e-5	1.6e-3	1.6e-3	1.7e-4	4.6e-5	1.2e-3	1.2e-3	2.7e-4	2.7e-4	0.92293	0.01046	-0.02080
	298.174	8.0722	0.92466	1.8e-4	4.8e-5	1.6e-3	1.6e-3	1.6e-4	2.9e-5	1.2e-3	1.2e-3	2.7e-4	2.7e-4	0.92294	0.01046	-0.02082
	298.174	8.0718	0.92466	1.7e-4	4.9e-5	1.6e-3	1.6e-3	1.3e-4	2.6e-5	1.2e-3	1.2e-3	2.7e-4	2.7e-4	0.92294	0.01045	-0.02084
	298.174	8.0715	0.92473	1.7e-4	1.5e-5	1.6e-3	1.6e-3	1.9e-4	6.2e-5	1.2e-3	1.2e-3	2.7e-4	2.7e-4	0.92295	0.01045	-0.02085
	298.174	8.0712	0.92477	2.5e-4	7.7e-5	1.6e-3	1.6e-3	1.7e-4	2.1e-5	1.3e-3	1.3e-3	2.7e-4	2.7e-4	0.92295	0.01045	-0.02087
V27	298.168	8.1437	0.92479	2.5e-4	2.3e-5	1.4e-3	1.4e-3	2.3e-4	4.5e-5	1.2e-3	1.2e-3	2.7e-4	2.7e-4	0.92152	0.01065	-0.01708
	298.168	8.1436	0.92480	1.9e-4	5.1e-5	1.4e-3	1.4e-3	2.1e-4	3.0e-5	1.2e-3	1.2e-3	2.7e-4	2.7e-4	0.92152	0.01065	-0.01709
	298.168	8.1435	0.92459	2.7e-4	2.4e-5	1.4e-3	1.4e-3	2.2e-4	4.6e-5	1.2e-3	1.2e-3	2.7e-4	2.7e-4	0.92152	0.01065	-0.01709
	298.168	8.1434	0.92462	2.0e-4	7.0e-5	1.5e-3	1.5e-3	1.5e-4	5.9e-6	1.2e-3	1.2e-3	2.7e-4	2.7e-4	0.92152	0.01065	-0.01710
	298.170	8.1433	0.92433	6.2e-4	1.5e-4	1.6e-3	1.6e-3	1.7e-4	1.9e-5	1.2e-3	1.2e-3	2.7e-4	2.7e-4	0.92154	0.01065	-0.01710
	298.170	8.1432	0.92459	2.5e-4	2.2e-5	1.4e-3	1.4e-3	1.9e-4	2.7e-5	1.2e-3	1.2e-3	2.7e-4	2.7e-4	0.92154	0.01065	-0.01711
	298.170	8.1432	0.92458	2.1e-4	3.9e-5	1.5e-3	1.5e-3	1.8e-4	1.8e-5	1.2e-3	1.2e-3	2.7e-4	2.7e-4	0.92154	0.01065	-0.01711
	298.170	8.1431	0.92462	1.9e-4	2.2e-5	1.5e-3	1.5e-3	1.6e-4	1.3e-5	1.2e-3	1.2e-3	2.7e-4	2.7e-4	0.92154	0.01065	-0.01711
V28	298.174	8.2531	0.92624	3.3e-4	1.3e-4	1.5e-3	1.5e-3	1.1e-4	2.3e-5	1.2e-3	1.2e-3	2.7e-4	2.7e-4	0.92010	0.01121	-0.00920
	298.173	8.2530	0.92622	2.7e-4	3.1e-5	1.4e-3	1.4e-3	1.1e-4	1.3e-5	1.2e-3	1.2e-3	2.7e-4	2.7e-4	0.92010	0.01121	-0.00918
	298.173	8.2527	0.92606	2.8e-4	7.4e-5	1.5e-3	1.5e-3	1.3e-4	2.0e-5	1.2e-3	1.2e-3	2.7e-4	2.7e-4	0.92010	0.01121	-0.00922
	298.173	8.2526	0.92617	1.8e-4	2.2e-5	1.5e-3	1.5e-3	1.6e-4	2.1e-5	1.2e-3	1.2e-3	2.7e-4	2.7e-4	0.92011	0.01121	-0.00923
	298.173	8.2524	0.92608	2.9e-4	5.8e-5	1.5e-3	1.5e-3	2.0e-4	5.6e-5	1.2e-3	1.2e-3	2.7e-4	2.7e-4	0.92011	0.01121	-0.00925
	298.174	8.2522	0.92598	2.2e-4	7.2e-5	1.5e-3	1.5e-3	1.8e-4	2.6e-5	1.2e-3	1.2e-3	2.7e-4	2.7e-4	0.92011	0.01120	-0.00924
	298.174	8.2521	0.92596	2.1e-4	5.1e-5	1.5e-3	1.5e-3	2.0e-4	3.2e-5	1.2e-3	1.2e-3	2.7e-4	2.7e-4	0.92011	0.01120	-0.00929
V29	298.174	8.2725	0.92711	2.7e-4	1.7e-5	1.5e-3	1.5e-3	2.2e-4	4.0e-5	1.2e-3	1.2e-3	2.7e-4	2.7e-4	0.91994	0.01137	-0.00730
	298.174	8.2722	0.92672	2.8e-4	2.1e-5	1.5e-3	1.5e-3	2.1e-4	3.1e-5	1.2e-3	1.2e-3	2.7e-4	2.7e-4	0.91994	0.01137	-0.00732
	298.174	8.2722	0.92707	3.7e-4	2.9e-5	1.5e-3	1.5e-3	2.1e-4	6.1e-5	1.2e-3	1.2e-3	2.7e-4	2.7e-4	0.91995	0.01137	-0.00737
	298.174	8.2721	0.92706	3.2e-4	4.2e-5	1.4e-3	1.4e-3	1.6e-4	2.6e-5	1.2e-3	1.2e-3	2.7e-4	2.7e-4	0.91995	0.01137	-0.00734
	298.174	8.2719	0.92663	3.0e-4	4.5e-5	1.5e-3	1.5e-3	2.0e-4	2.6e-5	1.2e-3	1.2e-3	2.7e-4	2.7e-4	0.91995	0.01137	-0.00734
	298.174	8.2719	0.92704	6.2e-4	2.4e-4	1.5e-3	1.5e-3	1.5e-4	1.8e-5	1.2e-3	1.2e-3	2.7e-4	2.7e-4	0.91995	0.01137	-0.00733
V30	298.175	8.2865	0.92749	1.4e-4	1.5e-5	1.5e-3	1.5e-3	2.0e-4	4.3e-5	1.3e-3	1.3e-3	2.7e-4	2.7e-4	0.91987	0.01151	-0.00574
	298.175	8.2865	0.92742	1.8e-4	3.6e-5	1.5e-3	1.5e-3	1.7e-4	1.7e-5	1.3e-3	1.3e-3	2.7e-4	2.7e-4	0.91987	0.01151	-0.00573
	298.175	8.2864	0.92734	1.8e-4	1.8e-5	1.5e-3	1.5e-3	1.9e-4	3.9e-5	1.3e-3	1.3e-3	2.7e-4	2.7e-4	0.91987	0.01151	-0.00577

	298.175	8.2863	0.92735	1.9e-4	2.0e-5	1.5e-3	1.5e-3	1.3e-4	2.0e-5	1.3e-3	1.3e-3	2.7e-4	2.7e-4	0.91987	0.01151	-0.00576
	298.175	8.2861	0.92728	1.2e-4	1.0e-5	1.5e-3	1.5e-3	1.7e-4	2.4e-5	1.3e-3	1.3e-3	2.7e-4	2.7e-4	0.91987	0.01151	-0.00601
	298.175	8.2860	0.92719	8.7e-5	1.4e-5	1.5e-3	1.5e-3	1.4e-4	2.1e-5	1.2e-3	1.2e-3	2.7e-4	2.7e-4	0.91987	0.01151	-0.00581
	298.175	8.2858	0.92718	2.4e-4	2.2e-5	1.5e-3	1.5e-3	1.3e-4	2.3e-5	1.2e-3	1.2e-3	2.7e-4	2.7e-4	0.91987	0.01150	-0.00581
	298.175	8.2858	0.92712	1.1e-4	8.8e-6	1.6e-3	1.6e-3	1.4e-4	2.5e-5	1.2e-3	1.2e-3	2.7e-4	2.7e-4	0.91988	0.01150	-0.00582
V31	298.174	8.2969	0.93016	2.9e-4	3.2e-5	1.6e-3	1.6e-3	1.3e-4	2.7e-5	1.2e-3	1.2e-3	2.7e-4	2.7e-4	0.91980	0.01162	-0.00451
	298.174	8.2971	0.93013	2.9e-4	5.1e-5	1.6e-3	1.6e-3	1.4e-4	1.7e-5	1.2e-3	1.2e-3	2.7e-4	2.7e-4	0.91980	0.01163	-0.00449
	298.175	8.2973	0.93033	3.5e-4	1.3e-4	1.7e-3	1.7e-3	1.1e-4	2.1e-5	1.2e-3	1.2e-3	2.7e-4	2.7e-4	0.91982	0.01163	-0.00445
	298.176	8.2971	0.93029	2.2e-4	2.1e-5	1.7e-3	1.7e-3	1.4e-4	2.6e-5	1.2e-3	1.2e-3	2.7e-4	2.7e-4	0.91982	0.01163	-0.00446
	298.176	8.2973	0.93030	2.2e-4	1.9e-5	1.7e-3	1.7e-3	1.1e-4	1.5e-5	1.2e-3	1.2e-3	2.7e-4	2.7e-4	0.91982	0.01163	-0.00444
	298.176	8.2974	0.93027	2.3e-4	1.9e-5	1.6e-3	1.6e-3	1.3e-4	1.7e-5	1.2e-3	1.2e-3	2.7e-4	2.7e-4	0.91982	0.01163	-0.00443
P3	303.158	7.2105	0.99999	3.2e-4	9.5e-6	2.0e-3	2.0e-3	1.4e-4	3.0e-5	1.1e-3	1.1e-3					
V32	303.156	7.4006	0.99148	8.1e-4	4.1e-5	1.8e-3	1.8e-3	9.4e-5	6.6e-6	1.2e-3	1.2e-3	2.7e-4	2.8e-4	0.99157	0.00822	-0.04198
	303.156	7.4007	0.99149	3.6e-4	2.0e-5	1.9e-3	1.9e-3	1.4e-4	1.8e-5	1.2e-3	1.2e-3	2.7e-4	2.8e-4	0.99157	0.00822	-0.04198
	303.156	7.4007	0.99159	2.2e-4	3.5e-5	1.9e-3	1.9e-3	1.2e-4	2.1e-5	1.2e-3	1.2e-3	2.7e-4	2.8e-4	0.99157	0.00822	-0.04198
	303.157	7.4007	0.99157	2.5e-4	2.1e-5	1.9e-3	1.9e-3	1.2e-4	2.5e-5	1.2e-3	1.2e-3	2.7e-4	2.8e-4	0.99157	0.00822	-0.04198
	303.158	7.4007	0.99156	1.4e-4	6.6e-6	2.0e-3	2.0e-3	1.0e-4	2.1e-5	1.2e-3	1.2e-3	2.7e-4	2.8e-4	0.99158	0.00822	-0.04197
	303.158	7.4007	0.99156	3.6e-4	1.8e-5	2.0e-3	2.0e-3	1.2e-4	2.6e-5	1.2e-3	1.2e-3	2.7e-4	2.8e-4	0.99158	0.00822	-0.04198
	303.158	7.4007	0.99153	1.5e-4	1.6e-5	2.0e-3	2.0e-3	1.0e-4	9.1e-6	1.2e-3	1.2e-3	2.7e-4	2.8e-4	0.99158	0.00822	-0.04197
	303.158	7.4008	0.99152	1.4e-4	1.3e-5	2.0e-3	2.0e-3	9.3e-5	8.7e-6	1.2e-3	1.2e-3	2.7e-4	2.8e-4	0.99158	0.00822	-0.04197
V33	303.156	7.4670	0.98914	7.0e-4	6.4e-5	2.0e-3	2.0e-3	1.6e-4	5.6e-5	1.1e-3	1.1e-3	2.7e-4	2.8e-4	0.98888	0.00835	-0.03915
	303.156	7.4672	0.98906	4.5e-4	7.8e-5	1.9e-3	1.9e-3	1.2e-4	1.1e-5	1.1e-3	1.1e-3	2.7e-4	2.8e-4	0.98887	0.00835	-0.03914
	303.157	7.4672	0.98895	4.0e-4	2.1e-5	2.0e-3	2.0e-3	1.0e-4	8.1e-6	1.1e-3	1.1e-3	2.7e-4	2.8e-4	0.98888	0.00835	-0.03913
	303.158	7.4672	0.98908	1.3e-4	2.1e-5	2.0e-3	2.0e-3	1.2e-4	1.4e-5	1.1e-3	1.1e-3	2.7e-4	2.8e-4	0.98888	0.00835	-0.03913
	303.158	7.4673	0.98898	3.4e-4	1.4e-5	2.0e-3	2.0e-3	1.1e-4	1.9e-5	1.1e-3	1.1e-3	2.7e-4	2.8e-4	0.98888	0.00835	-0.03913
	303.158	7.4674	0.98910	1.9e-4	3.3e-5	2.0e-3	2.0e-3	1.6e-4	2.2e-5	1.1e-3	1.1e-3	2.7e-4	2.8e-4	0.98888	0.00835	-0.03912
	303.158	7.4674	0.98899	3.7e-4	3.4e-5	2.1e-3	2.1e-3	1.3e-4	1.4e-5	1.1e-3	1.1e-3	2.7e-4	2.8e-4	0.98887	0.00835	-0.03912
V34	303.158	7.5219	0.98691	3.2e-4	3.3e-5	1.7e-3	1.7e-3	1.2e-4	1.4e-5	1.2e-3	1.2e-3	2.7e-4	2.8e-4	0.98682	0.00851	-0.03633
	303.158	7.5219	0.98698	3.6e-4	1.6e-5	1.7e-3	1.7e-3	1.2e-4	1.8e-5	1.2e-3	1.2e-3	2.7e-4	2.8e-4	0.98682	0.00851	-0.03633
	303.158	7.5219	0.98700	1.5e-4	9.6e-6	1.7e-3	1.7e-3	1.2e-4	2.5e-5	1.2e-3	1.2e-3	2.7e-4	2.8e-4	0.98682	0.00851	-0.03633
	303.158	7.5218	0.98698	4.1e-4	4.3e-5	1.7e-3	1.7e-3	1.4e-4	3.2e-5	1.1e-3	1.1e-3	2.7e-4	2.8e-4	0.98682	0.00851	-0.03634
	303.158	7.5217	0.98700	3.4e-4	3.1e-5	1.7e-3	1.7e-3	1.1e-4	1.1e-5	1.1e-3	1.1e-3	2.7e-4	2.8e-4	0.98682	0.00851	-0.03634
	303.158	7.5215	0.98692	3.0e-4	2.5e-5	1.7e-3	1.7e-3	1.5e-4	1.4e-5	1.1e-3	1.1e-3	2.7e-4	2.8e-4	0.98683	0.00851	-0.03635
	303.158	7.5215	0.98693	3.9e-4	3.0e-5	1.7e-3	1.7e-3	1.6e-4	4.1e-5	1.1e-3	1.1e-3	2.7e-4	2.8e-4	0.98683	0.00851	-0.03636
	303.158	7.5213	0.98689	2.4e-4	3.0e-5	1.7e-3	1.7e-3	1.0e-4	1.1e-5	1.1e-3	1.1e-3	2.7e-4	2.8e-4	0.98684	0.00851	-0.03637
V35	303.158	7.5349	0.98700	3.4e-4	1.6e-5	1.8e-3	1.8e-3	1.6e-4	2.8e-5	1.2e-3	1.2e-3	2.7e-4	2.8e-4	0.98635	0.00856	-0.03556
	303.158	7.5351	0.98700	3.6e-4	5.9e-5	1.8e-3	1.8e-3	1.1e-4	8.8e-6	1.2e-3	1.2e-3	2.7e-4	2.8e-4	0.98635	0.00856	-0.03554
	303.158	7.5350	0.98698	4.0e-4	4.7e-5	1.8e-3	1.8e-3	1.8e-4	3.0e-5	1.2e-3	1.2e-3	2.7e-4	2.8e-4	0.98635	0.00856	-0.03555
	303.158	7.5349	0.98697	1.9e-4	2.7e-5	1.8e-3	1.8e-3	1.1e-4	1.0e-5	1.2e-3	1.2e-3	2.7e-4	2.8e-4	0.98636	0.00856	-0.03556
V36	303.158	7.5449	0.98689	2.4e-4	3.6e-5	1.7e-3	1.7e-3	1.1e-4	2.1e-5	1.1e-3	1.1e-3	2.7e-4	2.8e-4	0.98600	0.00861	-0.03491
	303.158	7.5450	0.98685	4.7e-4	4.3e-5	1.8e-3	1.8e-3	1.5e-4	2.4e-5	1.2e-3	1.2e-3	2.7e-4	2.8e-4	0.98600	0.00861	-0.03489
	303.158	7.5450	0.98677	2.1e-4	9.7e-6	1.8e-3	1.8e-3	1.2e-4	1.5e-5	1.2e-3	1.2e-3	2.7e-4	2.8e-4	0.98600	0.00861	-0.03491
	303.158	7.5450	0.98688	2.9e-4	2.5e-5	1.7e-3	1.7e-3	1.4e-4	3.3e-5	1.2e-3	1.2e-3	2.7e-4	2.8e-4	0.98600	0.00861	-0.03491
	303.158	7.5450	0.98677	2.1e-4	1.3e-5	1.8e-3	1.8e-3	1.0e-4	1.4e-5	1.2e-3	1.2e-3	2.7e-4	2.8e-4	0.98600	0.00861	-0.03491
	303.158	7.5449	0.98680	3.4e-4	1.8e-5	1.8e-3	1.8e-3	1.2e-4	2.3e-5	1.1e-3	1.1e-3	2.7e-4	2.8e-4	0.98600	0.00861	-0.03492
V37	303.157	7.5532	0.98692	8.3e-4	1.4e-4	1.8e-3	1.8e-3	1.8e-4	2.5e-5	1.2e-3	1.2e-3	2.7e-4	2.8e-4	0.98570	0.00865	-0.03435
	303.158	7.5533	0.98692	2.0e-4	1.1e-5	1.8e-3	1.8e-3	1.3e-4	2.2e-5	1.2e-3	1.2e-3	2.7e-4	2.8e-4	0.98571	0.00865	-0.03434
	303.158	7.5535	0.98669	4.8e-4	8.3e-5	1.8e-3	1.8e-3	1.3e-4	1.1e-5	1.2e-3	1.2e-3	2.7e-4	2.8e-4	0.98570	0.00865	-0.03433
	303.158	7.5529	0.98669	3.6e-4	4.6e-5	1.7e-3	1.7e-3	1.1e-4	1.2e-5	1.1e-3	1.1e-3	2.7e-4	2.8e-4	0.98572	0.00865	-0.03437
V38	303.158	7.5542	0.98670	1.5e-4	1.4e-5	1.8e-3	1.8e-3	1.4e-4	3.2e-5	1.1e-3	1.1e-3	2.7e-4	2.8e-4	0.98568	0.00866	-0.03428
	303.158	7.5542	0.98667	1.8e-4	2.5e-5	1.8e-3	1.8e-3	1.9e-4	3.5e-5	1.1e-3	1.1e-3	2.7e-4	2.8e-4	0.98568	0.00866	-0.03428
	303.158	7.5541	0.98662	6.5e-4	4.8e-5	1.8e-3	1.8e-3	1.2e-4	2.1e-5	1.1e-3	1.1e-3	2.7e-4	2.8e-4	0.98568	0.00866	-0.03429
	303.158	7.5540	0.98660	1.9e-4	1.2e-5	1.7e-3	1.7e-3	1.2e-4	1.8e-5	1.1e-3	1.1e-3	2.7e-4	2.8e-4	0.98568	0.00866	-0.03429
	303.158	7.5539	0.98662	3.2e-4	2.7e-5	1.8e-3	1.8e-3	1.1e-4	2.2e-5	1.1e-3	1.1e-3	2.7e-4	2.8e-4	0.98568	0.00866	-0.03430

	303.158	7.5538	0.98659	4.9e-4	1.1e-4	1.7e-3	1.8e-3	1.1e-4	1.7e-5	1.1e-3	1.1e-3	2.7e-4	2.8e-4	0.98569	0.00866	-0.03431
	303.158	7.5538	0.98661	1.9e-4	2.2e-5	1.7e-3	1.7e-3	1.0e-4	2.0e-5	1.1e-3	1.1e-3	2.7e-4	2.8e-4	0.98569	0.00866	-0.03431
	303.158	7.5537	0.98656	1.0e-4	2.6e-5	1.8e-3	1.8e-3	1.1e-4	2.9e-5	1.1e-3	1.1e-3	2.7e-4	2.8e-4	0.98569	0.00866	-0.03431
V39	303.156	7.5542	0.98643	3.7e-4	1.4e-5	1.7e-3	1.7e-3	1.0e-4	9.4e-6	1.1e-3	1.1e-3	2.7e-4	2.8e-4	0.98566	0.00866	-0.03428
	303.157	7.5543	0.98638	4.6e-4	4.7e-5	1.7e-3	1.7e-3	9.2e-5	1.0e-5	1.1e-3	1.1e-3	2.7e-4	2.8e-4	0.98566	0.00866	-0.03428
	303.157	7.5543	0.98641	5.1e-4	1.1e-4	1.7e-3	1.7e-3	1.2e-4	1.9e-5	1.1e-3	1.1e-3	2.7e-4	2.8e-4	0.98566	0.00866	-0.03427
	303.156	7.5543	0.98644	4.0e-4	2.9e-5	1.7e-3	1.7e-3	1.6e-4	1.7e-5	1.1e-3	1.1e-3	2.7e-4	2.8e-4	0.98566	0.00866	-0.03428
	303.156	7.5542	0.98641	3.7e-4	3.6e-5	1.7e-3	1.7e-3	1.5e-4	2.1e-5	1.1e-3	1.1e-3	2.7e-4	2.8e-4	0.98566	0.00866	-0.03428
V40	303.158	7.5577	0.98708	1.2e-4	3.1e-5	1.7e-3	1.7e-3	1.4e-4	2.1e-5	1.1e-3	1.1e-3	2.7e-4	2.8e-4	0.98555	0.00868	-0.03402
	303.158	7.5576	0.98705	4.2e-4	3.5e-5	1.8e-3	1.8e-3	1.6e-4	2.2e-5	1.1e-3	1.1e-3	2.7e-4	2.8e-4	0.98556	0.00868	-0.03403
	303.158	7.5575	0.98705	2.2e-4	1.9e-5	1.8e-3	1.8e-3	1.2e-4	1.3e-5	1.1e-3	1.1e-3	2.7e-4	2.8e-4	0.98556	0.00868	-0.03404
	303.158	7.5575	0.98709	2.7e-4	2.4e-5	1.7e-3	1.7e-3	1.6e-4	3.0e-5	1.1e-3	1.1e-3	2.7e-4	2.8e-4	0.98556	0.00868	-0.03404
	303.158	7.5574	0.98707	1.8e-4	1.3e-5	1.7e-3	1.7e-3	1.0e-4	1.6e-5	1.1e-3	1.1e-3	2.7e-4	2.8e-4	0.98557	0.00868	-0.03405
	303.158	7.5574	0.98710	3.5e-4	3.3e-5	1.7e-3	1.7e-3	1.2e-4	1.4e-5	1.1e-3	1.1e-3	2.7e-4	2.8e-4	0.98557	0.00868	-0.03405
	303.158	7.5572	0.98710	5.0e-4	2.9e-5	1.7e-3	1.7e-3	1.1e-4	2.0e-5	1.1e-3	1.1e-3	2.7e-4	2.8e-4	0.98557	0.00868	-0.03406
	303.158	7.5572	0.98711	3.3e-4	2.9e-5	1.7e-3	1.7e-3	1.2e-4	2.4e-5	1.1e-3	1.1e-3	2.7e-4	2.8e-4	0.98557	0.00868	-0.03406